University of Alberta

A Study of Passivity and Stress Corrosion Cracking (SCC) Of Alloy 800 In Simulated Steam Generator Crevice Solution Containing Thiosulfate and Sulphide Species

by

Santhoshkumar Kulandaivel

A thesis submitted to the Faculty of Graduate Studies and Research

in partial fulfillment of the requirements for the degree of

Master of Science

in

Materials Engineering

Department of Chemical & Materials Engineering

Fall 2011

Edmonton, Alberta

ABSTRACT

The passivity and stress corrosion cracking (SCC) behavior of Alloy 800 was studied in test solution containing thiosulfate and sulphide species. Cyclic polarization experiments in thiosulfate containing solutions indicated that with an increase in the concentration of thiosulfate, both the pitting potential and the passive range were decreased. The presence of deflection promoted material degradation. Cyclic polarization test in solution containing sulphide indicated that Alloy 800 was susceptible to anodic dissolution. Mott-Schottky results showed that the donor density of the passive film increased with an increase in the concentration of low valence sulphur species.

The SCC of Alloy 800, with an applied deflection of 0.356 mm, was studied under different applied potentials in test solution containing 0.075 M thiosulfate. Alloy 800 was susceptible to SCC in transpassive potential region (-110 mV). The x-ray photoelectron spectroscopy (XPS) and secondary ion mass spectroscopy (SIMS) analysis showed that the degradation of the passive film caused by the reduction reaction of thiosulfate was the cause of S^{y}-SCC.

ACKNOWLEDGEMENTS

I thank my supervisor Dr. Jingli Luo for her excellent support, guidance and encouragement throughout my studies at University of Alberta.

I would like to acknowledge Dr. Renkang Zhu for his valuable suggestions, discussions and support during the course of my research. I also acknowledge Luning Wang, Payam and Liang for their helpful discussions.

This work would not have been possible without the financial support of the Natural Sciences and Engineering Research Council and Atomic Energy of Canada Limited.

I also wish to express my deepest appreciation to my family for their constant encouragement throughout this work.

ABBREVIATION

AVT	All volatile treatment
CE	Counter electrode
CT	Compact tension
IGA	Intergranular attack
OTSG	Once through steam generators
PWR	Pressurized water reactor
RE	Reference electrode
SCC	SCC
S^y-SCC	Low valence sulphur SCC
SCE	Saturate calomel electrode
SG	Steam generator
SS	Stainless steel
TTS	Top of the tube sheet
WE	Working electrode

Table of Contents

List of Figures

List of Tables

Chapter 1 Introduction

Electricity is emerging as the deciding factor in energy and environmental policy. The most important challenge of the electricity industry is to generate power from low carbon sources because of the potential threats posed by global warming. Therefore, there is an increasing need around the world to reduce our dependence on traditional energy resources like coal and crude oil. Hydro power and nuclear power are the best clean energy resource alternatives for energy.

The following table shows the contributions from the different energy sources to the total electricity production for the year 2009.

Table 1.1 Total electricity generation in Canada (617.5 TWh) with break down of contributions from individual source[1].

Hydro	63.2%
Nuclear	14.8%
Conventional Steam	17.4%
Internal Combustion	0.2%
Combustion Turbine	4.1%
Tidal	0.01%
Wind	0.3%

Nuclear power is a promising clean energy resource. A lot of new nuclear power plants will be built in the next several decades. For example, in Ontario, nuclear power has supplied more than 50% of the electricity consumption, as shown in Figure 1.1. However, the most challenging task is the safe operation of the nuclear power plant. The degradation of the steam generator (SG) tube materials is one of the major safety concerns.

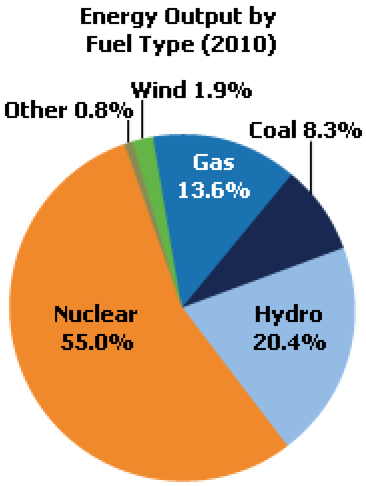

Figure 1.1 Ontario's electricity supply distribution[2].

Smooth operation of the nuclear power plants depends to a large extent on the trouble free operation of the SG[3-5]. The development of Ni-Cr-Fe based SG tube materials has been driven by the failure of various materials owing to their compatibility with the SG tube environment. Austenitic stainless steels such as type 304 and similar other varieties were initially considered as SG tube materials. These materials experienced transgranular stress corrosion cracking (SCC) in high temperature water containing only a few ppm of chloride and oxygen [6]. This has led to discarding of stainless steel (SSs) as SG tube materials. To overcome the deficiencies of austenitic SSs, Ni based alloys were developed. Alloy 600 was a Ni based alloy and it found application as a standard SG tube material for PWRs in the sixties [6]. In late sixties SCC of Alloy 600 from the primary side was detected in the high purity water [6]. This type of intergranular SCC(IGSCC) and SCC from the secondary side due to crevice and denting effects were the main causes of tube failures. Alloy 600 was further studied extensively and it was found by some researchers that it was susceptible to hydrogen-induced IGSCC. Besides hydrogen induced IGSCC, environmental assisted cracking of Alloy 600 has also been reported by several researchers later on [6-11]. Monel 400 is a Ni-Cu based alloy. This alloy unlike SSs, has been found to be resistant to chloride induced SCC [6].This alloy was employed as a SG tube material in early CANDU reactors and early Indian pressurized heavy water reactors (PHWRs) due to its good corrosion resistance in low oxygen environments[6, 12]. However, this alloy has been reported to be prone to intergranular attack (IGA) associated with pitting under certain conditions [12]. Deficiencies of Alloy 600 and Monel 400 have led to the development of Alloy 800, which is an austenitic, Fe-Cr-Ni alloy. Alloy 800 was chosen as a SG tube material for Kraft Werk Union and later Indian PHWRs owing to its very good resistance to SCC in pure water and chloride environments [13-15]. Alloy 800, irrespective of material condition, has also been reported to be resistant to SCC in high temperature water containing up to 8 ppm oxygen and 0.6 ppm dissolved Pb [6]. However, a study [3]relating to microstructural aspects indicates that the large, faceted primary TiN (hexagonal structure) particle/austenite matrix interface in the alloy may provide a preferred site for pit initiation in the chloride and acidic chloride environments at ambient temperature. Due to extensive research, another modified alloy called Alloy 690 was developed. This is an austenitic alloy containing Fe-Cr-Ni. The major difference between Alloy 690 and 800 is due to high Ni content in Alloy 690, whereas Fe is high in Alloy 800. Alloy 690 possesses superior SCC resistance in pure water as compared to Alloy 600. However, the alloy has also been reported to be susceptible to SCC and IGA in deaerated caustic environments[16, 17].Younes et al., noticed that Alloy 690 are susceptible to hydrogen to a lesser extent than those of Alloy 600. In normal and simulating abnormal secondary side SG coolant conditions[18], the behaviour of the alloy is found to be similar to that of Alloy 600. Studies on microstructural aspects of the corrosion reveal that the large, faceted primary TiN (hexagonal structure) particle/austenite matrix interface may act as a preferential site for pit initiation in the acidic chloride environments at ambient temperature. Tapping et al., evaluated the various SG degradation mechanisms observed for 30 years of operation. They concluded that either primary side SCC or secondary side SCC dominated the SG degradation mechanisms. This is shown in the Figure 1.1 [19].

Therefore in steam generators environmentally assisted SCC of nickel based alloys poses a major problem for the safe operation of nuclear power plants. This causes repeated shut downs and affects the economics of the plant operation. Low valence sulphur species has been observed to accelerate the SCC of sensitized Alloy 600 at low temperatures, at operating conditions less than full power [20].

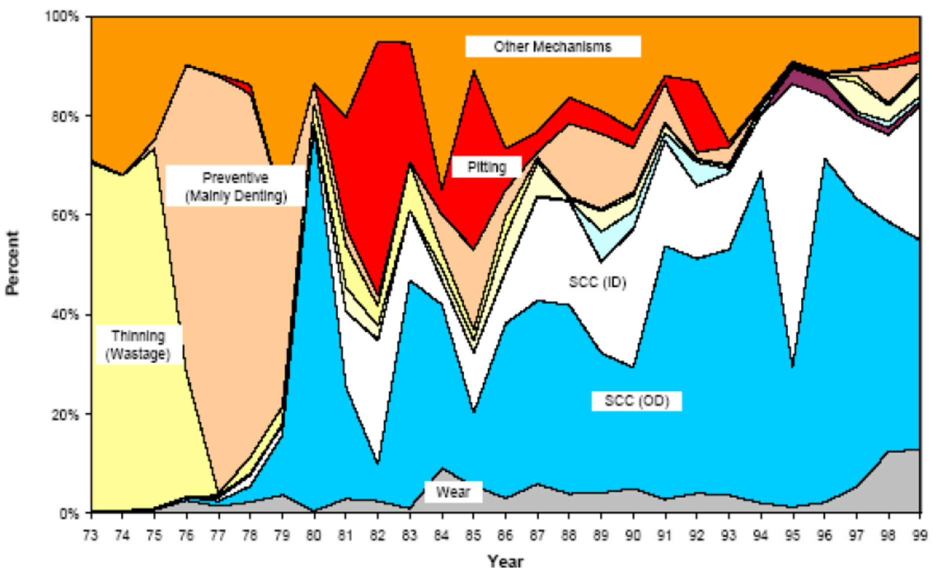

Figure 1.2 Evaluation of causes of SG tube degradation with time [19].

The Bruce unit 4 SGs experienced IGA/SCC at the top of tubesheet [21]. A detailed analysis revealed that the occurrence of this outer diameter IGA/SCC was likely caused by the low valence sulphur species such as thiosulphates and tetrathionates, since these compounds were found in the TTS sludge material. This attack in Bruce Unit 4 most likely occurred during startup evolutions, i.e due to the oxidizing conditions developed during the shutdown [20]. IGA identified in Alloy 600 SG tubes at the Palisades Nuclear Power Plant and Arkansas Nuclear One in 1983 was also associated with the presence of low valence sulphur species at low temperatures [22]. The amounts of sulphur species in the pits of tubes removed from Millstone 2 were found to exceed those of chloride, indicating that the sulphur species may have been involved in the pitting processes [22]. Thiosulfate-containing solutions have caused severe pitting of type 304 SS (UNS S30400) in the pulp and paper industry, where the aggressive effect of thiosulfate allows pitting to occur even in non-chloride, sulfate solutions [23].Therefore it is important to study the contribution of low valence sulphur species to the degradation SG tube materials at low temperatures.

Alloy 800 was introduced in the 1950s as a low nickel substitute for Alloy 600. Alloy 800 has been a preferred steam generator tubing materials for CANDU reactors and German power plants. Degradation of Alloy 800 SG tubing has only been found in a few cases at a limited number out of 19 PWRs in Europe despite the large number of SG tubes operating for years until today[24], [25].

However, operating experience in a few Germany PWR SGs and in SGs of one CANDU station over the last five years has challenged the assumption that Alloy 800 SG tubes will continue to demonstrate trouble (degradation) free performance, especially in the context of plant life extension. The degradation of Alloy 800 ex-service SG tubing due to the deleterious species such as sulphur and chlorine was reported [26]. Therefore it is necessary to understand the low valence sulphur corrosion and SCC susceptibility of Alloy 800 for effective corrosion control management and successful operation of the steam generator.

A lot of researchers have studied the effect of thiosulfate, one of the low valence sulphur species on stainless steel materials and Alloy 600. They studied the corrosion and SCC behavior of the various types of stainless steels and Alloy 600 in test solutions containing thiosulfate [27-43] .The data about passivity degradation and SCC due to low valence sulphur species on Alloy 800 is very limited.

This served as the motivation behind this work to study the relationship between passivity degradation and S^y-SCC of Alloy 800. Futher there is not sufficient experimental data about the sulphide, one of the low valence sulphur species, promoted corrosion and SCC behavior of Alloy 800. Therefore the first part of this research work is to study the effect of thiosulfate and sulphide on the passivity and SCC of Alloy 800.

The initiation of cracks due to pitting caused by the low valence sulphur species on the Alloy 800 SG tube surface is unavoidable, but not all of these cracks can grow and cause failure of the steam generator. Therefore it is important to focus on the growth behavior of the existent cracks in the Alloy 800 SG tube to obtain an appropriate model which explains the growth behavior of cracks in appropriate loading conditions. Using such a crack growth model one can have a reasonable engineering prediction on the growth behavior of the existent cracks.

The measurement of crack propagation rate is essential for the prediction of service life. This will help in the inspection and replacement of the section before SG tube failure occurs. Therefore the second part of this work will study the crack propagation rate of Alloy 800 by potential drop technique at room temperature in environments containing thiosulfate and sulphide.

The following chapter will review the literature associated with low valence sulphur species which can induce corrosion on SG tube material and other materials. Chapter 3 will describe the experimental techniques used in this study. Chapter 4 will discuss the results. Chapter 5 will highlight the conclusions and future work.

Chapter 2 Literature Review

2.1 Introduction

Low valence sulphur is produced from sulfate impurities and released resins accumulated in heat transfer crevices. N_2H_4 can react with these impurities to produce lower valence sulphur according to the thermodynamic inclination of such reactions to occur. Sulphur species of lower valencies +2.5, +2 and -2(tetrathionate, thiosulfate and sulphide respectively) tend to accelerate the entry of hydrogen into metals and tend to accelerate general and localized corrosion of Alloys 600 and 690. Thus, with these undesirable effects and the inevitability of producing lower-valence sulphur from reactions with N_2H_4, there should be continuing concern for the undesirable effects of lower valence sulphur species. There is a long history in corrosion associated with the deleterious effects of "reduced sulphur" on the corrosion of commercial alloys [44]. Extensive damage was sustained by a steam generator in 1981 when sodium thiosulfate in a holding tank was inadvertently released to the primary coolant during a shutdown period [44].

In general lower valence sulphur species are detrimental to metals and this subject has been studied extensively, especially in oil and petroleum processing industries. Thus the inevitability of N_2H_4 reducing SO_4^{-2} is of historic significance and is a well founded concern for the performance of SG tubing [44]. Also Rochester and Eaker have shown that the sulphides can sometimes occur inside the cracks in OTSG upper bundle regions. Since reduced sulphur species are sometimes found inside advancing SCC, although the exterior environment contains S^{+6} , it is perhaps important to note that the S^y SCC is mainly associated with the reduced sulphur species in the external environment outside the advancing SCC. The reduction of SO_4^{-2} from the outside environment to S^{-2} inside the advancing SCC may occur by a reaction between SO_4^{-2} and metal to produce metal sulphides [44].

In this chapter, the concept and theory of SCC will be discussed initially and then the characteristics of S^y-SCC will be discussed in detail. Since passivity degradation is one of the reasons behind S^y-SCC, the passivity concepts will also be discussed. Further the concepts of crack propagation studies using potential drop system will be discussed.

2.2 SCC

SCC is a term used to describe service failures in engineering materials by environmentally induced crack propagation which is the result of combined and synergistic interaction of mechanical deflection and corrosion reactions. The stress required to cause SCC are small, usually below the macroscopic yield deflection and are tensile in nature.

SCC is usually alloy/environment specific. It is often the result of a specific chemical species in the environment. For example, chloride ions can cause cracking in stainless steels and aluminum alloys. Further an environment that causes SCC in one alloy may not cause it in another.

In general SCC is observed in alloy/environment combinations that result in the formation of a film on the metal surface. These films reduce the rate of general or uniform corrosion.

The environmental parameters that are known to influence the rate of crack growth in aqueous solutions include but are not limited to:

- Temperature
- Pressure
- Solution composition
- pH
- Electrochemical potential
- Solution viscosity
- Stirring or mixing

SCC is a slow process in which cracks initiate and propagate at a slow rate until the stresses in the remaining ligament of metal exceed the fracture strength. Therefore the SCC process consists of three periods as shown in Figure 2.1.

- Crack initiation and period I propagation
- Steady state crack propagation
- Final failure

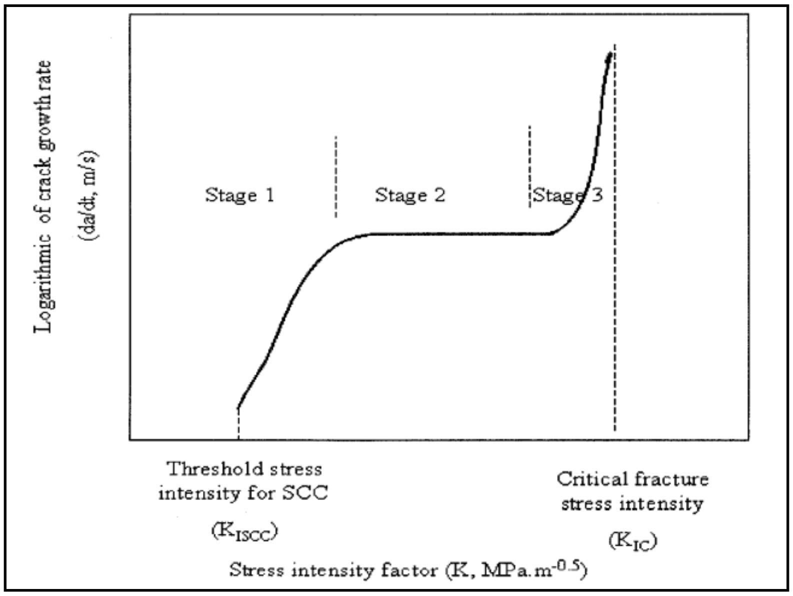

Figure 2.1 Schematic diagram of crack-propagation rate as a function of crack-tip deflection-intensity [45].

SCC can be discussed in terms of initiation (incubation & nucleation) and propagation. Different mechanisms are proposed to explain SCC. The basic corrosion reactions that dominate the SCC process in synergy with mechanical deflection are anodic and cathodic. Anodic SCC involves the dissolution of metal during the initiation and propagation of cracks. Cathodic SCC involves embrittlement by the corrosion product hydrogen. This process involves the adsorption of hydrogen at the cathodic sites on the metal surface or on the walls of a crack and its subsequent entry into the metal lattice. Usually the crack initiates at the surface discontinuities or pits developed on the surface during operation. Since the SCC of iron-based and Ni-based alloys is controlled by a film rupture model, this mechanism requires explanation.

The film rupture model is based on anodic dissolution at the crack tip that leads to crack growth. The crack growth rate is described by the following Faraday relationship.

$$\frac{d_a}{d_t} = \frac{i_a M}{zF\rho} \qquad \textbf{(2.1)}$$

where i_a is anodic current density at the crack tip, M is atomic weight, Z is the valence, F is Faraday's constant and ρ is density of the material.

According to this model, localized plastic deformation leads to the rupture of the passive film at the crack tip and the exposed bare metal to the environment undergoes anodic dissolution which causes crack propagation.

It is proposed that once the crack starts, it will lead to crack growth as the rate of film rupture is greater than the passive film growth at the crack tip. The crack growth is not a continuous process because the crack tip repassivates and then ruptures repeatedly to cause crack growth [45]. This is illustrated in the Figure 2.2 .

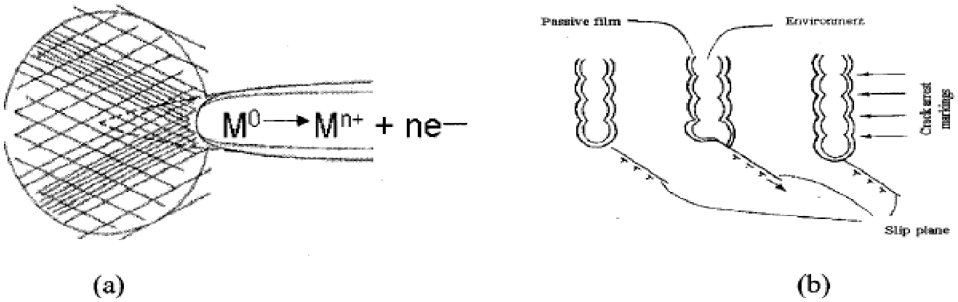

Figure 2.2 Schematic representation of crack propagation by the film-rupture model (a) Crack tip remains bare. (b) Crack tip repassivates and it is ruptured repeatedly [45].

2.3 Low Valence Sulphur SCC (S^y-SCC)

All volatile treatment has been used by CANDU 6 SGs. This treatment used a volatile reducing agent like hydrazine to scavenge oxygen from the feed water and to maintain reducing conditions in the SGs. However, N_2H_4 may reduce sulfate impurities that accumulate in heat transfer crevices to lower valences. Sulphur, in its reduced state, has been known to interfere with the protective oxide films that form on high-nickel alloys such as those used as tubing materials in CANDU SG. By assisting in the breakdown of oxides, reduced sulphur can cause intergranular attack and pitting of SG tubing material over a wide pH range. Reduced sulphur has also been observed to accelerate SCC of sensitized Alloy 600 at low temperatures (i.e., operating conditions less than full power)[46]. Lower valence sulphur species accelerate degradation of alloys in two ways, as illustrated in the Figure 2.3.

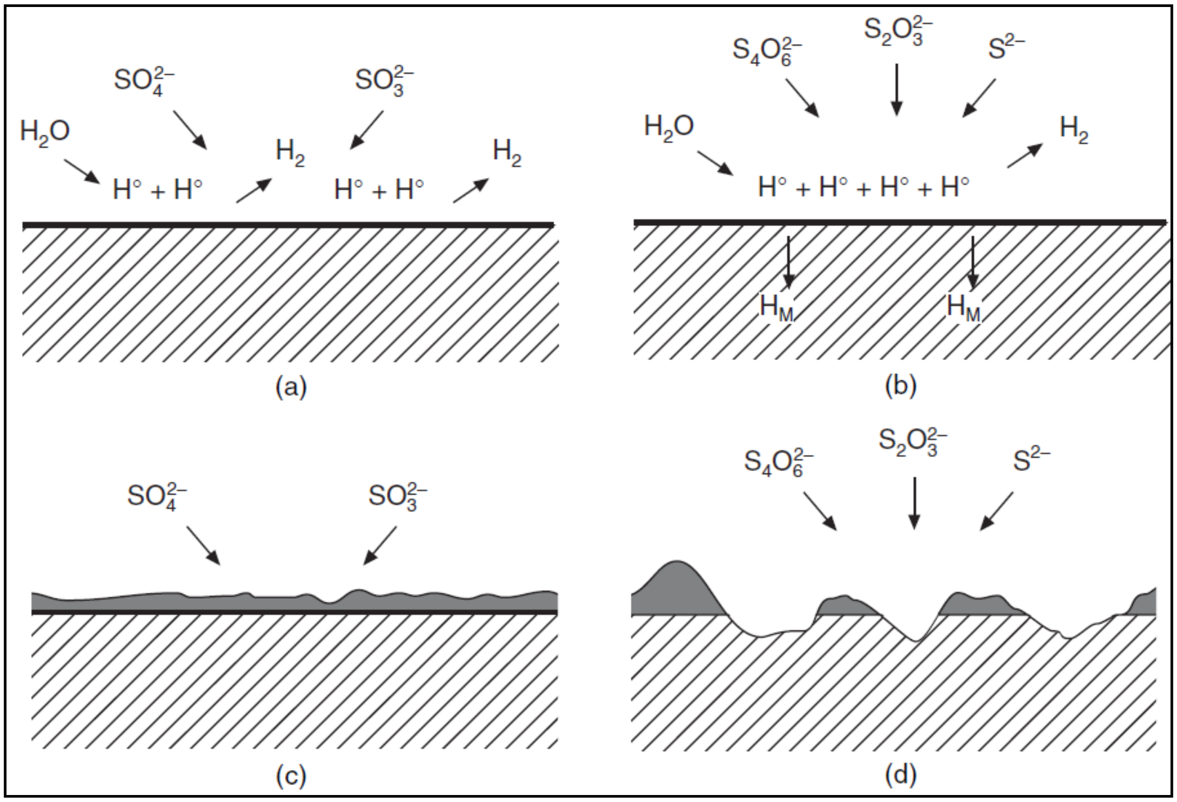

Figure 2.3 Decreasing valence of sulphur promotes entry of hydrogen and degradation of the protective film [44].

The materials that are commonly prone to S^y-SCC are 304 and 316 SS, and Alloy 600. Alloy 800 has austenitic structure and it has similar properties to 304, 316 SS and Alloy 600. There is no accepted comprehensive mechanism available in literature to explain S^y-SCC. Different researchers have used different test conditions and therefore the correlation of the results is quite difficult. The following discussion will serve to provide a better understanding of S^y-SCC for various materials.

Newman et al., studied SCC of a sensitized type 304 stainless steel at room temperature using controlled potentials and two concentrations of sodium thiosulfate. They found that sensitized type 304 stainless steel in thiosulfate solutions was susceptible to SCC only when repassivation of simulated grain boundary material was retarded in a simulated crack tip environment. They further found that the addition of sufficient concentration of sodium sulfate ions to dilute thiosulfate solution inhibits SCC[28].

Haruna et al., studied the SCC of type 316L stainless steel in a chloride solution containing thiosulfate ions using slow strain rate testing. They reported that the stress corrosion crack growth rate was almost wholly decided by the chemistry of the concentrated Cl^- solution at the crack tip and that $S_2O_3^{-2}$ acted only as an accelerator to pit formation[47]. Ashour et al., studied the effect of thiosulfate on SCC of type 316 stainless steel in a solution containing sodium thiosulfate and 3.5% aqueous sodium chloride. They reported that $Na_2S_2O_3$ accelerated pitting and SCC of type 316 SS in 3.5% NaCl [33]. Roychowdhury et al., studied the SCC behavior of sensitized AISI type 304 stainless steel in dilute thiosulfate solutions as a function of thiosulfate concentrations and applied potentials. The susceptibility to SCC was observed to increase with thiosulfate concentrations and applied potentials. They concluded that a film rupture anodic dissolution type of mechanism was operative during SCC of sensitized SS304 in thiosulfate solutions [34]. Laycock et al., studied the pitting behavior of austenitic stainless steels(304, 316L, 904L) using potentiodynamic polarization scans in 1M sodium chloride solutions with various thiosulfate additions at temperatures from 20^oC to 90^oC. They reported that a minimum concentration of thiosulfate was required for activation of pitting corrosion in each alloy. They found that the critical factor in the thiosulfate stabilization of pitting was the chloride : thiosulfate ratio. For type 304 SS at 20^oC in 1 M NaCl solution, the most aggressive ratio was 250:1[23].

Laitinen et al., studied the localized corrosion behavior of austenitic stainless steels UNS S30403 and UNS S31603 and duplex SS UNS S31803 in simulated paper machine environments containing chloride, sulfate and thiosulfate at 65^oC and a pH value of 3. Electrochemical testing of the materials was carried out by cyclic polarization scans and scratch tests. They reported that the pits on UNS S30403 and UNS S31603 were enriched in Cr and Cu and depleted in Fe, when compared to the base metal. When $S_2O_3^{2-}$ was present in the solution, pits contained very high amounts of S and no Cl^-. Without $S_2O_3^{2-}$ addition to the solution, pits contained only small amounts of S and Cl^-. Further they suggested that the environment inside pits reduced $S_2O_3^{2-}$ migrating from the solution or S dissolving from sulphide inclusions to H_2S according to potential-pH diagram. It was proposed that H_2S accelerated dissolution of SS by forming sparingly soluble metal sulphides and by acidifying the local environment[37].

Singh et al., studied the SCC and subsequent corrosion fatigue cracking behavior of a heat-treated duplex stainless steel in paper-machine white waters containing chloride and thiosulfate ions. They did potentiodynamic and slow strain rate tests and confirmed that the crack initiation was due to an SCC film rupture process during paper machine shutdowns where ionic concentrations of species increase due to white water evaporation. They suggested that crack initiation occurs by pitting within ferrite grains or near grain boundaries where metallurgical changes produced during heat treatments play an important role [38]. Chen et al., studied the susceptibility of Type 321 SS to SCC under simulated petrochemical conditions containing thiosulfate and chloride using a slow strain rate tensile test and a static load U-bend test at the free corrosion potentials. They found that SCC of type 321 stainless steel in simulated petrochemical process environment containing thiosulfate and chloride is induced by pitting [39]. Isaacs et al., studied the SCC of type 304 stainless steel in thiosulfate solutions using constant extension rate tests. They reported that 0.1ppm $Na_2S_2O_3$ was the minimum concentration at which SCC of 304 SS was observed. The rate of SCC increased with the potential and the rate of cracking was proportional to the current. They suggested that cracking is a result of dissolution of the chromium depleted grain boundary and is controlled by the rupture and formation of a salt layer at the crack tip rather than a passive oxide film [40].

Park et al., studied the pitting corrosion of type 304 and 316 stainless steel in neutral chloride solutions containing various concentrations of thiosulfate and chloride by a series of galvanostatic and potentiostatic experiments in conjunction with adsorption measurements made by a radiotracer method. They concluded that thiosulfate changes the growth behavior of pits. They observed from the radiotracer experiments that the extent of pit initiation and propagation were influenced by the adsorption behavior of thiosulfate [41].

Duret-Thual et al., investigated the role of thiosulfates in pitting induced by chlorides on Fe-17Cr alloys in neutral medium using electrochemical and XPS analysis. They reported that the detrimental effect of the thiosulfates on pitting resistance increases with increasing sulphur content in the alloy. The XPS results provide evidence that the thiosulfates are reduced on the metallic surface whereas they do not interact strongly with the passive film surface. Sulphide islands are formed at the bare alloy surface and prevent repassivation [48].

Yang et al., studied the effect of change in concentrations of thiosulfate on electrochemical behavior and SCC susceptibility of untreated and sensitized Alloy 600 at room temperature. They conducted SSRT tests using untreated and sensitized Alloy 600 at various applied potentials and different concentrations of $Na_2S_2O_3$. They found that the chloride content required to generate pitting was a function of the logarithm of the thiosulfate concentration in the range of 1 to 0.001 M.

Further they reported that sensitized Alloy 600 at -300 mV vs. SCE and +400 mV vs. SCE indicated susceptibility to SCC in low temperature thiosulfate solutions was electrochemically dependent. Untreated Alloy 600 showed no susceptibility to SCC in low temperature thiosulfate solutions [27]. Ho et al., studied pitting corrosion of Inconel 600 in aqueous chloride and chloride-thiosulfate solutions at low temperatures. They studied the effect of solution concentration on pitting using anodic polarization scans and pitting resistance of Alloy 600 at various solution concentrations and temperatures. They found that the pitting potential of Alloy 600 increases with increasing concentration of chloride. The concentration of thiosulfate higher than 0.001 M inhibits chloride pitting of Inconel 600 in the low concentration chloride solution. The efficiency of inhibition increases with increasing concentration of thiosulfate. Thiosulfate plays an important role in the growth process of pits [30].

Gonzalez et al., studied the SCC susceptibility of unsensitized and sensitized alloy 601 in sodium thiosulfate and sodium chloride solutions using slow strain rate testing. They reported that unsensitized alloy was immune to SCC and showed only ductile failure. The susceptibility to SCC increased with increase in the sensitization of the alloy [32]. Tsai et al., studied the corrosion fatigue crack growth behavior of sensitized alloy 600 in 0.1 M soldium thiosulfate solution at room temperature under applied anodic potential conditions using fracture mechanics technique. They reported that at a frequency of 0.1 Hz, the FCG rates in sensitized alloy 600 in 0.1 M $Na_2S_2O_3$ solution increased with increasing potential [49].

Fang et al., studied the effects of the valence of sulphur as sulphur oxyanions and sulphide (S^{-2} or HS^{-}), on passivation of alloys 600, 690, and 800 in various heat treatments at 25°C and 95°C using potentiodynamic polarization. They reported that the stability of the passive films decreased with decrease of the sulphur valence from +6 to -2. They reported that intergranular corrosion occurred mainly in solutions of thiosulfate ($S_2O_3^{-2}$), sulfate (SO_4^{-2}), sulfite (SO_3^{-2})and tetrathionate ($S_4O_6^{-2}$), whereas S^{-2} or HS^{-} produced pitting. They concluded that increasing the concentration of $S_2O_3^{-2}$ from 10^{-4} M to 1.5 M significantly increased the passive current density and lowered E_b. The transient instability of protective films was assessed using a SCC (SCC) parameter (PSCC) that incorporates the ratio of current densities obtained in fast and slow potentiodynamic scans [42]. Ge et al., studied the effect of sulphide on the passive film formed on 316 stainless steel. They showed that the passive current of stainless steel increases with the addition of sulphide.

They showed that the increase in sulphide concentration led to an increase in acceptor density N_A and donor density N_D. This confirms that sulphide changes the composition structure of the passive film on SS and decreases the corrosion resistance of the film [43].

To summarize, thiosulfate plays a crucial role in the growth process of pits and the initiated pits leads to the SCC of various materials as discussed above. Further there is not enough experimental data available about S^y-SCC for Alloy 800. Therefore S^y-SCC for Alloy 800 is not clearly understood. Also there is no experimental data available in the literature on the effect of sulphide on the corrosion and SCC behavior of Alloy 800.

2.3.1 Factors influencing S^y-SCC

S^y-SCC depends upon seven primary variables namely pH, potential, species, alloy composition, alloy structure, temperature and deflection. The effect of each of these variables on S^y-SCC is discussed in detail below.

2.3.1.1 pH

The potential - pH diagrams in Figure 2.4 and Figure 2.5 imply that S^y-SCC is likely to occur over the full range of pH. However, the data available is not sufficient to confirm such an implication. In high pH solutions, low valence sulphur species accelerate S^y-SCC. $Na_2S_2O_3$ exhibits the same intensity of SCC as does PbO in alkaline solutions and produces S^y-SCC in Alloys 800,690 and 600 at 350°C [44]. Between the pH range of 3 to 8, Alloy 690 exhibited more stability against S^y-SCC [42].

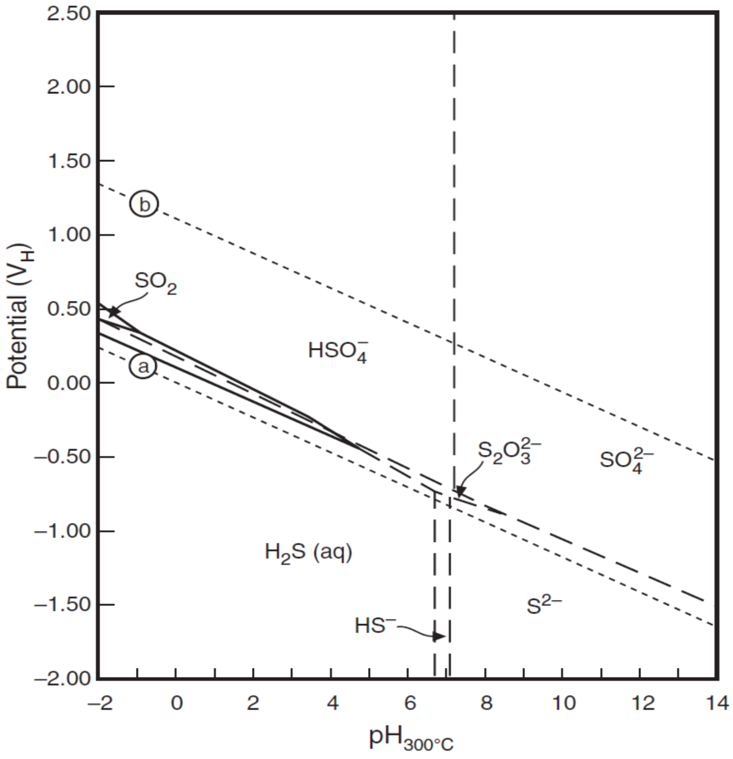

Figure 2.4 Potential vs. pH diagram for the stability of the sulphur species in aqueous environments at 300 °C [44].

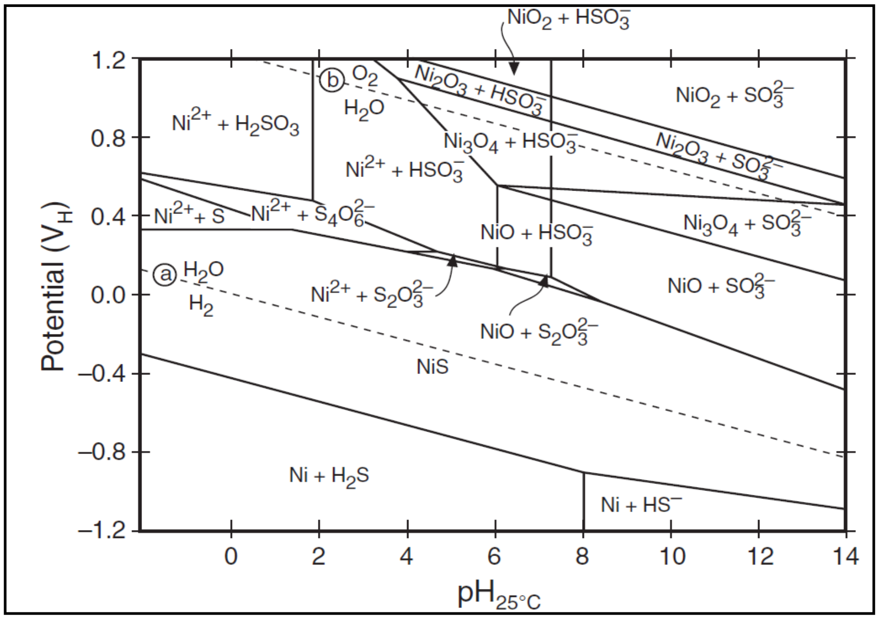

Figure 2.5 Potential vs. pH diagram for the stability of the Ni-S-H_2O species in aqueous environments at 25 °C [44].

2.3.1.2 Potential

The potential dependence for S^y-SCC at 22°C for sensitized Alloy 600 in thiosulfate solution is similar to that for SCC in alkaline solutions as shown in the Figure 2.6 & Figure 2.7 [44]. Figure 2.8 also shows that a heat treatment equivalent to Alloy 600TT produced accelerated S^y-SCC at a temperature as low as 95°C and at potentials that are oxidizing to the open-circuit potential [44].

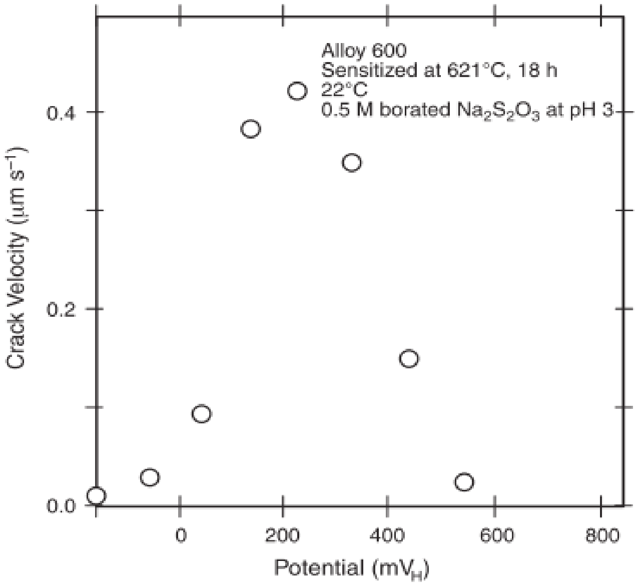

Figure 2.6 Crack velocity vs. potential for sensitized Alloy 600 exposed at 22 °C in 0.5M borated $Na_2S_2O_3$ at pH 3 [44].

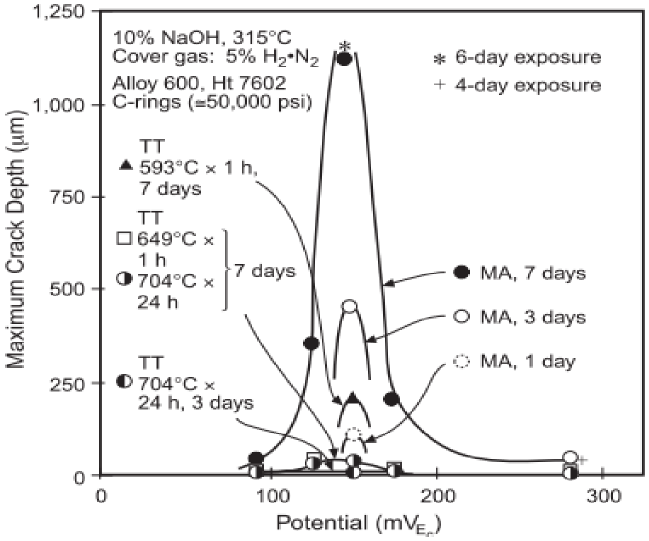

Figure 2.7 Maximum crack depth vs. potential for Alloy 600 exposed in 10% NaOH at 315 °C for mill annealed and various thermal treatments [50].

2.3.1.3 Species

S^y-SCC depends mainly on lower valence sulphur, and the +6 valence does not accelerate S^y-SCC in the high pH environments. It was clearly proved that N_2H_4 reduces sulfates and resins to lower valence sulphur in normal AVT conditions at typical SG temperatures. Also it was shown that the amount of reduced sulphur does not depend on the concentration of N_2H_4 in their range of concentrations. It appears that, once oxygen is reacted, N_2H_4 has no more effect on the electrochemical potential. Further reduced sulphur is preferentially concentrated in the steam phase. Due to its volatility, H_2S is preferentially concentrated in the steam phase when the pH of the system is near neutral or acidic [44]. Further the low valence sulphur species is promoted in the reduction by Ni in alloy. Figure 2.5 shows the potential vs. pH diagram at 25^{o}C. Although this diagram is not directly applicable at higher temperatures, it should generally be indicative of the tendencies [6]. The most significant information from this diagram is the broad range of stability of NiS over the range of pH and potential. This means that NiS is stable, as in nature, in preference to NiO. This diagram also shows that sulphates can be reduced by nickel to NiS due to thermodynamic favorability. Further, it is also possible that sulphates may also be reduced by Fe, and Cr to lower valence states.

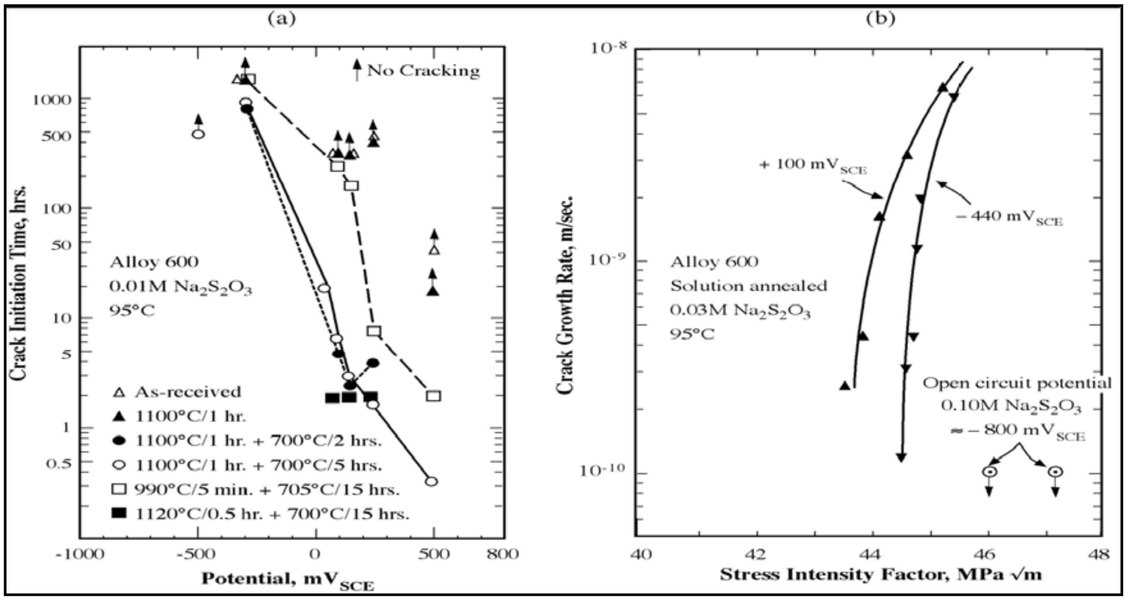

Figure 2.8 (a) Crack initiation time vs. potential for Alloy 600 in both annealed and annealed plus sensitized heat treatments exposed to 0.01 M $Na_2S_2O_3$ at 95°C. (b) Crack growth rate vs. stress intensity for Alloy 600 solution annealed and exposed to $Na_2S_2O_3$ at various potentials and 95°C[44].

2.3.1.4 Alloy composition

Table 2.1 compares the composition of the alloys 600, 690 and 800. Table 2.2 shows that Alloys 800, 690 thermally treated (TT), and 600 mill annealed (MA) are susceptible to S^y-SCC in strong alkaline solutions. Alloys 600 MA and 800 are susceptible in near-neutral conditions, but alloy 690 was not affected in near neutral conditions. This conclusion was drawn from the results in 10% NaOH and 10% NaOH + 0.1M CuO as indicated in Table 2.2. This pattern indicates that the effect of reduced sulphur is broadly significant for alloys used for SG tubes. Such effects of S^y-SCC are known for SSs and low-alloy steels from extensive work in the petroleum and oil industries [44].

Table 2.1 Chemical composition of alloys 600, 690 and 800 in wt [%] [42].

Element	Alloy 600	Alloy 690	Alloy 800
C	0.69	0.018	0.02
Ni	Bal. (~74.24*)	59.85	33.9
Cr	14.97	30.03	21.8
Fe	8.26	9.20	Bal. (~42.26*)
Cu	0.22	< 0.01	–
Co	0.04	0.003	0.019
Ti	0.29	0.20	0.55
Al	0.27	0.36	0.26
Mn	0.26	0.20	0.62
Mo	0.51	–	–
Si	0.24	0.14	0.55
P	0.009	0.004	0.007
S	5 ppm	< 0.001	0.004
B	0.004	0.002	–
Pb	< 1 pm	–	–
Zn	< 0.01 ppm	–	–
Se	< 1 ppm	–	–
Bi	< 1 ppm	–	–
N	–	0.01	0.015

Table 2.2 Results from visual examination of specimens exposed(A) to alkaline solutions at 350°C with added species (Cracked samples/tested samples) [44].

Material	10% NaOH	10% NaOH + 0.1 M CuO	10% NaOH + 0.1 M PbO	50% NaOH + 5% $Na_2S_2O_3$	0.75% M Na_2SO_4 + 0.25% M $FeSO_4$	0.75% M Na_2SO_4 + 0.25% M $FeSO_4$
Alloy 800 7-73243	3/3	3/3	4/4	4/4	4/4	0/4 (3/4)(B)
Alloy 800SP 81373	15/15	15/15	15/15	15/15	15/15	11/15 (15/15)(B)
Alloy 690TT WF816T	0/15	0/15	15/15	14/14	0/15	1/15
Alloy 690TT 764408	0/15	0/15	15/15	15/15	0/15	0/15
Alloy 600MA 1450	8/9	0/9 (2/9)(B)	0/9 (3/9)(B)	2/9	6/9 (8/9)(B)	9/9

(A) 500-h exposure; C-ring specimens; 2% strain.
(B) visual examination after bending the sample.

2.3.1.5 Alloy microstructure

There was little information available on the effect of change in alloy microstructure on S^y-SCC. Figure 2.8 (a) shows the accelerating effect of sensitization on S^y-SCC. The MA material sustains no SCC in thiosulfates at low temperatures and Alloy 600TT may be susceptible to SCC in thiosulfates at low temperatures [44].

2.3.1.6 Temperature

The susceptibility to S^y-SCC was found to increase with increase in temperature.

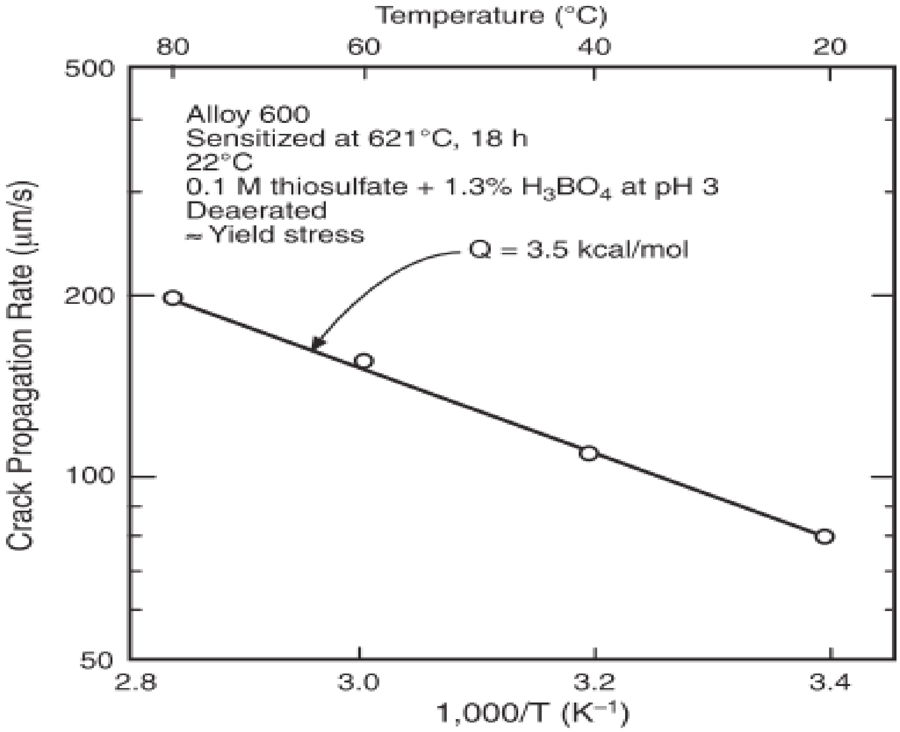

Figure 2.9 Crack propagation rate vs. 1000/T for sensitized Alloy 600 [44].

The above figure shows that the activation energy for SCC of sensitized Alloy 600 is low and most likely related to chemical or liquid phase processes [44]. The crack propogation rate of Alloy 600 increased with increase in the temperature of the test solution containing 0.1 M thiosulfate.

2.3.1.7 Stress

Figure 2.8 (b) shows that the crack propagation rate of solution-annealed Alloy 600 increases rapidly with stress intensity according to period I behavior. This rate decreases with decreasing potential and is negligible at the deaerated corrosion potential. The higher rates are likely related to the film breakdown conditions based on the values of the applied potentials [44].

2.4 Passivity of metals

Passive films play an important role in the corrosion resistance of any metal and more importantly of SG alloys. Most commercially available corrosion resistant alloys depend on passive films for their resistance. Faraday's experiment in the1840s helped to understand the phenomenon of passivity. In the presence of concentrated " fuming" nitric acid, iron is virtually inert, despite the highly oxidizing conditions of the solution. When the acid is diluted with water, the iron remains inert initially but when the surface is lightly scratched it corrodes vigourously, evolving brown, nitrous oxide gas. Faraday suggested that an invisible surface oxide film, preformed in the concentrated nitric acid, is unstable in the diluted solution and is destroyed when mechanically disturbed by scratching.

Passivity of metals can be classified into two types.

1. When there is a large thermodynamic driving force for oxidation the metal is passive and it substantially resists corrosion in an environment. This is also known as thick film passivity.
2. A metal is passive if the rate of dissolution decreases , on increasing its potential to more positive values, and also exhibits low rates at higher potentials. This is also known as thin film passivity.

Evans diagram for materials which have the tendency to type 1 passive film is shown in **Figure 2.10** (a). Evans diagram for materials which form the type 2 passive film is shown in **Figure 2.10** (b). The mechanism of passivity can be explained in terms of mixed potential theory. At corrosion potential (E_{corr}), the metal corrodes uniformly and the metal is free of passive film. As the potential increases in the noble direction, dissolution of metal increases until the potential reaches passivation potential (E_{pp}). The current corresponding to E_{pp} is called the critical current density (I_{crit}). Above E_{pp}, the potential is called passive potential. The current density decreases from critical current density and is called passive current density. The dissolution rate of the material is decreased significantly in the passive range, and materials are designed to operate at passive potential dissolution rate. When the potential of the material increases above the passive potential, transpassive dissolution of the material will occur with evolution of oxygen in most of the metals.

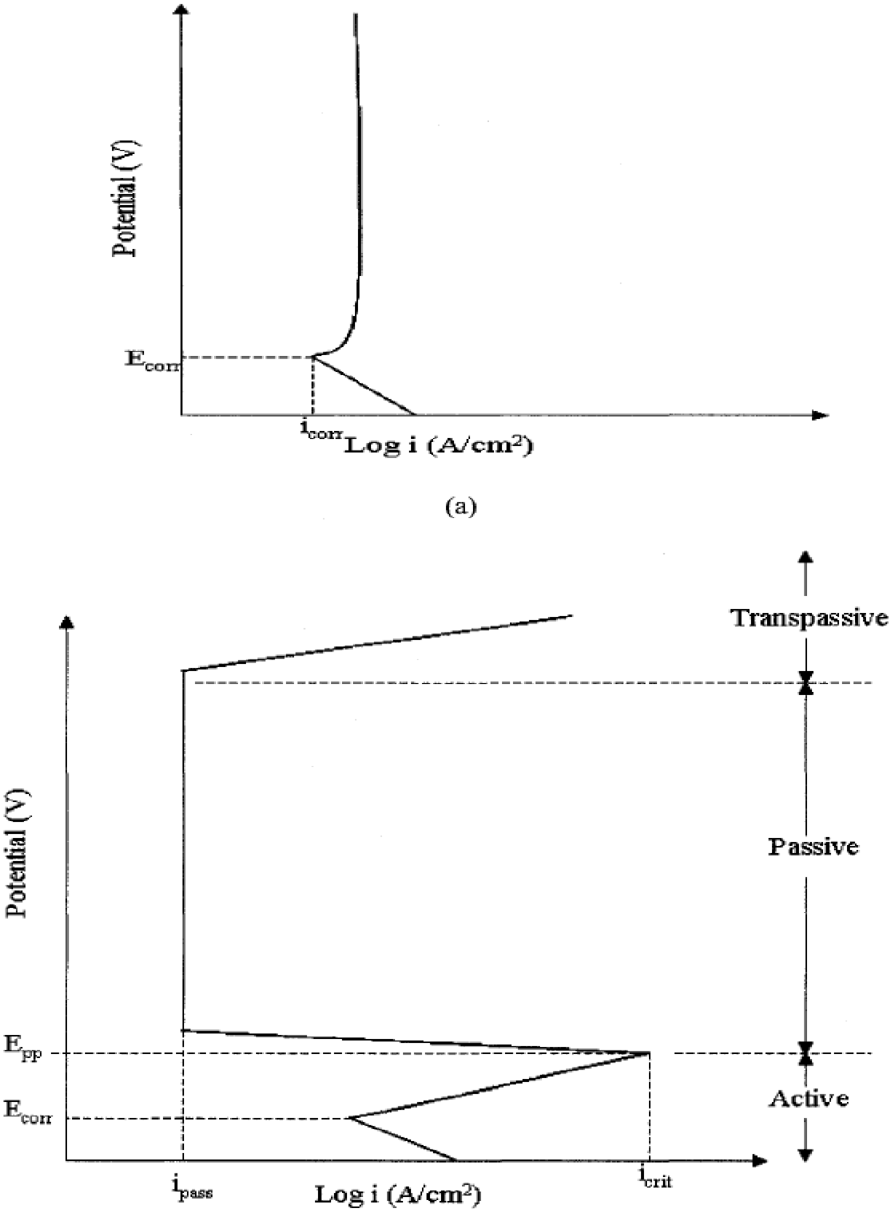

Figure 2.10 Schematic of Evans diagram of passivation. (a) Thick film passivation (b) Thin film passivation [51].

Passive film grows by interaction between the metal atoms and the solution. It was found that passive films formed on Ni-Cr alloys are comprised of two layers, an inner layer which mostly consists of metal oxide and an outer layer consisting metal hydroxides. The outer layer of Ni-Cr alloys consists of chromium and nickel hydroxides while the inner layer consists of chromium and nickel oxides.

The composition of passive film mainly depends on the electrochemical behavior of the base metal. Different mechanisms have been postulated to explain the passive film growth. The relevant mechanism necessary for this research work is described in detail below.

A point defect model was proposed by Chao et al.,. (1981) and later reviewed by Macdonald [52]. PDM was based on the following experimental data

1. The passive film is bilayer in structure, with an inner layer comprising a highly defective barrier layer which is semiconductive in nature.
2. Growth of the barrier layer varies linearly with the logarithm of the steady state current when there is no change in oxidation state of the cation in the passive range.
3. The electric field within the passive film is independent of the applied voltage.

A schematic diagram of passive film growth and dissolution of PDM is shown in Figure 2.11, where m = metal atom, M_M = metal cation in cation site, O_o = oxygen ion in anion site,
$V^{\chi'}_{M}$ = cation vacancy, V_m = vacancy in metal phase, $V_{0=}$ anion vacancy

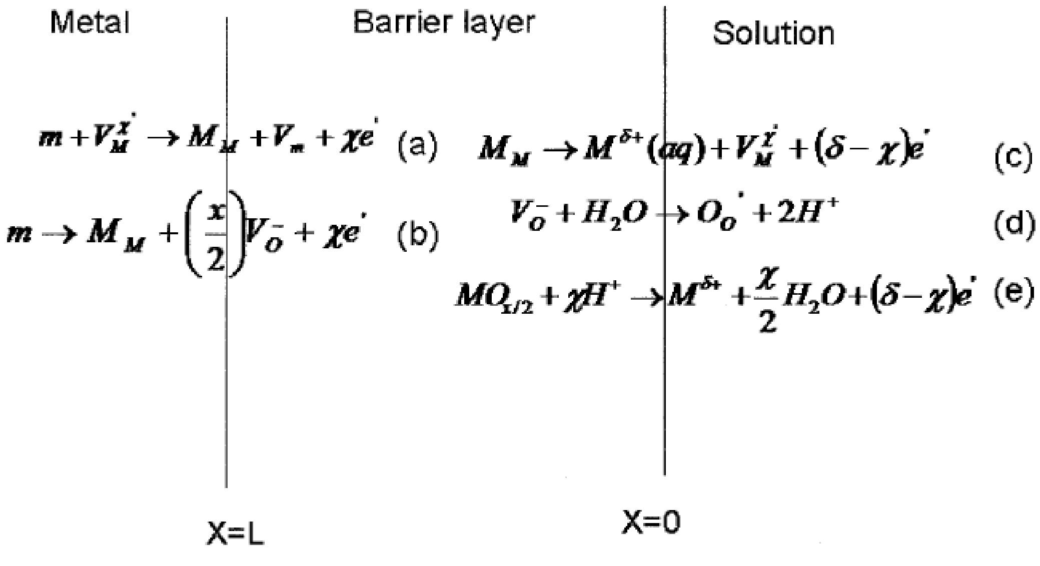

Figure 2.11 Schematic of physio - chemical processes that occur within a passive film according to point defect model [52].

During passive film growth, a metal cation vacancy produced at the film/solution interface moves toward the metal/film interface, whereas an oxygen anion produced at the metal/film interface moves toward the film/solution interface leading to the formation of the passive film.

The reactions a, c, and d are lattice conservatory and do not have any impact on the passive film growth while reactions b and e are responsible for the passive film growth.

2.5 Potential drop technique

Potential drop techniques can be used to measure growth of a flaw or a crack in any conductive material. This technique involves connecting the specimen to a circuit such that a constant current is flowing through it, and measuring the potential change in the specimen during the crack propagation process. As the crack grows it would change the geometry of the specimen and so the resistance of the specimen would change accordingly. Consequently, the change in potential can be correlated to crack growth.

Potential drop techniques can involve either alternating or direct currents. If a direct current is injected into the material, then the technique is known as a direct current potential drop/difference (DCPD) technique. If an alternating current is used, then it is known as alternating current potential drop/difference (ACPD) technique.

The actual individual application technique depends upon the sensitivity of the crack measurements, the nature of the specimen, the deflection conditions and the experimental environment. The DCPD has been used by many researchers, when attempting to investigate crack propagation. It was reported by McKeighan and Smith that the first successful use of the potential drop method for crack length determination was achieved by Barnett and Troiano, who investigated the effect of hydrogen embrittlement in notched tension specimens of steel [53, 54].

Necar Merah also used DCPD to monitor crack growth under high gross inelastic deformation (plastic and creep) conditions. They proposed a correction of the measured length at high temperatures, based on the analysis of DCPD-NOD (notch opening displacement) [55].

The DCPD technique is applied by inputting a direct current into a specimen, and measuring the potential difference across the crack. The current goes through the body of the specimen as opposed to the surface skin as in the case of an alternating current. At a constant current, the voltage value becomes a function of the resistance of the specimen indicating the crack growth behavior. At certain temperatures, the major factors affecting DCPD measurements are the cross-sectional area of the direct current path, the length of the path, and the resistivity of the material. Large currents are usually injected across the entire body of materials in the DCPD technique, causing specimen heating and thereby altering specimen physical properties. In addition, large currents can decrease the safety of the working environment. One technique to avoid the increase in temperature related to the use of large currents is the use of thermally stable connections. Another method is to use the “reversed” DCPD technique. The reversed DCPD method was successfully used by Catlin et al., as early as 1985 [56].

2.5.1 DCPD Calibration

DCPD calibration is very important in determining the relationship of voltage drop to crack depth. It can be done either experimentally, numerically or analytically. For situations where geometry is simple, analytical methods would be the best choice. For complicated geometries, experimental calibration was often used to provide an easier and as well as equally reliable method of determining the relationship between crack depth and voltage difference. In more critical situations, finite element analysis can be used to simulate a situation that is difficult to set up such as unique geometry and extremely high temperature and pressure.

All voltage readings should be normalized regardless of the calibration used. Potential normalization could minimize system error, and remove any specimen related effects [57]. The normalized voltage can be achieved by dividing the voltage difference between measured voltage and reference voltage by the same reference voltage. The reference voltage can be the initial voltage value in the measurement or it can be obtained by measuring the voltage of the non-cracked specimen at the experimental condition.

2.6 Summary

It is very clear that all the SG alloys are susceptible to S^y-SCC. Low valence sulphur assisted passivity degradation is considered to be one of the main reasons for materials to be susceptible to S^y-SCC. There are still many areas in S^y-SCC that are not clearly understood. There is no proper correlation between the low valence sulphur assisted passivity degradation and S^y-SCC. Further there is no proper crack propagation model for S^y-SCC based on the measurement of crack propagation rate to predict the service life. Additionally there is not enough data available for the passivity and SCC behavior of Alloy 800 in test solutions containing thiosulfate and sulphide.

In the first part of this work, effort is concentrated on the relationship between passivity and S^y-SCC of Alloy 800 at room temperature. The second part of this work focuses on the measurement of crack propagation rate of Alloy 800 for S^y-SCC to predict the remaining service life of SG tube.

Chapter 3 Experimental Procedure

3.1 Test material

Commercial Alloy 800(UNS N08800) tube (from Sandvik, Heat #:516809) was used in this study. It had the dimension of 1.14 mm average wall thickness and a 15.88 mm outer diameter (OD). The composition of Alloy 800 used in the experiments was shown in the table below:

Table 3.1 Composition of Alloy 800 in wt %.

Fe	Ni	Cr	Al	Mn	Si	Ti	Cu	S	C	P	Co	Cu	N
43.2	32.7	21.8	.29	.5	.46	.48	.02	.001	0.01	.012	.010	.02	.016

3.2 Solution Composition

The main components of typical crevice solutions in CANDU SG are believed to be Na_2SO_4, NaCl, KCl, $CaCl_2$ and SiO_2. The three solutions used to represent base crevice solutions are listed in Table 3.2.They are designated as NC, BC, and AC[58]. The basic compositions of a simulated crevice solution suggested by AECL are listed in Table 3.2 [46].The solution composition simulates the present crevice condition in CANDU SG tubes. AECL proposed a test matrix based on chemical and thermal stability, for testing the SG tubing materials in a reduced sulphur environment. Thiosulphates are chemically stable only in neutral or alkaline solutions, but not in acidic solutions, due to its decomposition:

$$S_2O_3^{-2}(aq) + 2H^+(aq) \rightarrow SO_2(g) + S(s) + H_2O \qquad \textbf{(3.1)}$$

Table 3.2 Summary of the base crevice chemistries

Simulated Crevice Environments	Compositions
Neutral (NC)	0.15 mol/kg Na_2SO_4 0.30 mol/kg NaCl 0.05 mol/kg KCl 0.15 mol/kg $CaCl_2$ 0.05 mol/kg SiO_2
Basic (BC)	NC + 0.40 mol/kg NaOH
Acidic (AC)	NC + 0.05 mol/kg $NaHSO_4$

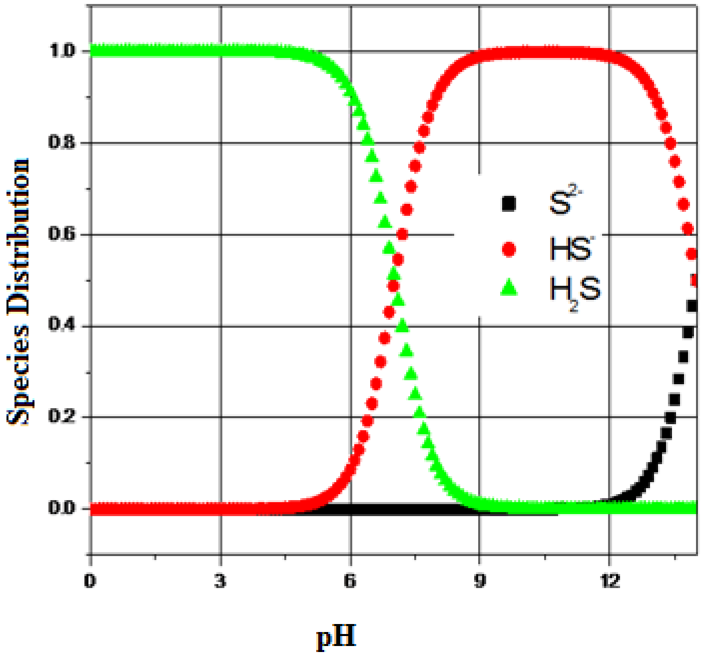

Figure 3.1 Chemical stability of sulphide at various pH values.

The chemical stability of sulphide is shown in the Figure 3.1. In the pH range discussed H_2S can be stable in the pH range of 0-4.5, HS^- is stable in the pH range of 9-12. In this work, the test solution was kept at pH 12 and therefore the major species present in the test solution should be HS^-.

Table 3.3 Simulated SG crevice solution compositions.

Environments	Test ID	Chemical Compositions	
		Base Compositions	**Sulphur additives**
pH = 6.33	NC-1	0.30 mol/kg NaCl 0.05 mol/kg KCl 0.15 mol/kg$CaCl_2$ 0.05 mol/kg SiO_2	
pH = 6.33	NC-2-1		0.075 mol/kg $Na_2S_2O_3$
pH = 6.33	NC-2-2		0.01 mol/kg $Na_2S_2O_3$ + 0.13 mol/kg Na_2SO_4
pH = 6.33	NC-2-3		0.001 mol/kg $Na_2S_2O_3$ + 0.148 mol/kg Na_2SO_4
pH = 12	NC-3-1		0.075 mol/kg Na_2S + 0.075 mol/kg Na_2SO_4
pH = 12	NC-3-2		0.01 mol/kg Na_2S + 0.14 mol/kg Na_2SO_4
pH = 12	NC-3-3		0.01 mol/kg Na_2S + 0.149 mol/kg Na_2SO_4
Concentration of S and Cl was maintained constant at 0.15 mol/kg in all test solutions			

Table 3.3 shows the compositions of various test solutions used in this study. The base composition is the same for all the test solutions. The concentration of chloride is maintained constant as 0.15 mol/kg in all the test solutions. The concentrations of sulphur additives (thiosulfate & sulphide) were changed from 0 mol/Kg to 0.075 mol/Kg to study the effect of change in concentration. In all the test solutions, the concentration of sulphur is maintained constant at 0.15 mol/Kg by the addition of sodium sulphate.

3.3 Sample Preparation

3.3.1 NACE C-ring Specimen

The effect of stress on S^y-SCC is investigated using a C-ring specimen. The C-ring is a versatile, economical specimen for quantitatively determining the susceptibility to SCC of all types of alloys in a wide variety of product forms. The stress of principal interest in the C-ring specimen is circumferential stress. The stress is not uniform. First there is a gradient through the thickness, varying from a maximum tension on one surface to a maximum compression on the opposite surface. Secondly, the stress varies around the circumference of the C-ring from zero at each bolt hole to a maximum at the arc opposite the stressing bolt. Thirdly the circumferential stress varies across the width of the C-ring specimen, the extent of variation depending on the width to thickness and diameter to thickness ratios of the C-ring specimens.

In the case of the notched C-ring specimen, a triaxial stress state is present adjacent to the root of the notch. In addition the circumferential stress at the root of the notch is expected to be in the plastic range. C-ring specimens were made from Alloy 800 steam generator tube according to the NACE standard TM0177-2005[59], as shown in Figure 3.2. The deflection of 0.356 mm was applied on all the stressed C-ring specimen using nylon screw and nut to avoid galvanic corrosion. Since this amount of deflection caused the plastic deformation, quantitative analysis was not valid. All the C-ring specimens used in this work have the same dimensions. Therefore, by maintaining the deflection value constant for all the stressed specimens, the effect of stress on S^y-SCC and corrosion behaviour will be studied by comparing the materials behaviour of the specimens with and without stress. The C-ring specimen was ground with 1200 grit silicon carbide paper. A notch of approximately 0.15 mm was made, then cleaned ultrasonically in distilled water and dried in air. These types of samples were used in potentiostatic tests, potential drop tests and cyclic polarization tests to study the effect of stress on material behaviour.

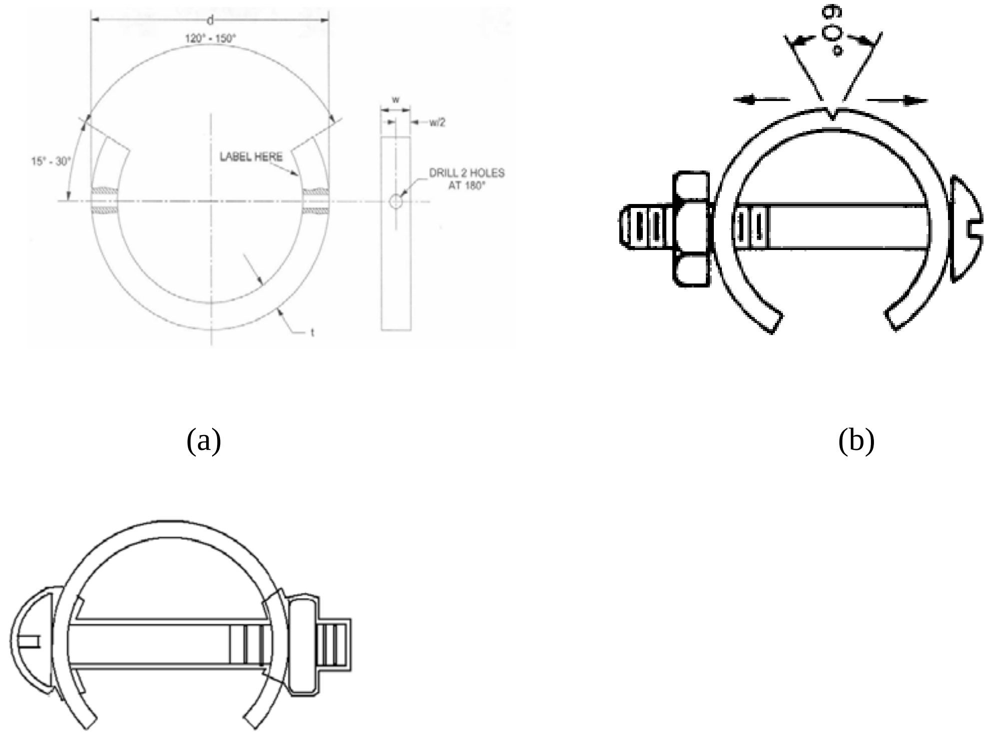

(a) (b)

(c)

Figure 3.2 Schematic representation of C-ring specimen (a) dimensions (b) C-ring specimen with notch (c) C-ring specimen without notch.

3.3.2 Specimen without deflection

The samples without deflection were cut from a long tube into 2 cm X 0.5 cm approximate dimensions, connected with copper wire and it was mounted in epoxy using resin and hardener with a ratio of 5:1 and cured for 12 hours at room temperature. The surface of the specimen was ground with SiC paper in the sequence of 240,320,400,600,800, and 1200 grit. Then cleaned ultrasonically in distilled water and dried in air. These types of specimens were used in Cyclic polarization and Mott-Schottky tests.

3.4 Experimental Procedure

3.4.1 Cyclic Polarization

It is one of the types of electrochemical experiments. All the electrochemical experiments were carried out with a three electrode cell. The Alloy 800 sample mounted on epoxy was used as the working electrode (WE). A saturated calomel electrode (SCE) was used as the reference electrode (RE). A platinum wire with platinum mesh was used as the counter electrode (CE). The potential was applied between the reference electrode and the working electrode and the current was measured between the working electrode and the counter electrode. The scan rate was 1.0 mV/s. The instrument used for this measurement was the Gamry electrochemical measurement system.

Electrochemical polarization experiments can be used to determine the corrosion susceptibility of SG tubing since the potentiodynamic polarization curve provides information on the corrosion rate as a function of ECP under a specific environment. The objective of cyclic polarization test is to determine the acceptable ECP/pH zones. The polarization curve is an experimentally determined potential vs. current density diagram. A metal or alloy will develop a potential difference across its interface spontaneously, and it is called open circuit potential (E_{oc}). It represents the potential at which the rates of anodic and cathodic reactions on the surface balance.

The polarization curves can represent the effect of potential on the electrochemical kinetics, such as open circuit potential, passive potential range, primary passivation potential (E_{pp}), pitting potential (E_p), repassivation potential (E_{repass}) and transpassive potential (E_t), as shown in Figure 2.10 (b).

In most cases, linear increase of the potential of the interface from E_{oc} results in an exponential increase in the current density. By plotting the potential-current data on semi logarithmic axes, such behavior appears as a straight line designated as the “active region” in the figure. The measured current density continues to increase to a maximum, I_{crit}, at E_{pp} (called the primary passivation potential) and then begins to decrease. This decrease in current density happens at the “active-passive transition”, meaning that dissolution of the metal has gone from a state of active dissolution to passive dissolution due to the formation of the passive film.

The current density starts to drop at E_{pp}, and remains at low values, I_{pass} (the passive current density), for a certain range (the “passive potential range”). The potential at the point, from which current density increases again, is called transpassive potential (E_t).

However, for example in acidified Cl^- solutions, the current density increase is observed at lower potential, and is accompanied by the formation of corrosion pits on the metal surface. That is why we call this potential a pitting potential (E_p). The definition of pitting potential was illustrated schematically in Figure 3.3.The polarization behavior of different materials is strongly dependent upon the electrolyte and alloy composition.

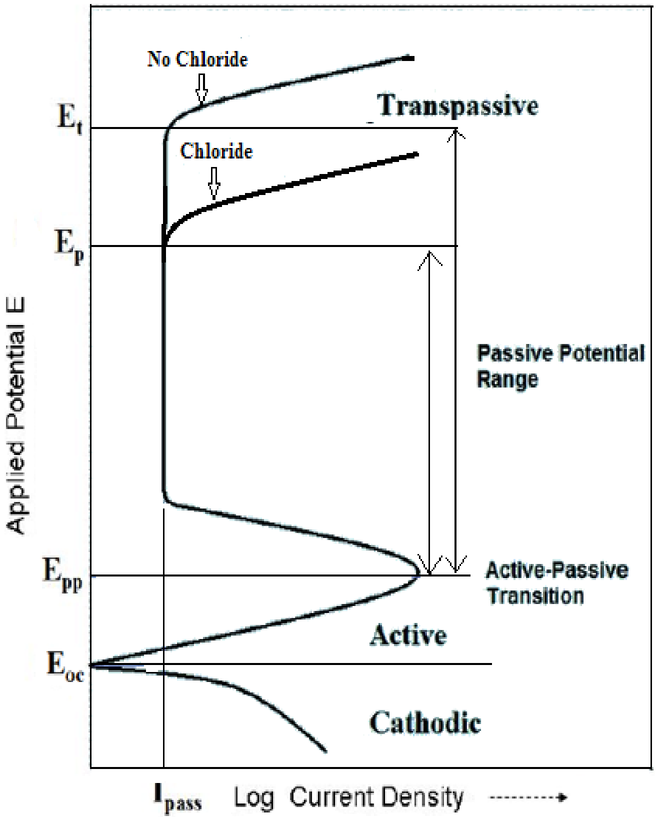

Figure 3.3 Schematic polarization curve showing the effect of chloride ion on the pitting potential.

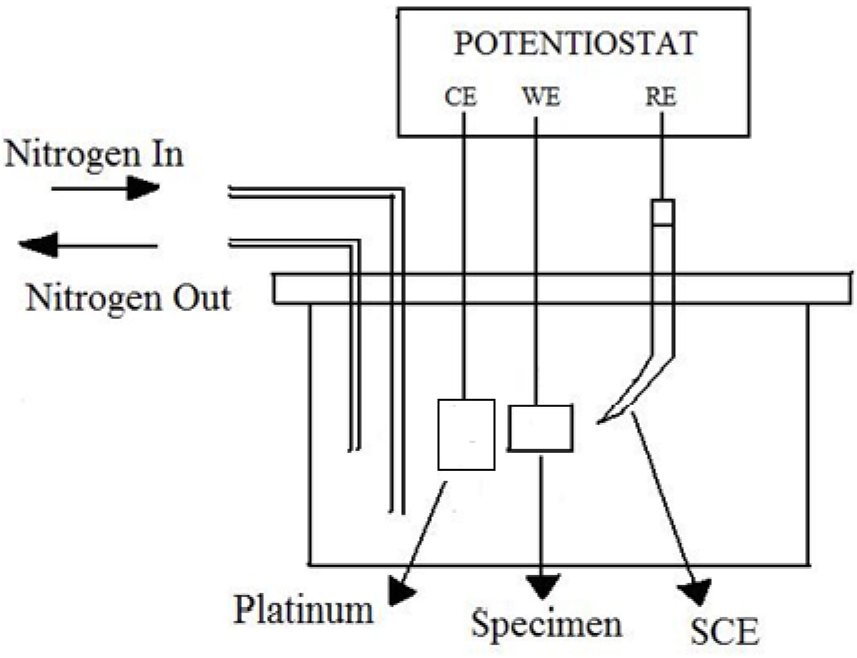

Figure 3.4 Schematic diagram of electrochemical cell setup.

3.4.2 Potentiostatic Test

The main objective of potentiostatic test was to study the susceptibility of Alloy 800 to SCC under fixed applied potential. A three electrode electrochemical cell was used to do this test. Alloy 800 C-ring specimen prepared according to NACE standard [59] was used as WE as explained in the Section 3.3.1.A glue was applied between the screw and the C-ring to reduce crevice corrosion. Further the glue was applied on the inside surface of the C-ring specimen to make sure that only the outer surface of the C-ring was exposed to the corrosive environment.

The potentials were chosen in the following potential regions on the cyclic polarization curve:

- Active - passive region.
- Passive region.
- Transpassive region.

The constant applied potential was maintained and the change in current value was measured using a GAMRY electrochemical measurement system. It was known that when SCC occurs under constant applied potential, value of the measured current will increase.

3.4.3 Mott-Schottky Test

Mott-Schottky plots were determined for various test conditions with a Gamry EIS measurement system. The main objective of this test method is to analyze the semiconductive properties of the passive film formed on Alloy 800. Capacitance measurements were performed at fixed frequency of 1000 Hz. The potential was scanned in the anodic direction of the passive range at 5mV per step. The passive range was determined from cyclic polarization test. AC impedances were measured as a function of the potential. The capacitance values were calculated from the imaginary part of impedance, assuming an equivalent circuit with resistance and capacitance in series. The impedance of the space charge layer is much smaller than that of the charge transfer resistance of the passive film at 1000 Hz.

The relationship between the differential capacitance and the potential drop in the semiconductor can be written in the following Mott-Schottky equation:

$$C^{-2} = \frac{2}{\varepsilon\varepsilon_o q N_q}\left(U - U_{fb} - \frac{kT}{e}\right) \qquad \textbf{(3.2)}$$

where q is the elementary charge (negative for electrons and positive for holes). ε the dielectric constant. ε_0 the permittivity in vacuum, N_q the acceptor or donor concentration, U the applied potential, U_{fb} is the flat band potential.

The linear region in the plot of C^{-2} vs. U is determined. The intercept of this linear region with the potential axis allows the determination of the flat band potential and the slope of the linear region yields the donor density. The higher value of donor density indicates a defective passive film structure, which in turn increases the susceptibility to SCC. The specimens without deflection as explained in the Section 3.3.2, was used in this test.

3.4.4 Potential Drop Test

A C-ring specimen with a notch of 0.15mm depth made according to NACE standard [59] as explained in the Section 3.3.1, was used in this test. A deflection of 0.356 mm was applied. Alloy 800 wires were used as potential and current leads to avoid errors in the measured signal due to bi-metallic corrosion.

Four different Alloy 800 wires were spot welded to the notched C-ring samples so that the potential drop system can be used to monitor the crack length changes during the tests, which is schematically shown in the Figure 3.5 Two wires were spot welded to the sides of the sample as current wires C & D. The other two wires (signal wires) A & B were spot welded on either side of the specimen’s notch across the width of the specimen.

Crack growth measurement was done using potential drop method. The wires on the sides of the sample C & D were connected to the current supplier device which supplied the constant current of 6A. The signal wires on the sides of the notch A & B were connected to the signal reader device. The limiting value of voltage was set as 6V. As the cracking occurs at the notch, the resistivity of the sample increases and the potential measured using signal wires A & B will increasee. This change in the measured potential value due to crack growth can be converted into the crack propagation rate.

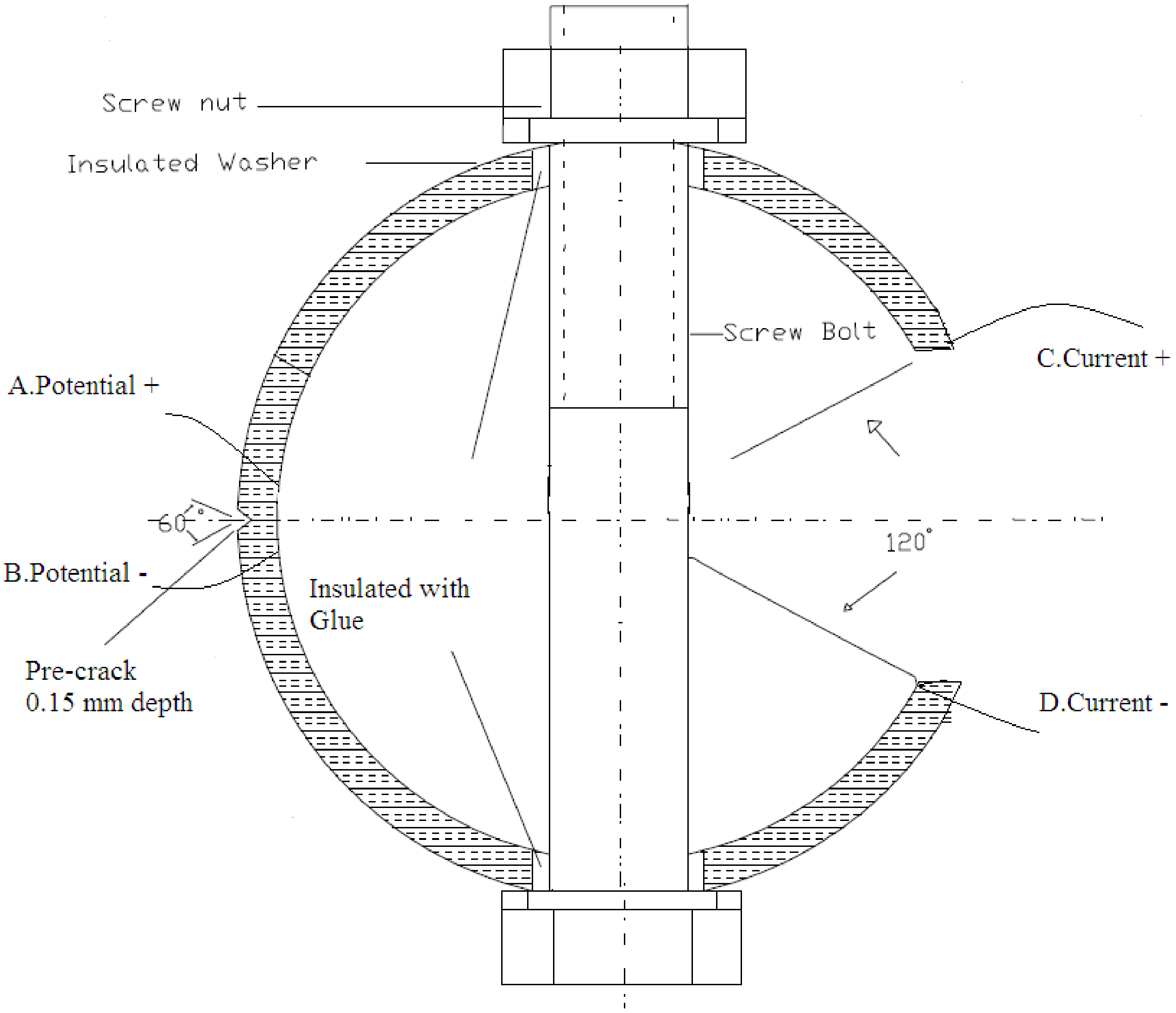

Figure 3.5 The illustration of voltage measurement and DC current flowing through the Alloy 800 C-ring specimen.

3.4.5 Immersion Test

The C-ring specimens with stress and a notch were exposed to the test solution in an airtight cell. The test solution was nitrogen purged and the test cell was completely sealed. The samples were exposed to the test solution for approximately 90 days. The objective of this test was to find out if the increase in the time of exposure to the aggressive test solution makes Alloy 800 susceptible to SCC.

Chapter 4 Results & Discussion

4.1 Cyclic polarization behaviour of Alloy 800

4.1.1 Effect of change in concentration of thiosulfate on the cyclic polarization behaviour

The safe operating conditions of the nuclear plant are estimated using the ECP-pH (electrochemical potential vs. solution pH) diagrams that are preliminarily determined from the polarization behaviour[20]. Therefore its important to run cyclic polarization test to study the polarization behaviour. Figure 4.1 shows the cyclic polarization behaviour of Alloy 800 in the simulated SG crevice solution without and with thiosulfate. The results indicated that there was no significant effect of concentration of thiosulfate on the passive current density. Table 4.1 compares the values of passive current density, corrosion potential (E_{corr}), passive range, repassivation potential ($E_{repassivation}$) in NC-1, NC-2-1, NC-2-2 & NC-2-3 environments. The increase in the concentration of thiosulfate in the test solution decreased the passive potential ranges of Alloy 800, which was indicated in Figure 4.1. Figure 4.2 shows E_{pit} vs. concentration of thiosulfate. It is obvious that increase in the concentration of thiosulfate in the test solution decreased the pitting potential. However it’s difficult to explain the value of pitting potential at 0 mol/kg of thiosulfate in the test solution. Also significant difference in E_{pit}, $E_{repassivation}$ and E_{corr} was found between curves NC-2-1 and NC-1 in Figure 4.1. This implies the strong effect of thiosulfate on the corrosion behaviour of Alloy 800. This result indicate that thiosulfate cause the degradation of oxide film on Alloy 800. A similar effect of thiosulfate on the pitting potential of 316 SS in 3.5% NaCl solution was reported. Additionally similar behaviour was reported for 310 SS in ammonium chloride solution with sodium thiosulfate addition. They observed that the presence of sodium thiosulfate enhanced pitting corrosion as indicated by the decrease in pitting potential[62].

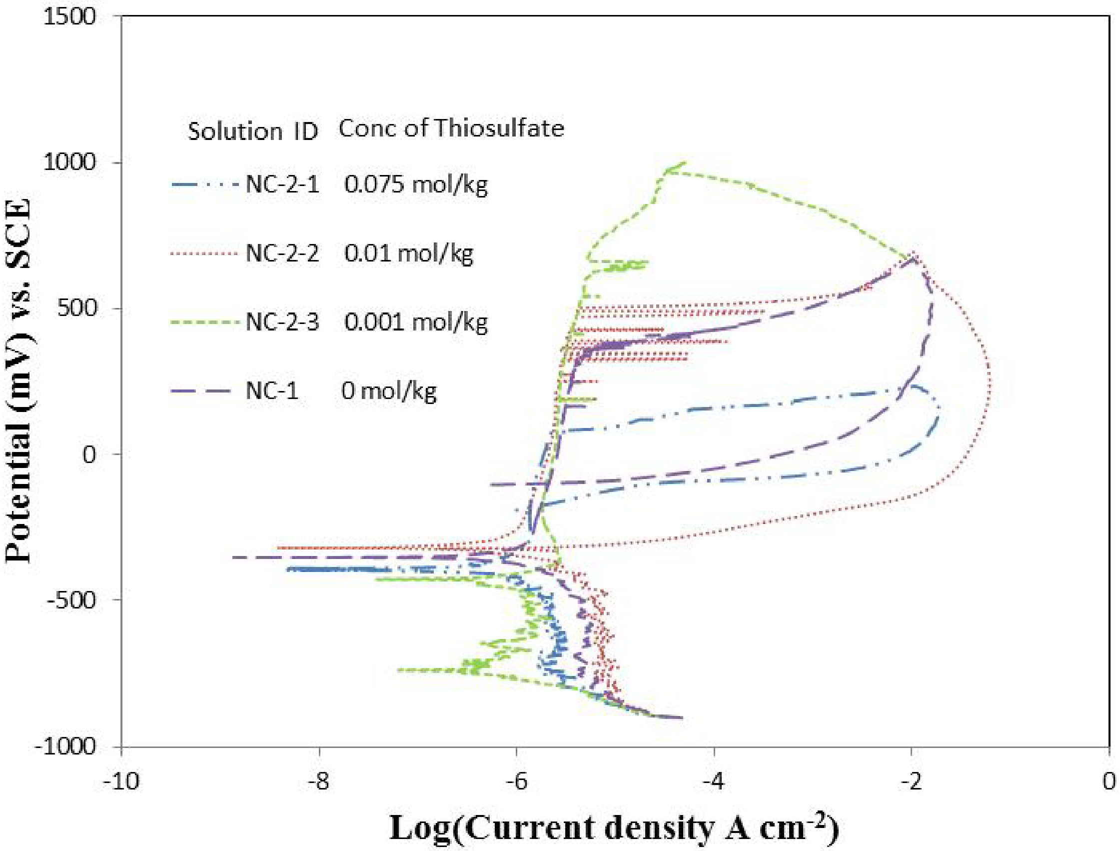

Figure 4.1 Cyclic polarization curves of Alloy 800 samples without deflection in NC-1, NC-2-1, NC-2-2, NC-2-3 environments.

Table 4.1 Corrosion potentials, passive current density, passive range, repassivation potentials obtained on the cyclic polarization curves in Figure 4.1.

Test Environment	**Passive Current density (μA cm^{-2})**	**$E_{repassivation}$ (mV)**	**E_{corr}(mV)**	**Passive range(mV)**
NC-2-1	1.5	-202	-392	3 to -268
NC-2-2	2.3	-320	-320	422 to -225
NC-2-3	3		-428	613 to -178
NC-1	2.4	-122	-352	275 to -263

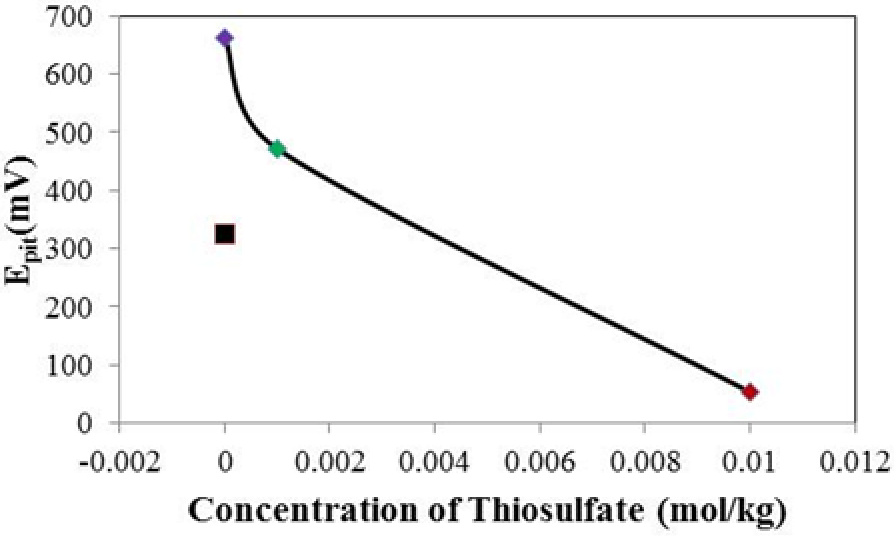

Figure 4.2 Effect of change in concentration of thiosulfate on the pitting potential.

Figure 4.3 compares the SEM morphologies of Alloy 800 samples used for cyclic polarization test in NC-2-1, NC-2-2 and NC-2-3 environments. Figure 4.3 (a) indicated that the density of pits is high in NC-2-1 environment. Figure 4.3 (b) indicated that the probability of pitting is less in NC-2-2 environment, when compared to NC-2-1. Figure 4.3 (c) showed that there was no pitting in NC-2-3 environment. Figure 4.3 (a) show that the material inside the pit got etched away and the surface surrounding the pit was passive. This indicate that the potential inside the pit was much more active than that outside [63]-[64]. Further the interior of the pits was at relatively lower local pH compared to outside [65]. Under these conditions, thiosulfate undergoes decomposition and reduction reaction to produce hydrogen sulphide. The resulting hydrogen sulphide is a well known catalyst for the dissolution of iron [66].

$$\begin{aligned}
&S_2O_3^{-2} + 6H^+ + 4e^- \rightarrow 2S + 3H_2O \\
&S + 2H^+ + 2e^- \rightarrow H_2S \\
&H_2S \rightarrow H^+ + S^{-2} \\
&Fe \rightarrow Fe^{2+} \\
&Fe^{2+} + S^{-2} \rightarrow FeS
\end{aligned} \qquad \textbf{(4.1)}$$

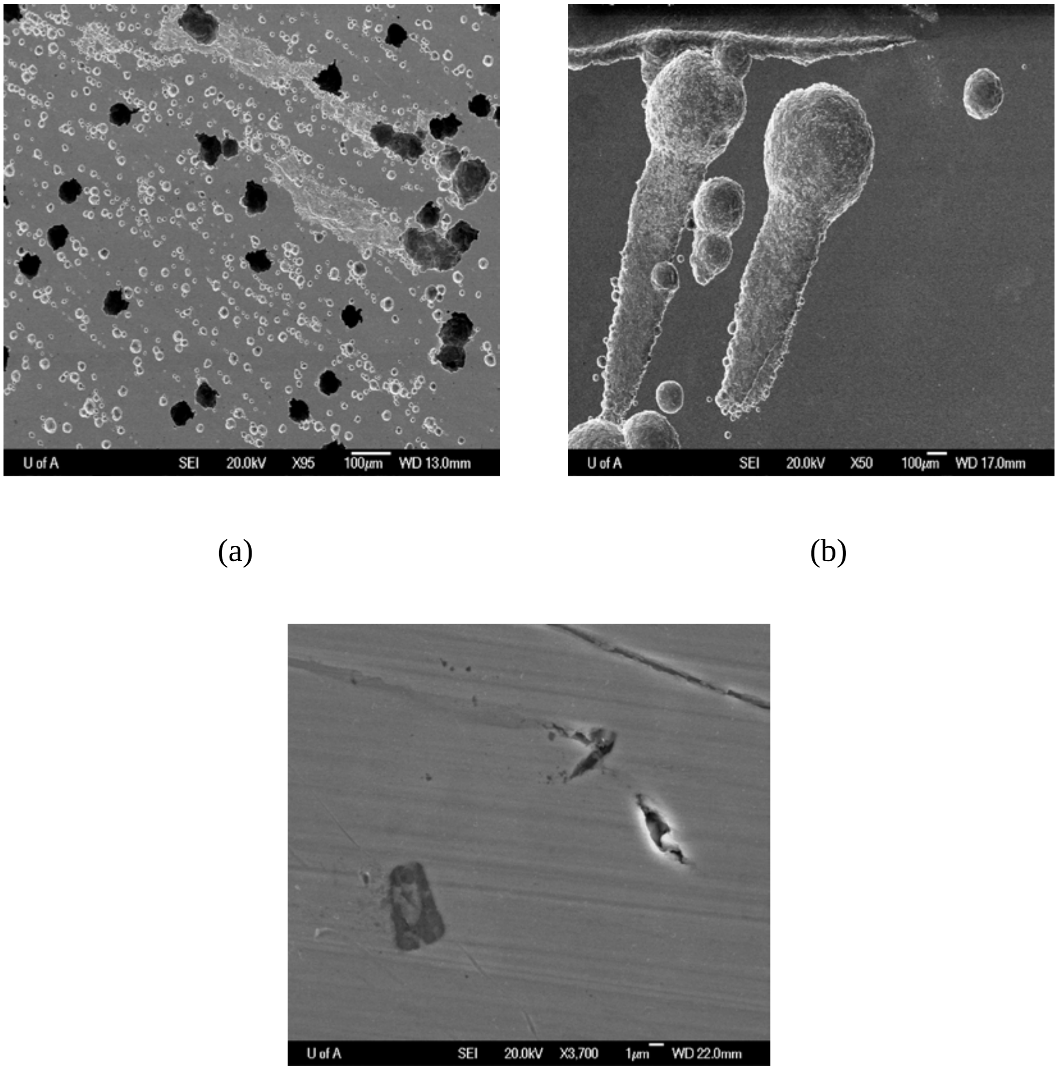

(a) (b)

(c)

Figure 4.3 SEM morphologies of Alloy 800 samples without deflection after the cyclic polarization tests in (a) NC-2-1, (b) NC-2-2, (c) NC-2-3 environments.

It should be noted that during cyclic polarization scan the potential was scanned from the negative to positive direction. Therefore during cyclic polarization scan the potential influenced the type of reaction that occurred on the surface of Alloy 800. It can be argued that the increase in the potential towards the positive direction favoured the reduction reaction of thiosulfate . Further from the SEM pictures in Figure 4.3 it can be seen, thiosulfate caused localized attack on the surface of Alloy 800. This further implies that the reduction reaction of thiosulfate is favourable to occur with increase in the potential towards positive value.

However it should be noted from the SEM picture in Figure 4.3 that thiosulfate attacked selective points on the surface of Alloy 800 while the potential is scanned towards positive direction.

This is probably due to the fact that there should be weak points on the oxide film on Alloy 800 surface, which eventually became favourite spot for thiosulfate to cause a localized attack. This reduction reaction of thiosulfate to sulphide during localized attack, eventually degrades the oxide film on Alloy 800 and increases its susceptibility to corrosion. Therefore the applied potential and the nature of the oxide film on Alloy 800 surface plays a significant role in the degradation of Alloy 800 in the test solution containing thiosulfate. The role of applied potential in the degradation of Alloy 800 in the test solution containing thiosulfate is discussed in detail in the section 4.2.

Additionally, it should be noted that for the pitting to occur due to the localized attack by thiosulfate , the dissolution reaction promoted by the reduction reaction of thiosulfate should occur at a faster rate than the repassivation reaction to form oxide film. This eventually leads one to further investigate the competition between the reduction reaction of thiosulfate and the oxidation reaction of metallic elements (Fe, Cr, Ni) present in Alloy 800 to determine the corrosion behaviour of Alloy 800. The stability of hydroxides formed by various metallic cations can be evaluated using the solubility product pK defined by [67].

$$pK = -\log \frac{\left[M^{m+}\right]\left[OH^{-}\right]^{m}}{\left[M(OH)_{m}\right]} \qquad \textbf{(4.2)}$$

A larger pK value indicates the low stability of hydroxides. Based on this idea, the readiness of dehydration of hydroxides can be evaluated. This will indirectly aid to do the comparison between the dehydration of metal hydorxides to form oxide film and reduction reaction of thiosulfate to form sulphide film. This phenomenon can be investigated based on the solubility product constant of the probable metal sulphide products of reduction reaction and metal hydroxides that can occur electrochemically on the surface of Alloy 800.

Table 4.2 K_{sp} values for probable products of reactions that can occur on Alloy 800 [68].

Reaction product	Solubility Product Constant (K_{sp})	pK
FeS	6×10^{-19}	18.2
$Fe(OH)_2$	8.0×10^{-16}	15
NiS	3×10^{-19}	18.5
$Ni(OH)_2$	2.0×10^{-15}	14.7
$Cr(OH)_2$	2.0×10^{-16}	15.7

Table 4.2 shows the K_{sp} values of probable products metal sulphide and metal hydroxides likely to occur on the surface of Alloy 800. The information about the K_{sp} values of oxides of iron, chromium and nickel is not available in the literature. However, it should be noted that the dehydration of metal hydroxides lead to the formation of metal oxide. Therefore, it is reasonable to compare the K_{sp} value of metal hydroxides with metal sulphides to explain the competition between reduction and oxidation reactions occurring on the surface of Alloy 800. The pK values of FeS and NiS is higher than the corresponding hydroxides and chromium hydroxide. Therefore the anodic dissolution reaction caused by metal sulphide formation occurs at a faster rate and prohibits the formation of protective oxide film through the repassivationn reaction caused by dehydration of hydroxides.

Therefore it is probable that the formation of metal sulphide before the formation of metal oxide on the surface of Alloy 800 lead to the degradation of the oxide film on Alloy 800 and increased its susceptibility to corrosion. However its difficult to compare the rate of metal dissolution promoted by the formation of sulphides of Fe, Cr and Ni, which are the major elements present in Alloy 800, due to lack of enough information in the literature. The competition between the reduction reaction of thiosulfate and the oxidation reaction of metallic elements in Alloy 800 is further investigated in Section 4.2

4.1.2 Effect of deflection on the cyclic polarization behaviour

Figure 4.4 compares the cyclic polarization curves for Alloy 800 samples with and without deflection/notch in the solution containing 0.075 mol/kg thiosulfate. Figure 4.4 shows that the presence of deflection shifts the cyclic polarization curve cathodically which is detrimental to the material. Further the passive range is decreased, pitting potential (E_{pit}) and corrosion potential (E_{corr}) shifted in the cathodic direction. There is increase in the passive current density of Alloy 800 due to the presence of deflection. The presence of deflection increases the susceptibility of Alloy 800 for material degradation in the test solution containing thiosulfate. Table 4.2 compares the values of passive current density, corrosion potential (E_{corr}), passive range, repassivation potential (E_{repass}), pitting potential (E_{pit}) obtained from Figure 4.4.

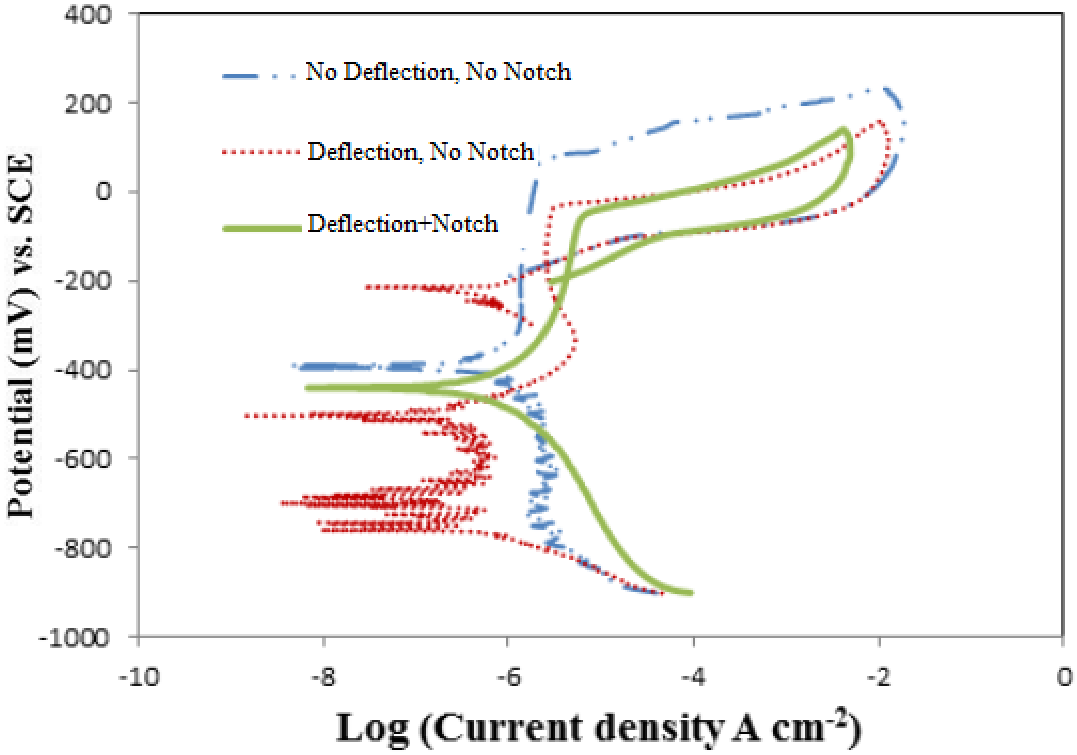

Figure 4.4 Cyclic polarization curves of Alloy 800 samples without deflection and with deflection in NC-2-1.

Table 4.3 Corrosion potentials, passive current density, passive range, repassivation potentials obtained on the cyclic polarization curves in Figure 4.3.

Deflection	Notch	Test Solution	Passive current density (μA cm^{-2})	E_{pit} (mV)	E_{repass} (mV)	E_{corr} (mV)	Passive range(mV)
NO	NO	NC-2-1	1.5	53	-202	-392	3 to -268
Yes	NO	NC-2-1	2.7	-57	-190	-504	-107 to -309
Yes	Yes	NC-2-1	3.6	-71	-209	-440	-121 to -349

4.1.3 Effect of change in concentration of sulphide on the cyclic polarization behaviour

Figure 4.5 compares the cyclic polarization behaviour of Alloy 800 in simulated SG crevice solution with varying concentration of sulphide species. The result indicated that the increase in the concentration of sulphide in the test solution increased the passive current density and decreased the corrosion potential of Alloy 800. This is shown in Figure 4.6. The presence of sulphide in the test solution promoted anodic dissolution reaction and inhibited the formation of stable passive film. A similar behaviour was reported for copper alloys in test solution containing sulphide by syrett et al., [69]. Additionally, Ge et al., reported similar behaviour for 316 stainless steel in simulated cooling water containing sulphide [43].

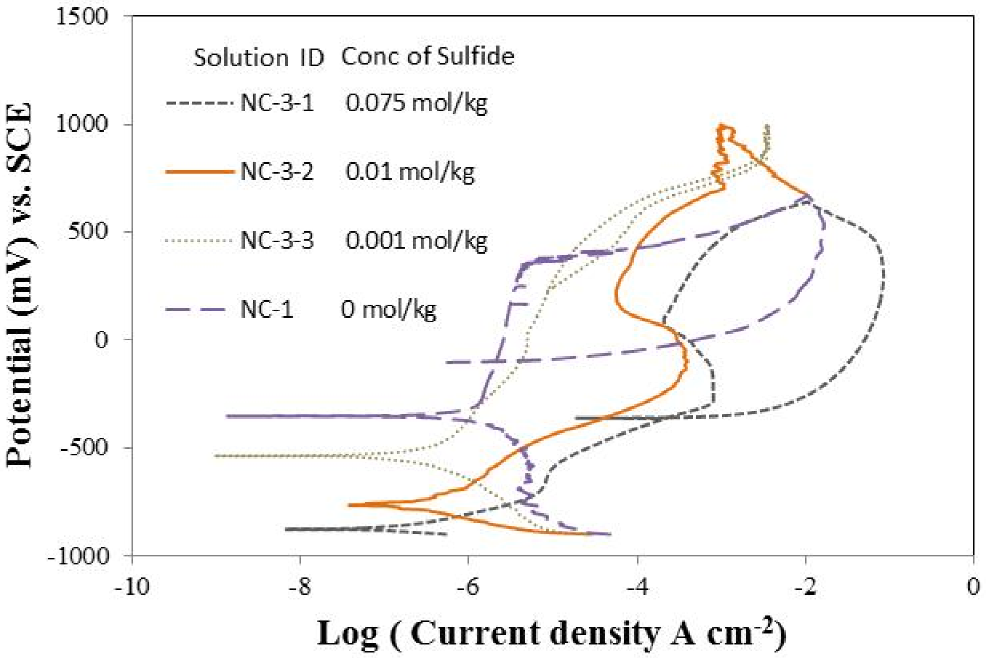

Figure 4.5 Cyclic polarization curves of Alloy 800 samples without deflection in NC-1, NC-3-1, NC-3-2, NC-3-3 environments.

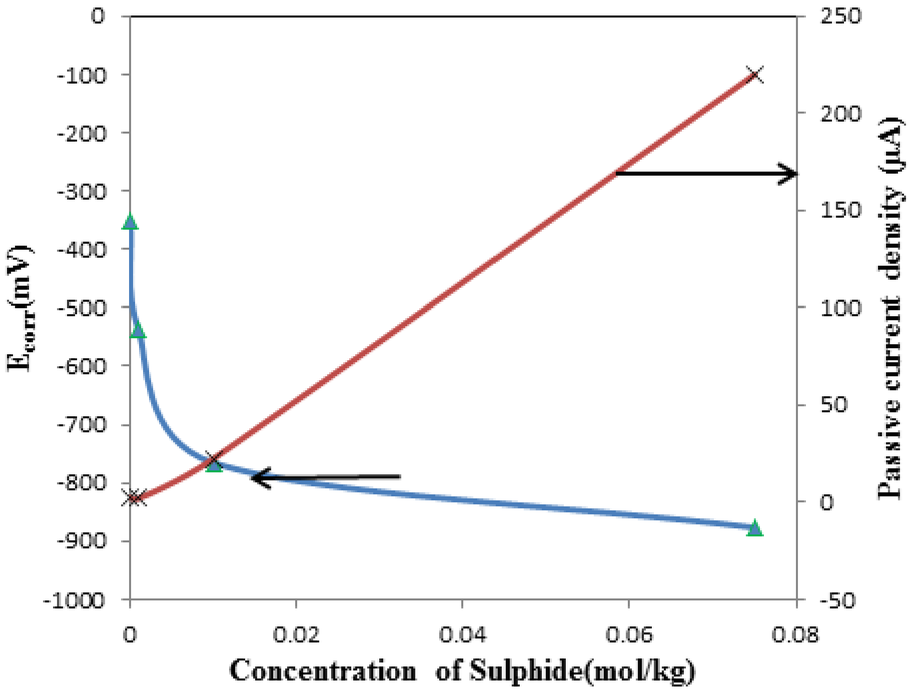

Figure 4.6 Comparison of corrosion potential & passive current density values obtained from Figure 4.5.

In NC-3-3 test solution which contains 0.001 mol/ kg sulphide, the material showed passive behaviour. However in the test solutions NC-3-2, NC-3-1 with 0.01 mol/kg and 0.075 mol/kg sulphide respectively, the material indicated metal dissolution behavior. At potentials more negative than the corrosion potential (E_{corr}), the cyclic polarization curves of 0.001 to 0.075 mol/kg sulphide, have an approximately linear trend, indicating that most probably hydrogen evolution reaction is rate controlling in this region. Additionally the dependence of current density on potential is more pronounced at higher sulphide concentrations (0.01 & 0.075 mol/kg). On the other hand, addition of sulphide of 0.001 mol/kg produced smaller effect on the cyclic polarization curve.

The above phenomenon could be explained by the reactive adsorption of sulphide on the surface which prevents the growth of passivating oxide layer and increases its defectiveness. The other way to explain this phenomenon is that the adsorbed sulphide interacts with cations in the outermost layer of oxide and leads to the formation of sulphur-containing compounds leading to an increase in defect concentration of this film, hence it increased its ionic conductivity and the current density through the oxide. The formation of sulphur containing compounds is explained by the following reactions [70-73].

$$\begin{gathered} M_M^{II} + HS_{ad}^{-} \rightarrow MHS_{ad}^{+} + V_M^{''} \\ MHS_{ad}^{+} \rightarrow MS_{1-x} + xHS^{-} + (1-X)H^{+} \end{gathered} \qquad \textbf{(4.3)}$$

In addition the above reaction leads to local acidification and thus an increase in the dissolution rate of the passivating oxide. Similarly at the highest sulphide concentration, there was evidence for anodic dissolution behaviour for Fe, Ni and AISI 316L[74-77]. It should be noted that during cyclic polarization scan the potential was scanned from the negative to positive direction. Therefore during cyclic polarization scan the potential influenced the type of reaction that occurred on the surface of Alloy 800. It should be noted from Figure 3.1 that the concentration of the species HS^- is high in the test solution at pH 12.

It can be argued that with increase in the potential towards the positive direction the oxidation reaction of HS^- is favoured as explained by the equation 4.2, which promotes anodic dissolution reaction. However, sulphide which is present in small concentration in the test solution can also undergo oxidation to form adsorbed sulphide on the surface of Alloy 800.Figure 4.7 (a), (b) & (c) shows the SEM morphologies of Alloy 800 samples after the cyclic polarization tests in NC-3-1, NC-

3-2, NC-3-3 environments, respectively. Figure 4.7 (a) shows features on the Alloy 800 sample that confirmed material degradation by anodic dissolution reaction more likely due to adsorbed sulphide in NC-3-1 environment. Figure 4.7 (b) shows some features of active dissolution of Alloy 800 in NC-3-2 environment. The material degradation due to anodic dissolution was low compared to NC-3-1 environment. Similar features of metal dissolution were not observed in the Figure 4.7 (c) in NC-3-3 environment. This clearly indicated that the higher concentration of sulphide (0.075 M) in the test solution promoted anodic dissolution reaction of Alloy 800.

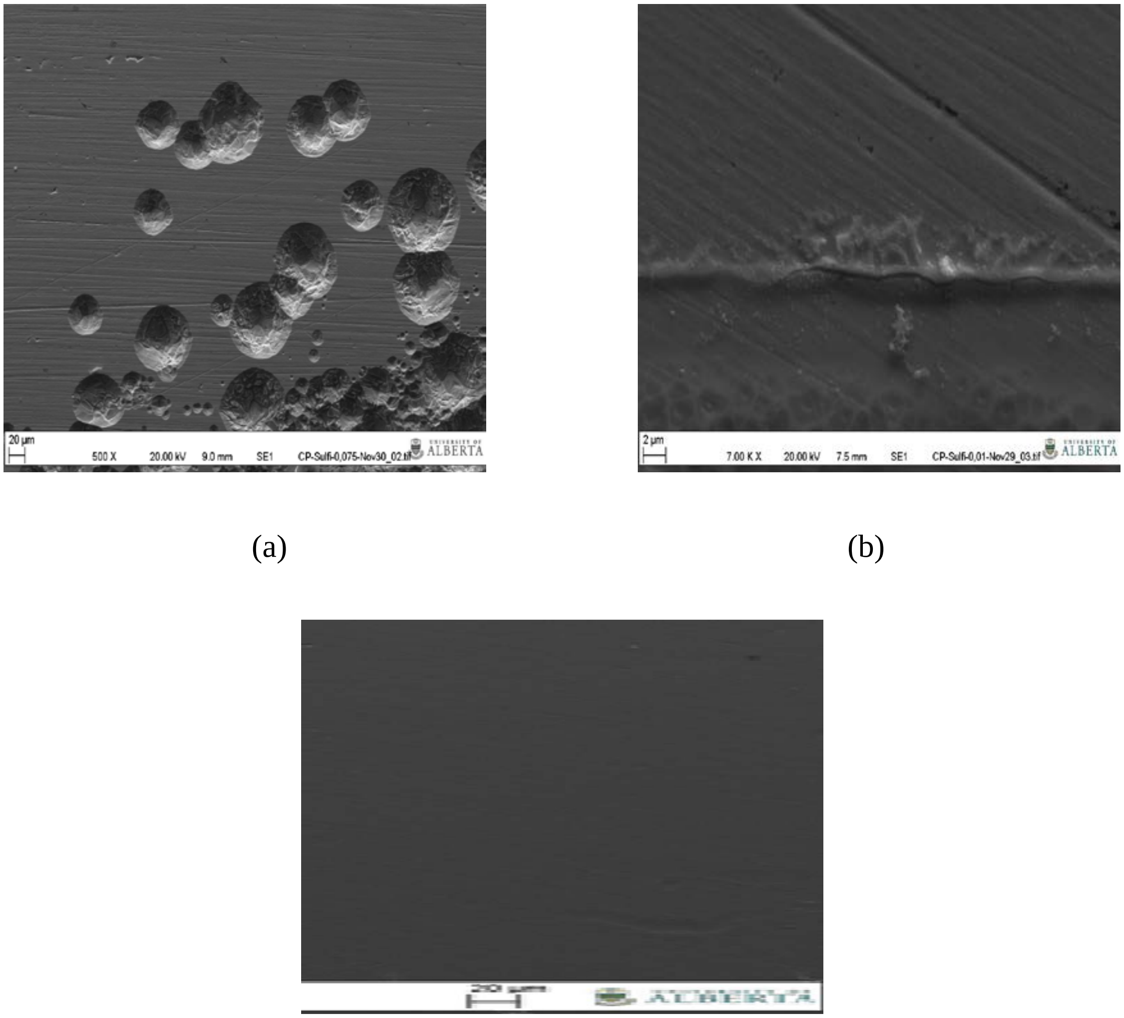

(a) (b)

(c)

Figure 4.7 SEM morphology of Alloy 800 samples without deflection used for cyclic polarization test in NC-3-1 (a), NC-3-2 (b), NC-3-3(c) environments.

Figure 4.8 (a) show the SEM morphology of the area on Alloy 800 sample used for cyclic polarization test in NC-3-1 environment. The area shown in Figure 4.8 (a) was selected for EDX mapping of different elements as shown in Figure 4.8 (b). The bright spots in the EDX map represent the significant presence of an element on the sample surface and the dark spots represent the partial presence of an element.

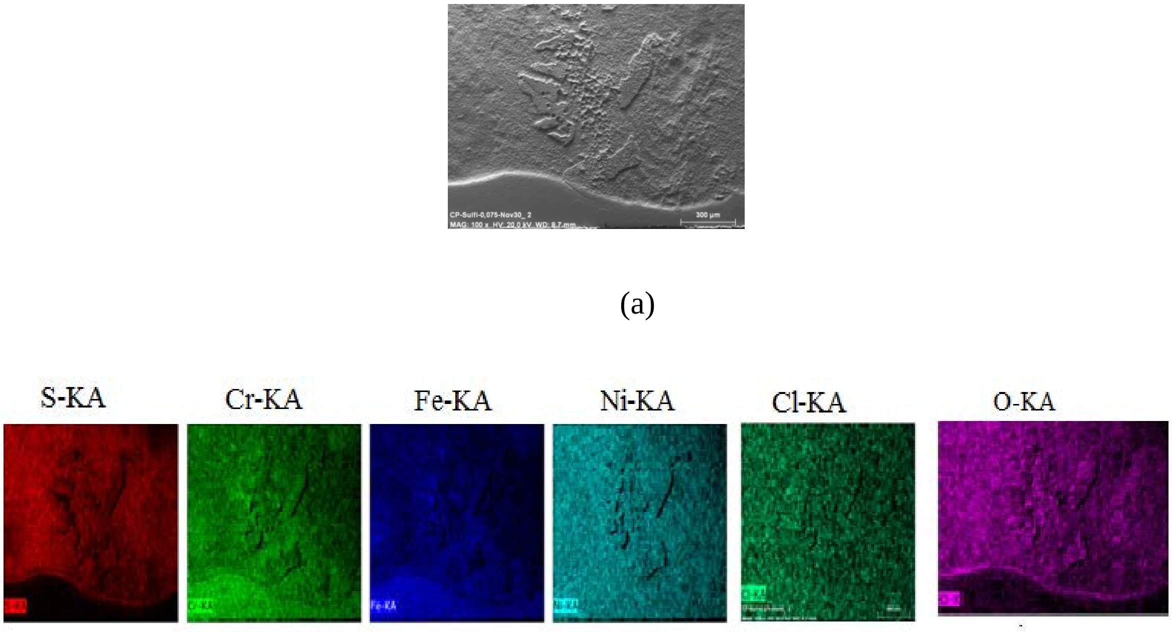

(a)

(b)

Figure 4.8 EDX mapping of Alloy 800 sample without deflection used for cyclic polarization test in NC-3-1 environment.

The comparison between the maps of Fe, Cr and Ni indicate that loss of Fe due to metal dissolution reaction was high compared to Ni and Cr. This is indicated by the large number of dark spots in the map of Fe in Figure 4.8 (b). The map of S in Figure 4.8 (b) indicated the presence of adsorbed sulphur on the surface of Alloy 800 and its role in promoting anodic dissolution. The map of Cl in Figure 4.8 (b) indicated its presence on the Alloy 800 sample surface.

When we compare the map of S with that of Fe, Cr and Ni in Figure 4.8, it can be noted that the areas were bright spot appeared on S map, darks spots can be seen on Fe map. However the intensity of darkness is intermediate in the same area of Cr and Ni maps.

Further when the maps of S and O is compared, the darks spots of intermediate intensity can be observed in the same area where bright spots appeared in S map. This implies that there are weak points on the oxide film, where sulphide could promote anodic dissolution. Further when we compare the maps of Fe, Cr and Ni it is observed that Fe is more susceptible to anodic dissolution reaction promoted by the presence of sulphide in the test solution.

4.2 Relationship between passivity degradation and S^y-SCC of Alloy 800

4.2.1 Effect of applied potential on S^y-SCC susceptibility of Alloy 800

Potentiostatic test method was employed to understand the SCC behaviour of Alloy 800 at a fixed potential. After potentiostatic tests the specimen surface was examined using SEM. Figure 4.9 shows the current vs. time plot of Alloy 800 polarized at active - passive potential region(-350 mV), passive potential region(-250 mV) and transpassive potential region (-110 mV). The test was conducted in three periods. The term period refers to the time interval. In each period the fixed potential was maintained for three days (72 hours). At the end of each period, the next period was started immediately. The experiment was conducted in three periods to have a good data resolution.

The result in Figure 4.9 (a) showed that the current increased dramatically with increase in the potential towards anodic direction. The current value is stable at -350 mV and -250 mV indicating the stable passive film at these potential regions. The result in the period 1 at -110 mV indicated that there was formation of stable passive film initially. Then the current increased probably due to anodic dissolution caused by localized corrosion. Then during the initial time in period 2 there was decrease in the current and it remained stable. This indicated the occurrence of repassivation. Then the current increased towards the end of period 2 indicating the occurrence of anodic dissolution. This indicated that there was periodic occurrence of anodic dissolution and repassivation. The same phenomenon was observed in period 3 as well.The anodic peaks observed could represent the anodic dissolution within the crack. It should be noted here that as the applied potential was increased in the positive direction further from the previous value of -250 mV, it is more likely that the reduction reaction of thiosulfate occurred at a faster rate than the oxidation reaction of Fe, Cr and Ni. The periodic occurrence of anodic dissolution and repassivation observed in the Figure 4.9 confirms the probable competition between the reduction reaction of thiosulfate (anodic dissolution) and oxidation reaction of Fe, Cr and Ni (repassivation) present in Alloy 800. It is more likely that the reduction reaction occurred at a faster rate than the formation of oxide film at -110 mV and played a dominant role in causing the SCC of Alloy 800. The experimental evidence behind this probable phenomenon was discussed below. Figure 4.10 (a) show the SEM morphology of Alloy 800 sample polarized at -350 mV. It indicated the formation of pits on the sample surface. Based on obtained SEM morphology pictures, Alloy 800 material was not susceptible to SCC at active-passive potential region at room temperature.The applied potential of -350 mV is near the corrosion potential. As explained earlier the reduction reaction of thiosulfate is favoured with increase in potential towards positive direction from the corrosion potential. Based on the obtained SEM picture it was observed that the localized attack due to reduction of thiosulfate is not significant. When we analyse in terms of the competition between reduction reaction of thiosulfate and oxidation reaction of metallic elements present in Alloy 800, it is more likely that oxidation reaction of Fe, Cr and Ni present in Alloy 800 occurred at a faster rate and played a dominant role at -350 mV, which made Alloy 800 resistant to SCC.

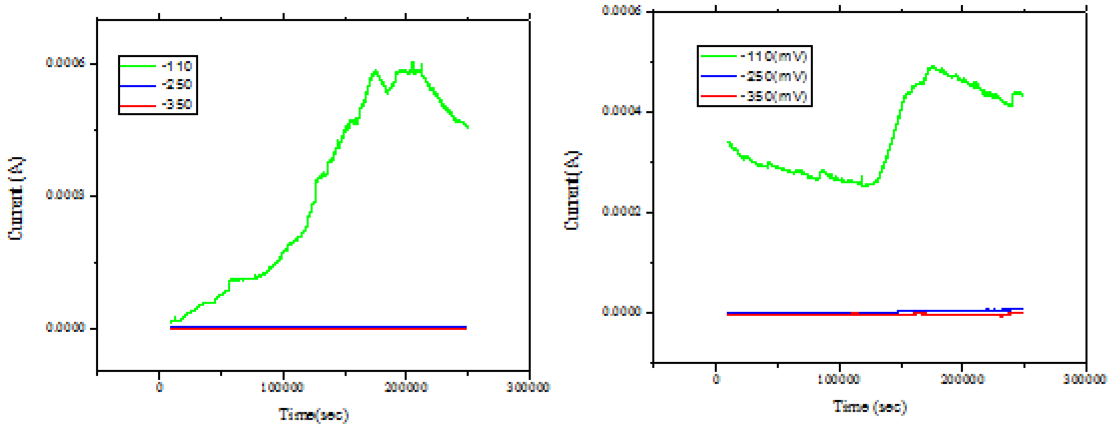

(a) (b)

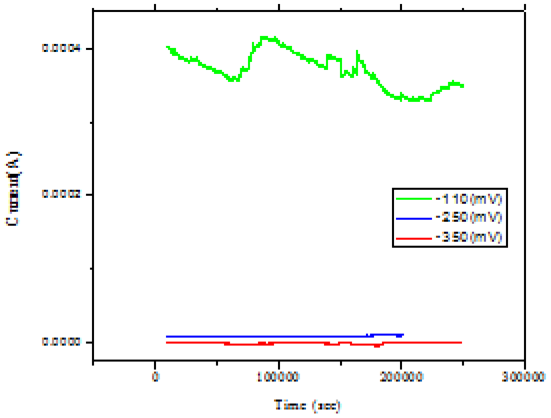

(c)

Figure 4.9 Current vs. time curves of Alloy 800 NACE C-ring sample with deflection & with a mechanical notch of 0.15mm depth in test solution NC-2-1 at active-passive (-350 mV), passive (-250 mV) and transpassive (-110 mV)regions during (a) Period 1 (b) Period 2 and (c) Period 3.

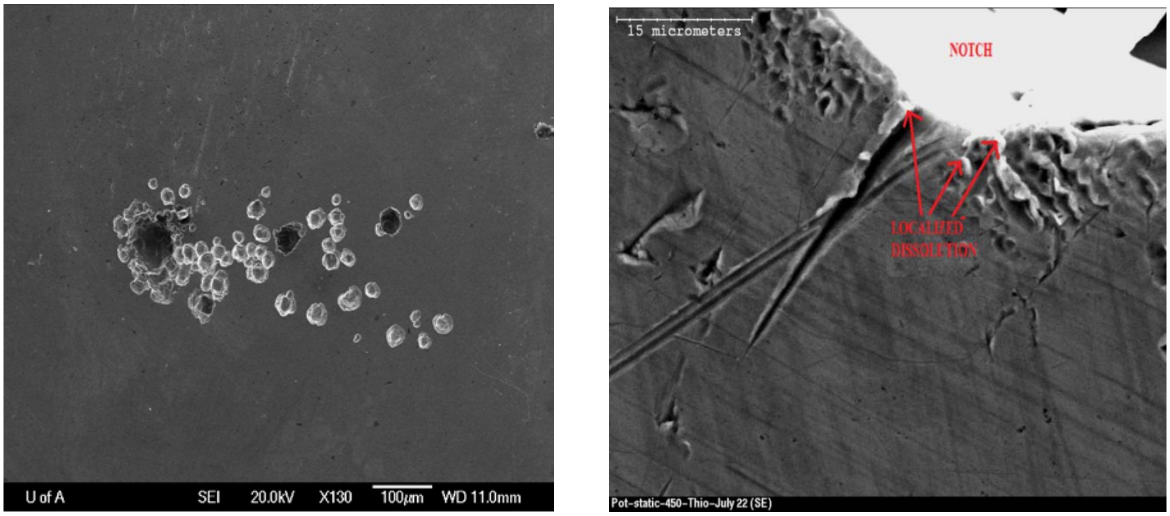

(a)

(b)

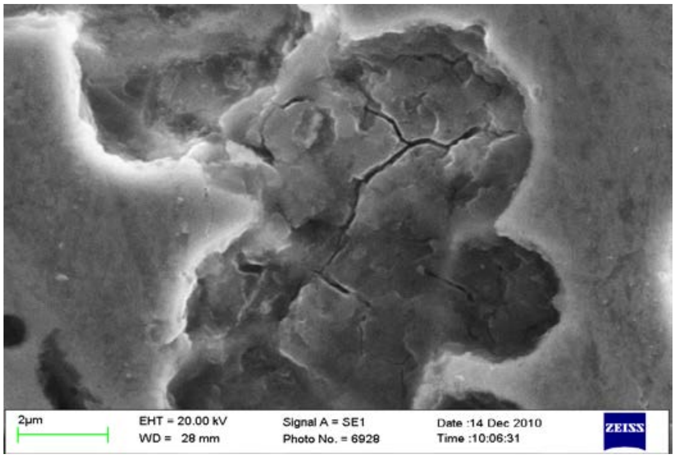

(c)

Figure 4.10 SEM morphology of NACE C-ring sample with deflection & with a mechanical notch of 0.15mm depth at (a) -350 mV (b) -250 mV (c) -110 mV in the test solution NC-2-1 after Potentiostatic test.

Figure 4.10 (b) shows the SEM morphology of Alloy 800 sample polarized at -250 mV. The observed features represent localized anodic dissolution. It should be noted here that as the applied potential was increased in the positive direction further from the previous value of -350 mV, it is more likely that the reduction reaction of thiosulfate occurred at a faster rate than the oxidation reaction of Fe, Cr and Ni, which eventually promoted anodic dissolution of Alloy 800 and lead to localized dissolution. However, there was no significant damage due to SCC on Alloy 800 surface. It implies that even though the reduction reaction of thiosulfate occurred at a faster than at -350 mV, the formation of oxide layer is still faster and stable enough to provide resistance to SCC. Figure 4.10 (c) shows the SEM morphology of Alloy 800 sample polarized at a fixed transpassive potential of -110 mV. The corrosion product was not present in this picture. This picture indicated that the pitting was initiated first and the pits had grown laterally and coalesced together and the anodic dissolution promoted by sulphur as explained previously caused a high stress concentration at the base of these pits and led to intergranular stress corrosion cracks, as found in the picture. This clearly showed that the SCC occurred by film rupture event initiated by pitting. Similar results were reported for Alloy 600 in a low temperature sulphur bearing environment intergranular SCC occurred in sensitized material and subsequently induced tubing failure [49]. Additionally, IGSCC of Alloy 800 SG tube due to low valence sulphur species reported for Bruce Unit 4 SG tubes, which is similar to this work[21].

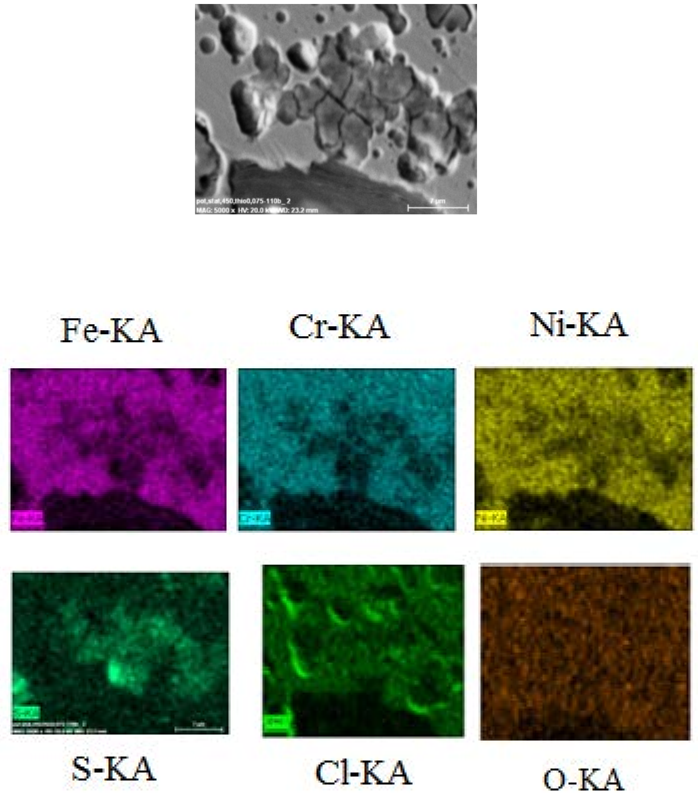

Figure 4.11 EDX map of Alloy 800 NACE C-ring sample with deflection & with a mechanical notch of 0.15mm depth at transpassive potential region (-110 mV) in the test solution NC-2-1 at room temperature after Potentiostatic test.

Figure 4.11 shows the SEM morphology of Alloy 800 sample, which was polarized at a fixed potential of -110 mV at transpassive potential region. This picture indicated the occurrence of anodic dissolution through pitting caused by the reduction reaction of thiosulfate. There was formation of corrosion product inside the pits. Figure 4.11 shows the EDX map of the same area where the presence of corrosion product was observed. The dark spots in the map represent the partial presence of an element. The bright spots indicate the significant presence of an element being analysed. The dark areas in the maps of iron, chromium and nickel indicate the loss of these elements. The bright spots in the map of sulphur indicate that there was a sulphur deposit inside the pits. This indicated that the sulphur promoted the anodic dissolution of Alloy 800, which in turn implies that the reduction reaction reaction of thiosulfate played a dominant role to cause metal dissolution than the repassivation reaction to form oxide film at -110 mV. The map of O has intermediate bright spots and it is more likely that there are weak points on the oxide film, which played a crucial role for sulphur to promote anodic dissolution of Alloy 800.

This phenomenon can be seen by comparing the maps of O and S in Figure 4.11. The bright spots in the map of chlorine indicated that it is present on the walls of the pit.Similar behavior was reported by Dinu et al., for Alloy 800 in a caustic solution [60] and Dhawale et al., for stainless steel in thiosulfate solution. Similar result was reported by laycock et al., for austenitic stainless steel. Laycock et al., proposed that sulphur species activated anodic dissolution on the bare metal surface created at pit initiation. Activation of dissolution was thought to occur by formation of a layer of adsorbed sulphur (Sads) on the dissolving surface, for instance, by electroreduction of the thiosulfate ion. Acceleration of dissolution by sulphur thought to be caused by a weakening of metal-metal bonds by Sads, leading to the reduction of the activation energy for dissolution [23].

4.2.2 Composition of the surface of Alloy 800 polarized at transpassive potential

XPS analyses was conducted to determine the chemical states of elements present on the surface of Alloy 800 sample polarized at a fixed potential of -110 mV. A survey spectrum was first recorded to identify all elements present at the surface, then high resolution spectra of the following regions were recorded: Fe2p, Cr2p, Ni2p, O1s, S2p. The obtained spectra was fitted, after background subtraction following the shirley procedure.

Table 4.4 summarizes the binding energy of the compounds of elements present on the surface of Alloy 800.The peak at the binding energy of 853.06 eV in the XPS spectra of Figure 4.12 was probably due to the metallic nickel (Ni)[78]. The peak at the binding energy of 856.369 eV was probably due to the presence of nickel hydroxides ($Ni(OH)_2$), based on the reference spectra [79]. Based on the reference spectra, the peak at the binding energy 711.645 eV in the Figure 4.13 was probably due to the presence of iron hydroxide ($Fe(OH)_3$). Further the peak at the binding energy of 710.945 eV was probably due to the presence of iron oxide (Fe_2O_3) [80], [81].The peak at the binding energy of 707.258 eV shows the probable presence of iron sulphide (FeS), based on the reference[82].

The peak at the binding energy of 574.066 eV in the Figure 4.14 was probably due to the presence of elemental chromium (Cr) based on the reference [83]. Further the peak at the binding energy 577.456 eV probably was due to the presence of Chromium hydroxide ($Cr(OH)_3$) [83].

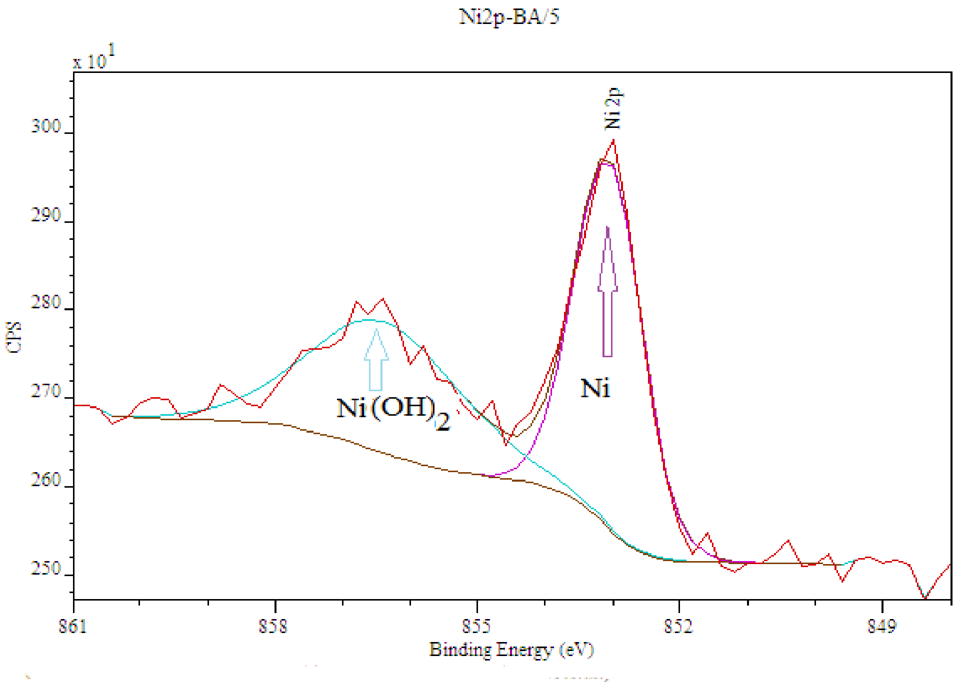

Figure 4.12 Spectra of Ni and its chemical state present on the surface of the Alloy 800 SCC sample failed at transpassive potential region(-110 mV) as determined by XPS.

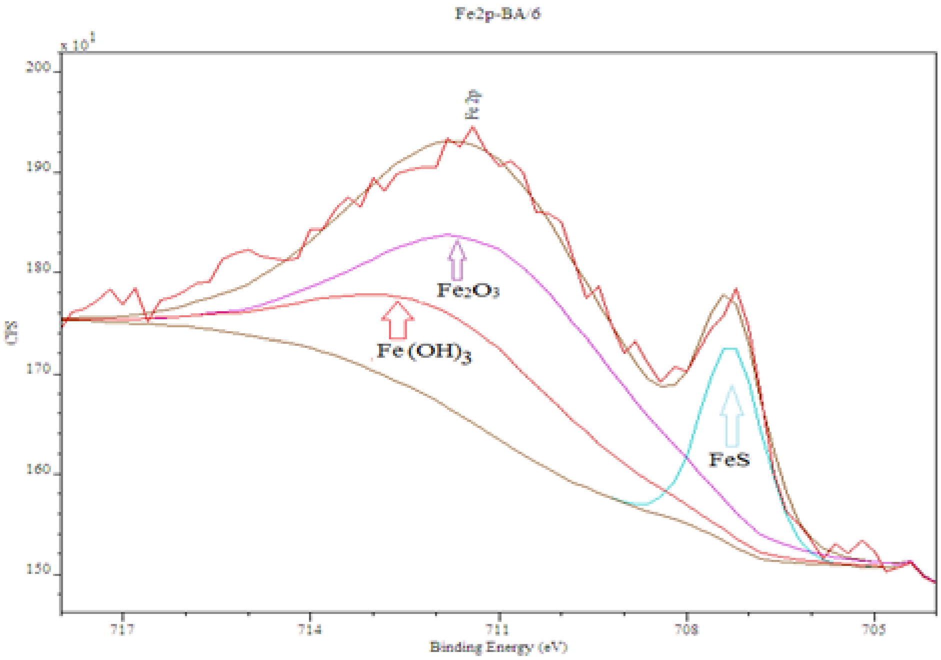

Figure 4.13 Spectra of Fe and its chemical state present on the surface of the Alloy 800 SCC sample failed at transpassive potential region(-110 mV) as determined by XPS.

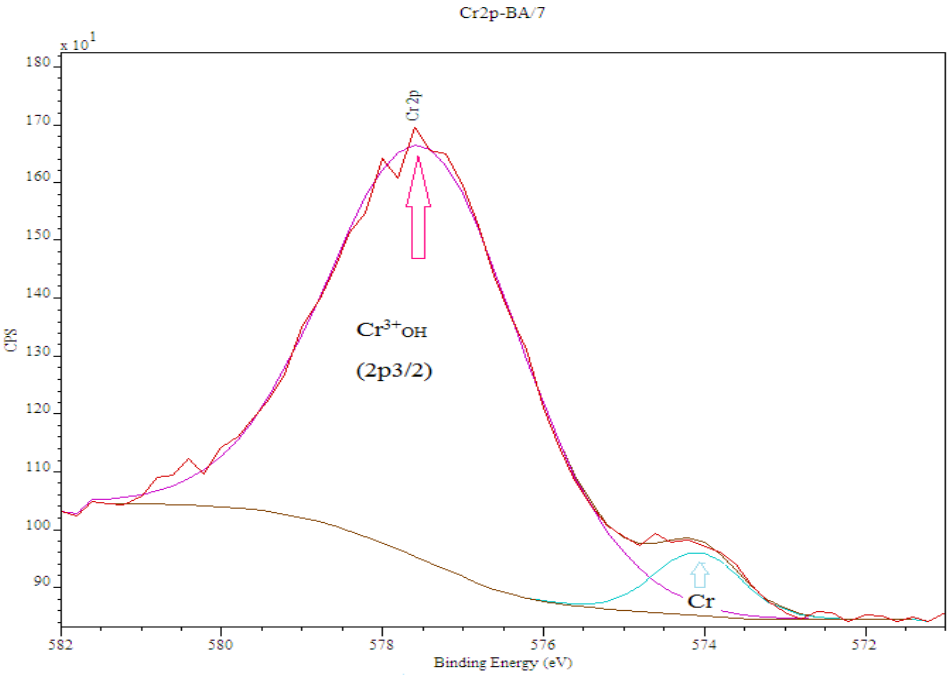

Figure 4.14 Spectra of Cr and its chemical state present on the surface of the Alloy 800 SCC sample failed at transpassive potential region (-110 mV) as determined by XPS.

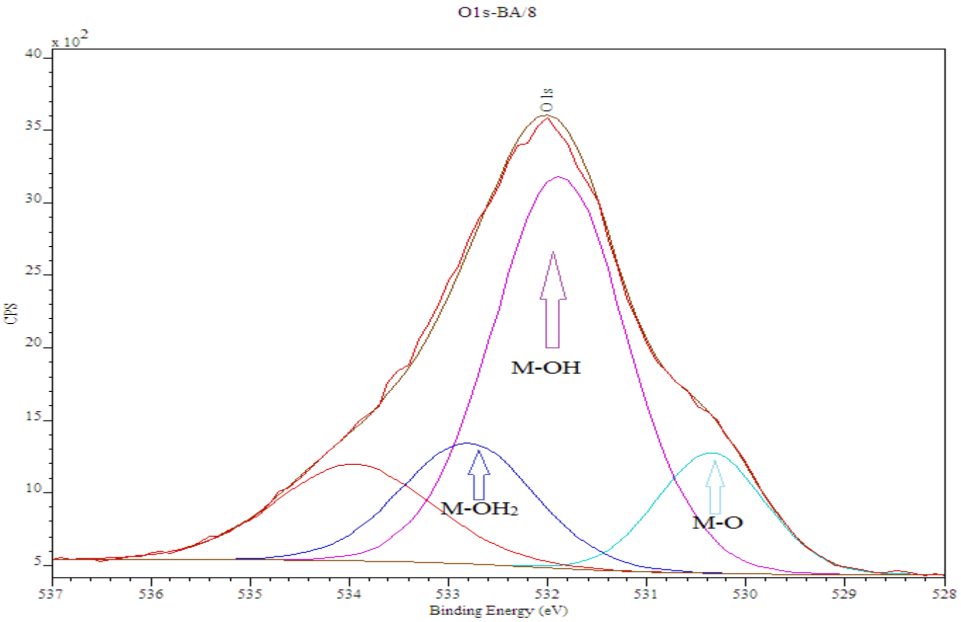

Figure 4.15 Spectra of O and its chemical state present on the surface of the Alloy 800 SCC sample failed at transpassive potential region(-110 mV) as determined by XPS.

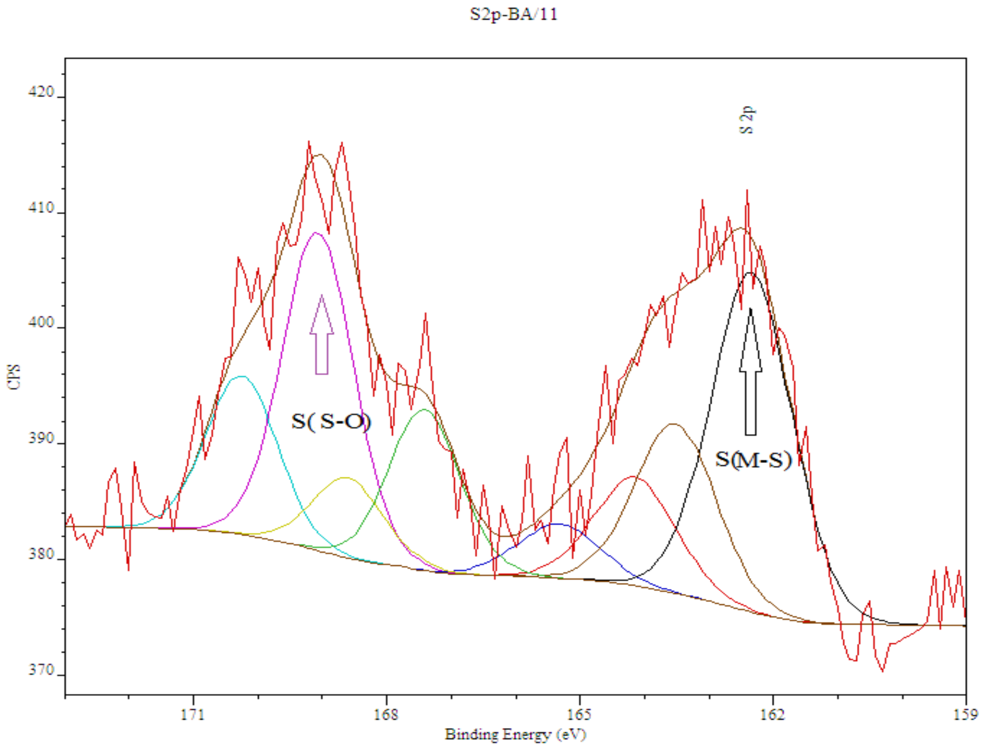

Figure 4.16 Spectra of S and its chemical state present on the surface of the Alloy 800 SCC sample failed at transpassive potential (-110 mV) as determined by XPS.

Table 4.4 Binding energy of Fe, Cr, Ni, O & S in various compounds.

Region	Compound	Binding energy (eV)	Reference
Ni	Ni^o	852.8	[84]
	$Ni(OH)_2$	856.4	[84]
	Ni^o	853.06	This work
	$Ni(OH)_2$	856.369	This work
S	$S_2O_3^{-2}$	168.5	[85]
	$S_2O_3^{-2}$	169.05	This work
	FeS	162.4	[82]
	FeS	162.33	This work
Fe	FeS	707.2	[82]
	FeS	707.258	This work
	$Fe(OH)_3$	711.9	[81]
	Fe_2O_3	711.5	[81]
	$Fe(OH)_3$	711.645	This work
	Fe_2O_3	710.945	This work
Cr	Cr^0	574.2	[83], [81]
	$Cr(OH)_3$	577.3	[83], [81]
	Cr^0	574.066	This work
	$Cr(OH)_3$	577.456	This work
O	O^{-2}	530	[86], [81]
	OH^-	531.4	[86], [81]
	H_2O	533.6	[81]
	H_2O	532.8, 533.95	This work
	O^{-2}	530.354	This work
	OH^-	531.8	This work

Table 4.5 Binding energy of sulphur in different oxidation states[48].

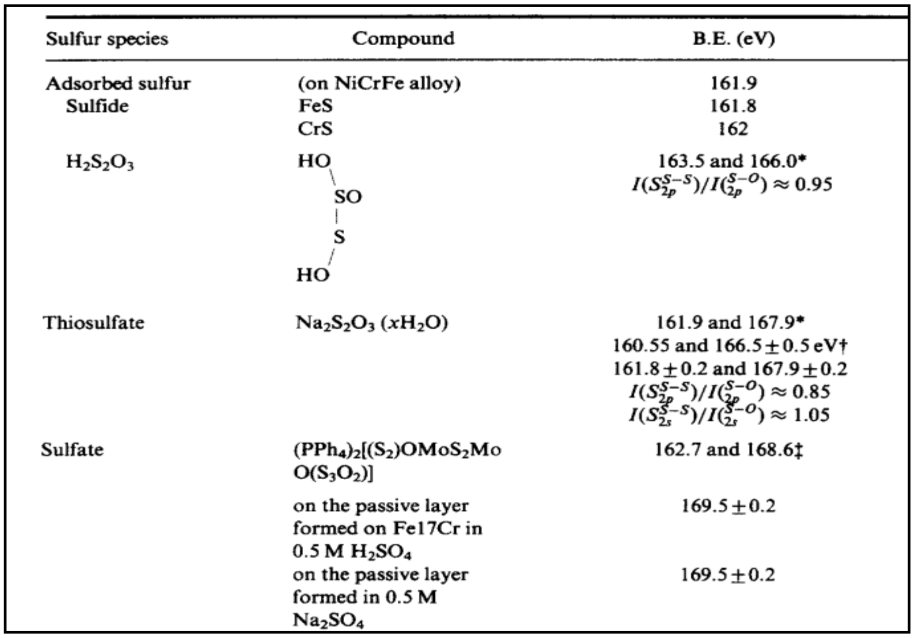

Sulfur species	Compound	B.E. (eV)
Adsorbed sulfur	(on NiCrFe alloy)	161.9
Sulfide	FeS	161.8
	CrS	162
$H_2S_2O_3$	HO \\ SO | S / HO	163.5 and 166.0* $I(S_{2p}^{S-S})/I(_{2p}^{S-O}) \approx 0.95$
Thiosulfate	$Na_2S_2O_3$ (xH_2O)	161.9 and 167.9* 160.55 and 166.5 ± 0.5 eV† 161.8 ± 0.2 and 167.9 ± 0.2 $I(S_{2p}^{S-S})/I(_{2p}^{S-O}) \approx 0.85$ $I(S_{2s}^{S-S})/I(_{2s}^{S-O}) \approx 1.05$
Sulfate	$(PPh_4)_2[(S_2)OMoS_2MoO(S_3O_2)]$	162.7 and 168.6‡
	on the passive layer formed on Fe17Cr in 0.5 M H_2SO_4	169.5 ± 0.2
	on the passive layer formed in 0.5 M Na_2SO_4	169.5 ± 0.2

The peak with the binding energy of 531.8eV in the XPS spectra of oxygen Figure 4.15 shows the probable presence of hydroxide(OH^-) [86]. The peak at the binding energy of 530.354 eV shows the probable presence of oxide(O^{-2}) [86]. The peaks at the binding energies 532.8 eV and 533.951 eV may be due to hydrates [81, 86] .The binding energies of sulphur in the adsorbed state, in sulphide(iron and chromium sulphide), in thiosulfate (Sodium thiosulfate) and in sulphate (adsorbed on the passive film) are reported in Table 4.5. There is no reliable work on the XPS spectra for S to identify its various chemical states. This makes it difficult to identify each individual deconvoluted peaks in XPS spectra of S2p, Figure 4.25. But this XPS spectra confirms the presence of oxidized form of sulphur and reduced form of sulphur, based upon XPS studies of thiosulfates [48]. They report two binding energies for sulphur, corresponding to sulphur-sulphur(S-S) and sulphur-oxygen (S-O) bonds.

The peak at 162.33 eV is very similar to the signal observed by Duret- Thual et al., for the reduced sulphur [48]. Therefore this probably indicates that on the bare metal surface(M), the decomposition of the thiosulfates have produced reduced sulphur species S(M-S). Based on the reference [82], the peak at 162.33 eV is probably due to the presence of iron sulphide FeS.

The probable presence of reduced form of sulphur confirms the role of the reduction reaction of thiosulfate in the SCC of the specimen tested potentiostatically at transpassive potential region.The peak at 169.05 eV is very similar to the S(S-O) signal peak observed by Duret – Thual et al.,[48]. Therefore this confirms that the oxidized sulphur species is adsorbed on the surface of the specimen.

Based on the above discussion of XPS analysis, it can be suggested that the $S_2O_3^{-2}$ participated in the electrochemical reactions. It can be suggested that the thiosulfate ion reduced to $S_{(ads)}$ and $H_2S_{(aq)}$ on the surface and eventually reacted with the dissociated Fe^{+++} to precipitate FeS which was identified by XPS analysis. The sequence of reactions is explained as follows. At first $S_2O_3^{-2}$, was oxidized to form S by the following reaction [87], [88].

$$S_2O_3^{-2} + 6H^+ + 4e^- \rightarrow 2S + 3H_2O \qquad \textbf{(4.4)}$$

Which contributed to the increase in the current in the figure. $S_2O_3^{-2}$ might also undergo disproportional reaction to form S and HSO^-_3 [87], [88].

$$S_2O_3^- + H^+ \rightarrow S + HSO_3^- \qquad \textbf{(4.5)}$$

S was further reduced and incorporated with H^+ according to the following reaction to form H_2S [87],

$$S + 2H^+ + 2e^- \rightarrow H_2S \qquad \textbf{(4.6)}$$

We suggest that it eventually may be reacted with dissolved Fe^{+++} to precipitate FeS according to the following reaction.

$$Fe^{3+} \rightarrow Fe^{2+} + e^-$$

$$Fe^{2+} + S^{-2} \rightarrow FeS \qquad \textbf{(4.7)}$$

It was also possible that the metal oxide reacted with H_2S to form sulphide in accordance with the following reaction.

$$MO + H_2S \rightarrow MS + H_2O \qquad \textbf{(4.8)}$$

4.2.3 Correlation between passivity degradation and S^y-SCC

The protective property of passive films fundamentally depends on their compositions and structures. When a metal was immersed in the corrosive test solution, the metal hydroxide layer will form. This layer will undergo dehydration to form metal oxide which acts as a protective barrier against SCC to occur. The investigations by Lu et al., indicated that the presence of lead hinders dehydration during the passivation of Alloy 690 and increases the concentration of hydroxides in the passive film [81]. Further they concluded that the susceptibility of Alloy 690 to SCC was due to lead induced passivity degradation. Lead induced passivity degradation was caused by changes in the compositions of the anodic films. Anodic films containing more M-OH and M-OH_2 bonds display the higher SCC susceptibility. Based on this, they found a strong correlation between lead-induced passivity degradation and PbSCC susceptibility [86]. Therefore the retarded dehydration results in the formation of less stable passive film containing more amorphous hydroxides that is less protective and increases the susceptibility to SCC.

In this work the effects of thiosulfate on the passivity degradation are investigated using the XPS peak analysis for the O_{1s} and $Cr_{2p3/2}$ peaks. The distribution of oxide and hydroxide in the passive film can be identified by deconvolution of O1s high resolution spectra. Figure 4.23 shows the XPS peak analysis for O_{1s} in which M-O and M-OH bonds were detected. Further M-OH_2 also can be detected. The higher amount of M-OH bonds confirm the occurrence of the phenomenon retarded dehydration.

The Cr2p3/2 core level spectra also reflect the trend of M-OH /M-O distribution in the films. This implies that the mechanism of passivity degradation at transpassive potential region is retarded dehydration and it can be correlated to the S^y-SCC for Alloy 800 similar to the work of Lu et al., [81, 86, 89].

The critical part of understanding this phenomenon is to find out the factors that promote retarded dehydration which in turn lead to passivity degradation and SCC of Alloy 800. The probable reduction reaction of thiosulfate to form sulphur on the surface during the passivation of Alloy 800 hinders dehydration and increased the concentration of hydroxides in the passive film. This further explains the competition between the reduction reaction of thiosulfate and the dehydration of hydroxides to form oxide film on the Alloy 800 surface.

4.2.4 SIMS analysis of Alloy 800 sample polarized at transpassive potential region

SIMS imaging analysis was done to get an idea about the chemical state of various ions present in the surface where SCC feature was observed. Even though XPS analysis can provide information about the chemical states its difficult for it to provide information about the distribution of various species in particular area on the surface of the specimen. The objective of SIMS in this work is to produce a map of different ions present at the SCC feature. This map helps to investigate the role of various species in the observed SCC feature.

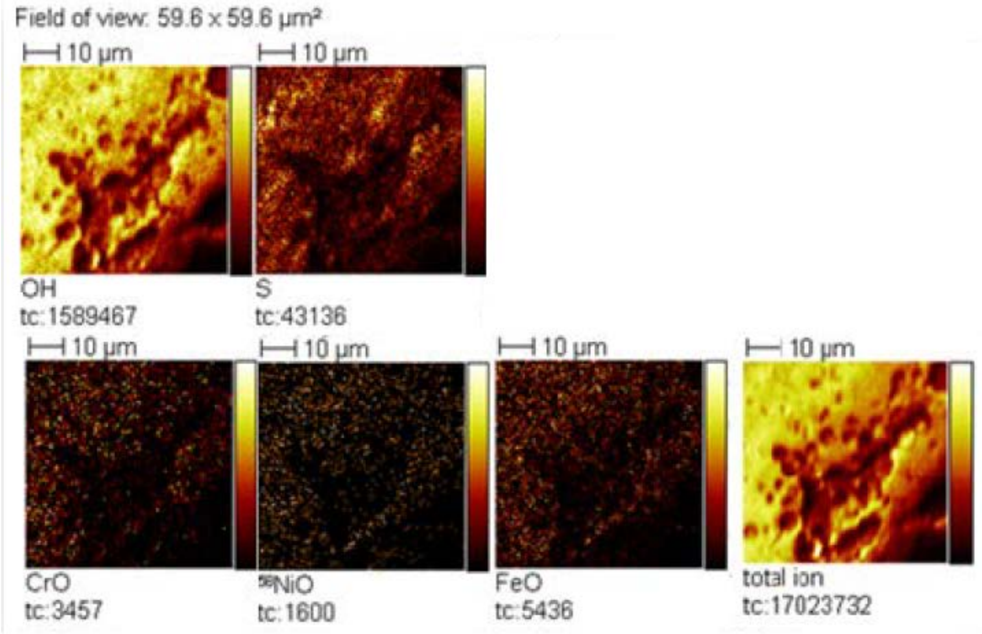

Figure 4.17 **SIMS image collected from the surface of the Alloy 800 sample tested potentiostatically at the transpassive potential region (-110 mV).**

The SIMS map in Figure 4.17 is from an area, where the corrosion product was observed as shown in the Figure 4.11. The bright spots in the map indicate the significant presence of a particular compound. The dark spots in the map indicate the partial presence of a compound. The comparison between the map of hydroxide (OH^-) and the maps of FeO, CrO and NiO indicated that there is significant presence of hydroxide and the presence of metal oxides is less. This clearly indicated the retarded dehydration of hydroxides.

The map of S suggests the role of it in causing passivity degradation. The map of S indicated the probable occurrence of the reduction of thiosulfate to low valence sulphur species. This clearly shows that at -110 mV the metal dissolution reaction promoted by adsorbed S occurred at a faster rate than the formation of oxide film and lead to SCC. In other words, at -110 mV, the reduction reaction of thiosulfate promotes entry of low valence sulphur species S into the passive film and reduces its stability and makes the material susceptible to SCC by causing passivity degradation. The information about other low valence sulphur species of thiosulfate was difficult to obtain due to the limited capability of SIMS.

4.2.5 Effect of thiosulfate on the localized dissolution of Alloy 800

The discussion in the previous section concluded the susceptibility of Alloy 800 to SCC at the potential in the transpassive region. This conclusion further gave the motivation to study the susceptibility of Alloy 800 to SCC at transpassive potential using a specimen without notch. Figure 4.18 shows the change in current with time at -110 mV in the transpassive region in NC-2-1 environment at room temperature. The anodic peaks observed represents the anodic dissolution [60].

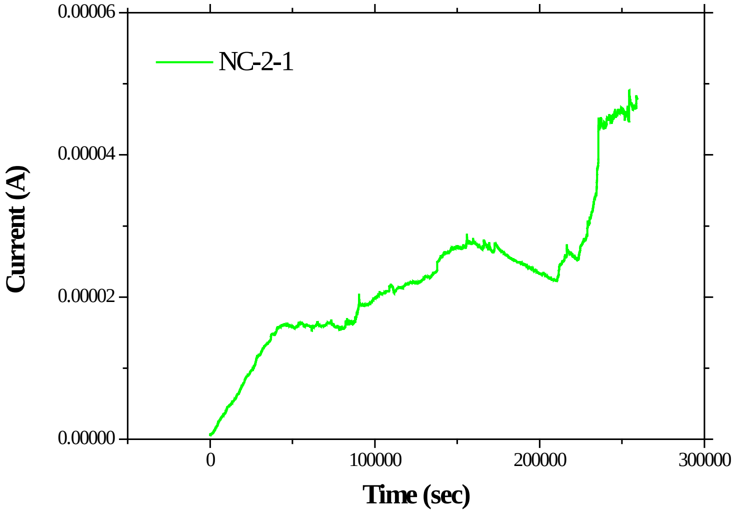

Figure 4.18 Current vs. time curves obtained on Alloy 800 NACE C-ring sample with deflection & without a mechanical notch at transpassive potential region(-110 mV) in test solution NC-2-1 for 3 days.

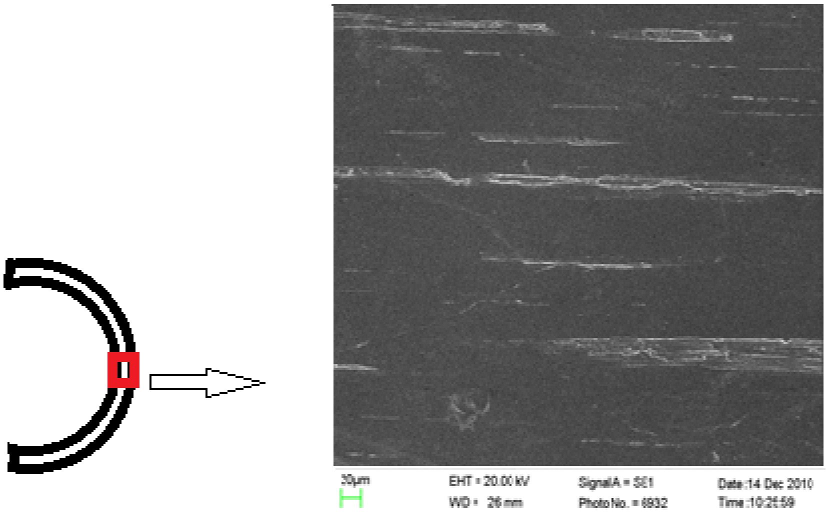

Figure 4.19 SEM morphology of NACE C-ring sample without deflection & without notch before Potentiostatic test.

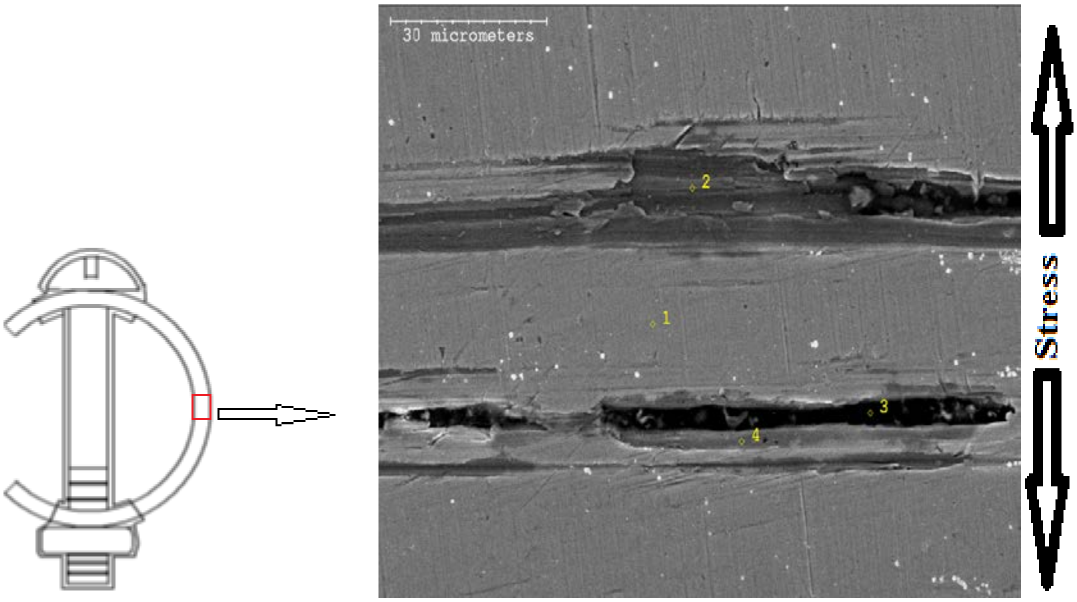

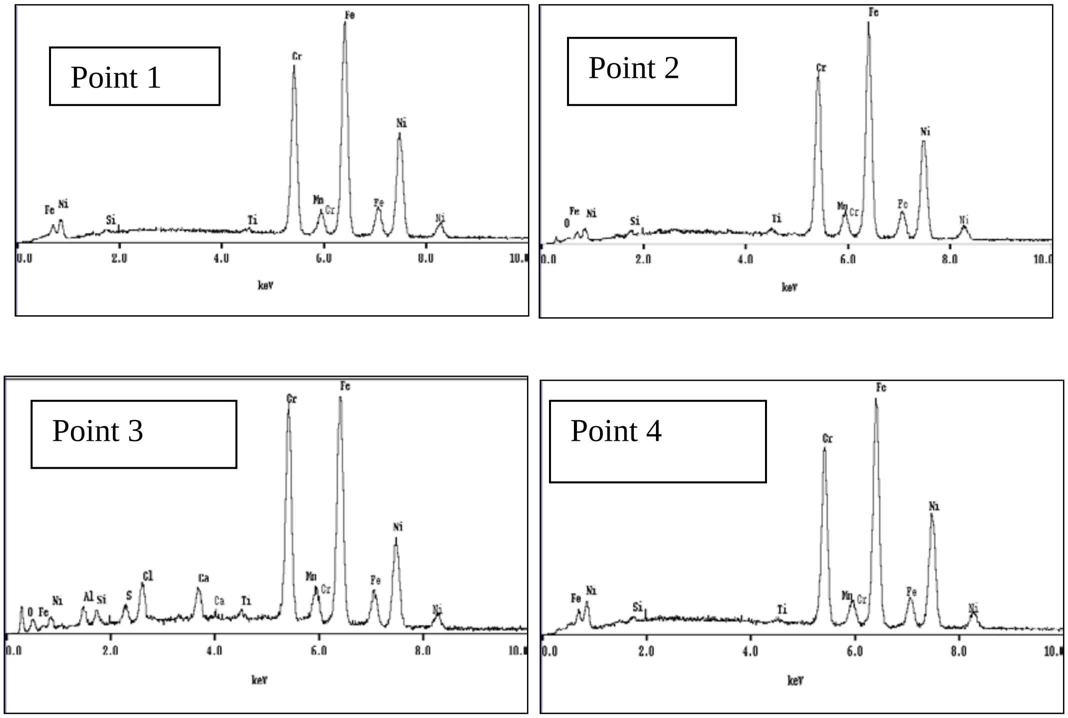

Figure 4.20 EDX analysis of NACE C-ring sample with deflection & without notch at transpassive potential in test solution NC-2-1 near neutral pH at room temperature after Potentiostatic test.

Figure 4.20 shows the SEM morphology of the polarized sample of Alloy 800 sample without notch at the transpassive potential region. These figures indicate the evidence for the localized dissolution. EDX analysis shown in the Figure 4.20 shows the presence of sulphur and chlorine in the initiated localized attack. This explains the synchronous role of sulphur and chloride in the initiation of the localized anodic dissolution. These evidence explains that the S^y-SCC of Alloy 800 at transpassive potential region more likely due to localized dissolution phenomenon. Further similar SEM features were observed in the Potentiostatic tests using SSRT sample by Lu et al., for PbSCC [86]. They concluded that the high SCC susceptibility in lead contaminated environments related to the passivity degradation of anodic films. The results obtained in this work was similar to the one observed for PbSCC by Lu et al., [86].Additionally previous researchers have confirmed that the SCC in solutions containing thiosulfate follows localized attack [34]. Further Lu et al., applied the model developed by ford to calculate the average crack propagation rate based on Faraday’s law for PbSCC. Based on the average crack propagation rate they calculated the value for film rupture ductility.

The same method cannot be applied in this work to calculate film rupture ductility because of the different test method and the lack of model in the literature for the specimen design used in this work. But it is still valid to relate the localized attack of the oxide film as the reason for susceptibility to S^y-SCC of Alloy 800.

4.2.6 Effect of low valence sulphur species on semi-conducting behaviour (structure) of the passive film

The passive films are regarded as semiconductors. The electrochemical behaviour of passive films is often interpreted in terms of their semiconductive nature. The corrosion resistance of a passive film is closely related to its electronic properties. Therefore the effect of low valence sulphur species promoted corrosion on the passive film was explored by measuring the capacitance of specimens passivated in the SG crevice chemistries with and without the presence of low valence sulphur species (sodium thiosulfate, sulphide). Further the effect of change in concentration of low valence sulphur species on the passive film was studied.

The Mott–Schottky relationships expresses the potential dependence of the capacitance of the space charge layer, C_{sc}, of a semiconductor electrode. A higher slope of the Mott-Schottky plot implies a lower acceptor density. The positive slopes of Mott-Schottky plots indicate that the passive films on the test material are n-type semiconductors. The Mott-Schottky slope of an n-type semiconductor can be formulated as follows,

$$\mathbf{Slope = 2/\ \varepsilon\varepsilon_0 q N_D} \qquad \mathbf{(4.9)}$$

ε- Dielectric constant; ε_0 - Permittivity of vacuum; q - Electron charge; N_D - Donor density.

Solution pH as well as potential and chloride or oxygen concentration are considered factors that affect the ratio of the different doping species, determining the type of semiconductivity of the oxide film. In fact, it is known that chromium hydroxide reveals a n-type semiconductivity whereas Chromium oxide has been described as a p-type semiconductor[90]. In the section 4.2.3 it was concluded that the presence of thiosulfate caused passivity degradation which in turn affected the formation of oxide film.

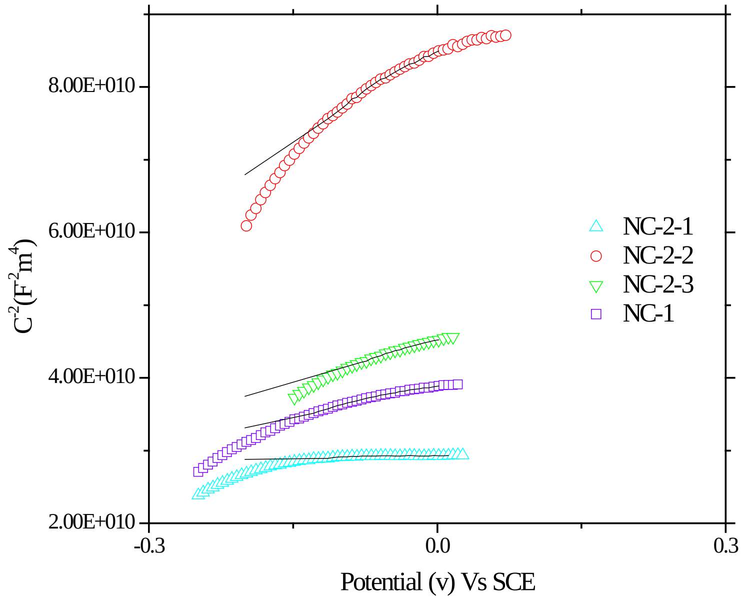

Figure 4.21 Mott Schottky plots obtained for Alloy 800 in test solutions NC-1, NC-2-1, NC-2-2, NC-2-3 in near neutral pH at room temperature.

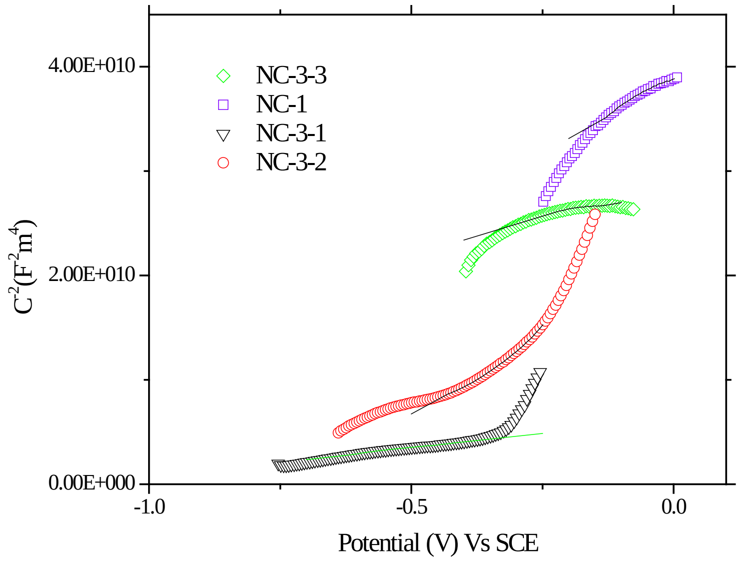

Figure 4.22 Mott Schottky plots obtained for Alloy 800 in test solutions NC-1, NC-3-1, NC-3-2, and NC-3-3 pH 12 at room temperature.

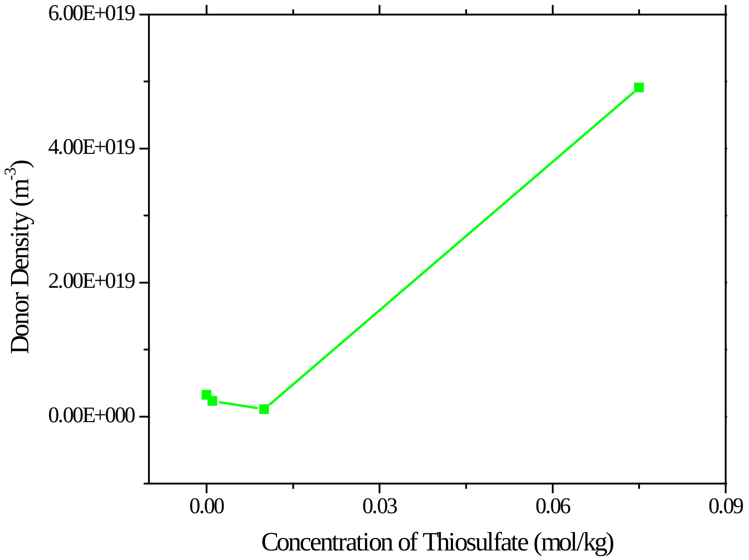

Figure 4.23 Donor density vs. concentration of thiosulfate.

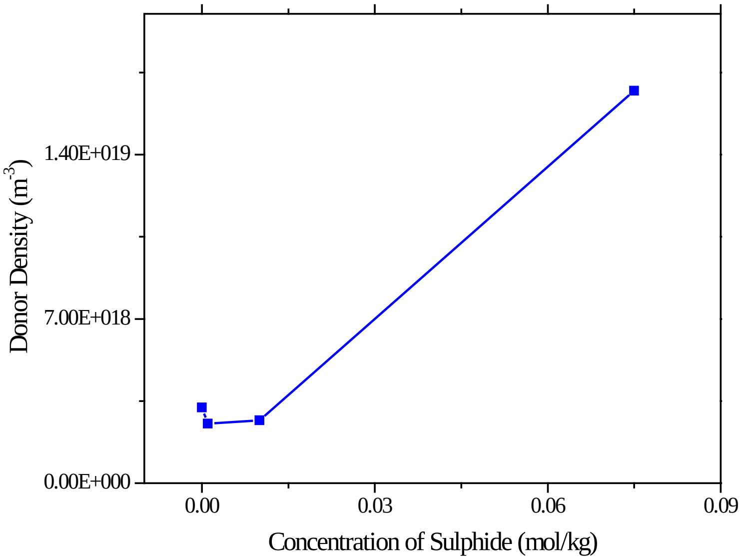

Figure 4.24 Donor density vs. concentration of sulphide.

Since the oxygen concentration in the passive film decides the type of semiconductivity of the oxide film, it can be suggested that the variation of thiosulfate in the test solution will have an impact on the semiconducting behaviour of the passive film, which was studied in this section. The density of acceptors and donors were calculated from the negative and positive slopes respectively, by considering the dielectric constant value of Cr_2O_3 (assuming ε=15.6) [91].Taking $\varepsilon = 15.6$, the donor densities of passive films can be determined from Mott-Schottky plots. The donor densities in the passive films are inversed proportional to the values of slope determined from the linear sections of Mott-Schottky plots. The donor density values determined from the Mott-Schottky plots are summarized in the Figure 4.23 to Figure 4.24. The following observations are obtained from the Mott-Schottky measurements.

Figure 4.23 shows the change in donor density of the passive film formed on Alloy 800, with change in the concentration of thiosulfate in the test solution. The passive film shows n-type semiconductive behaviour. This plot shows that the donor density of the passive film increases with increase in the concentration of thiosulfate in the test solution. For passive films that are n-type semiconductors, the donor is oxygen vacancies, and a higher donor density indicates a more defective passive film structure [92]. Therefore, the passivity degradation due to reduction reaction of thiosulfate probably lead to higher oxygen vacancies and higher donor density. This lead to the increased susceptibility to SCC.

To summarize the above conclusions, the presence of thiosulfate in the test environment resulted in the formation of passive film with more defective structure. Further previous research in our group confirmed that donor density can be related to passivity degradation[81, 86, 89, 93]. The increase in donor density contributes to the passivity degradation and which in turn increased the susceptibility to SCC[81, 86, 89, 93]. It was confirmed by Lu et al., that amorphours hydroxides lead to more defective structures in the passive film than crystalline oxides [89].Therefore the above explained behaviour of Alloy 800 in the presence of thiosulfate in the test environment, probably due to the formation of amorphous hydroxides with defective structures. The following observations are made from the Mott-Schottky measurements as shown in the Figure 4.24.

Figure 4.24 shows the change in donor density with change in concentration of sulphide in the test solution. The passive film shows n-type semiconductive behaviour. When the results are compared between NC-3-1 & NC-3-2 environments, the donor density increased with increase in the concentration of sulphide in the test solution.

4.3 Effect of low valence sulphur species on the crack propagation rate of Alloy 800

The objective of this test is to determine the crack propagation rate based on the change in the measured potential.

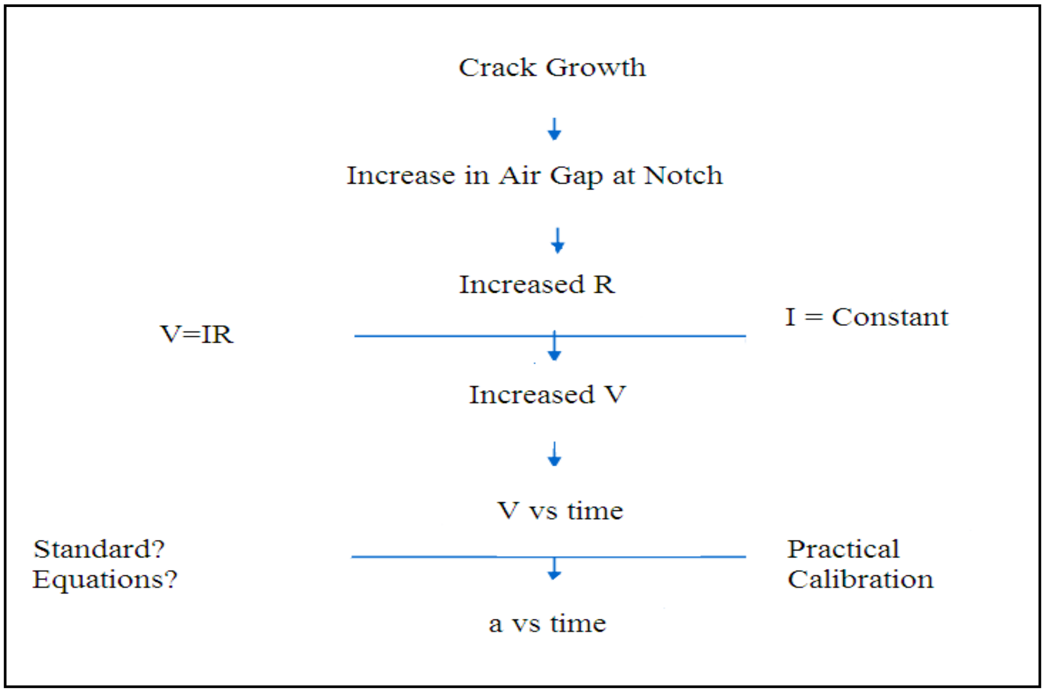

Figure 4.25 Schematic of potential drop test method [94].

When the crack propagates at the notch where stress concentration is high, there is an increase in air gap at the notch which causes an increase in the R(resistivity) value. A constant current is applied and therefore this increase in R value leads to increase in the V(potential) value, which is recorded with change in time.

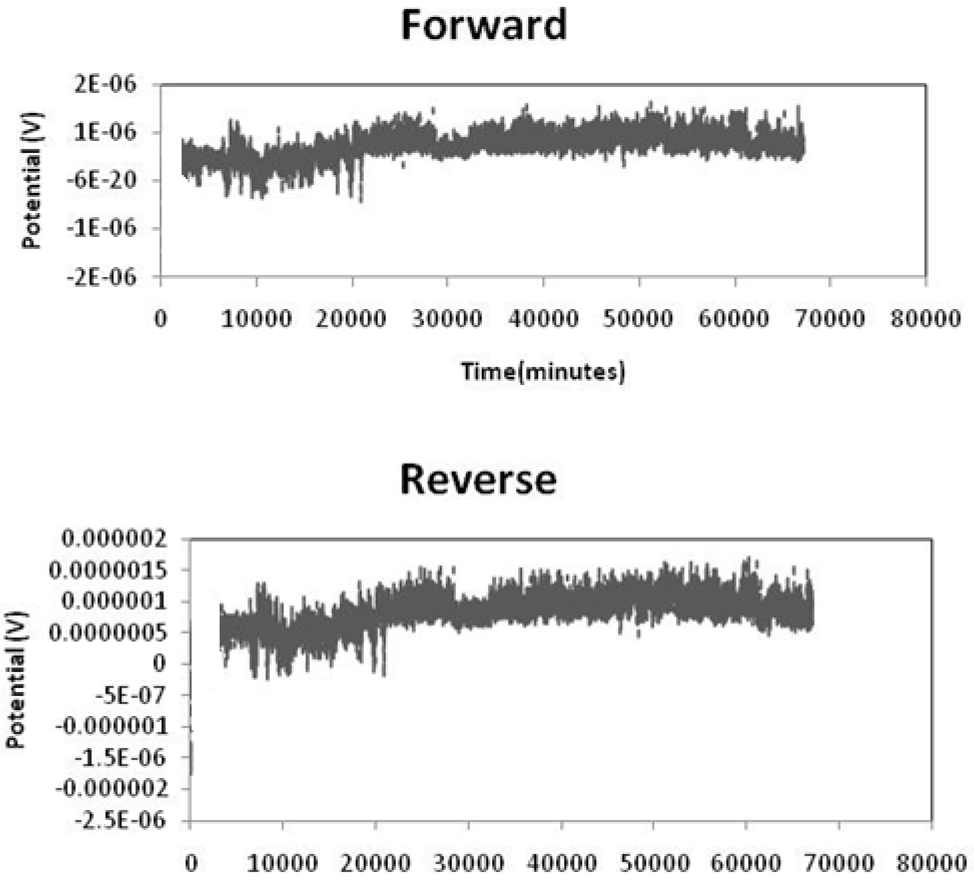

Forward

Reverse

Figure 4.26 Change of measured potential as a function of test time for C-ring specimen with notch in NC-3-1 test solution .

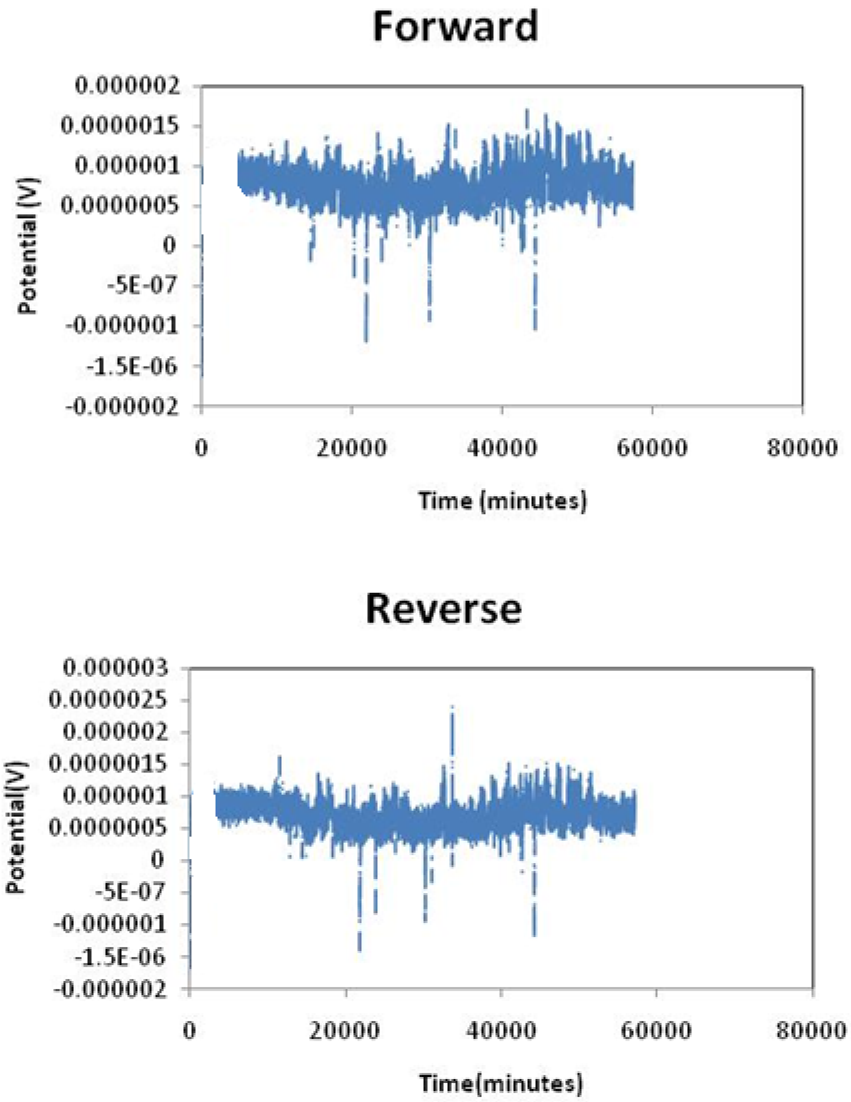

Figure 4.27 Change of measured potential as a function of test time for C-ring specimen with notch in NC-2-1 test solution.

Figure 4.26 & Figure 4.27 which is potential drop test result for specimen with 0.15mm depth notch in NC-2-1 and NC-3-1 environments; shows that there is no significant average increase in the potential drop signal. This shows that there is no significant change in air gap at the notch and which in turn means that there is no crack propagation. Further SEM morphology pictures confirm that there was no SCC on the test specimen. Therefore Alloy 800 was not susceptible to SCC under the given test conditions.

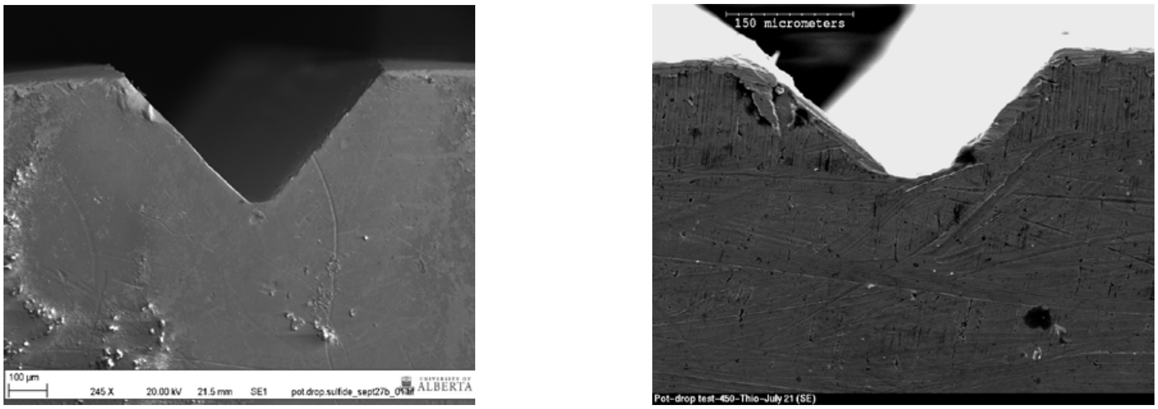

(a) (b)

Figure 4.28 SEM morphology of C-ring specimen with notch used in potential drop test in (a) NC-3-1 & (b) NC-2-1 test solutions.

Figure 4.28 confirms that there was no SCC feature on the sample used in potential drop test in NC-3-1 & NC-2-1 environments. From a corrosion perspective, the solubility of oxygen in a solution is one of the most significant effects. Figure 4.29 shows the effect of increasing oxygen concentration on the corrosion rate of iron in water. At any given temperature, the corrosion rate of iron increased with increasing oxygen concentration.

Figure 4.30 gives corrosion rates for various metals in solutions with no oxygen (hydrogen-saturated) and solutions saturated with oxygen. For all of the metals listed, the addition of oxygen to the solution significantly increases the corrosion rate. The presence of oxygen in a solution provides an additional reduction process, i.e., an additional reaction to consume electrons.

The iron atoms going into solution leave electrons at the anodic sites and the corrosion reaction can only go on as quickly as these electrons can be consumed in a cathodic reaction. Thus, the addition of oxygen allows more electrons to be consumed by an additional reduction reaction, and the corrosion rate of many of the metals increases.

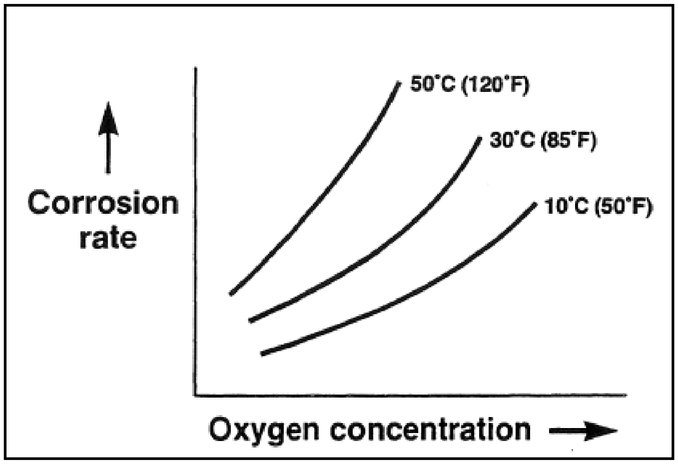

Figure 4.29 The effect of oxygen concentration on the corrosion rate of iron [95].

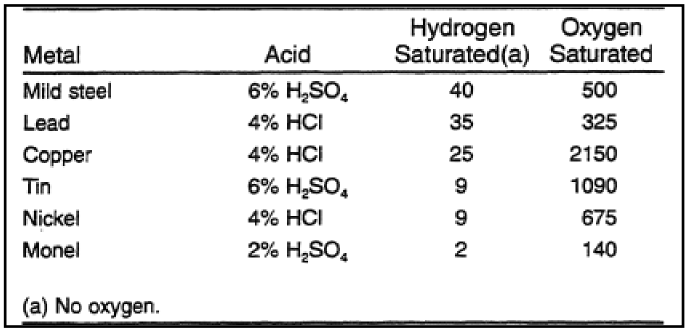

Metal	Acid	Hydrogen Saturated(a)	Oxygen Saturated
Mild steel	6% H_2SO_4	40	500
Lead	4% HCl	35	325
Copper	4% HCl	25	2150
Tin	6% H_2SO_4	9	1090
Nickel	4% HCl	9	675
Monel	2% H_2SO_4	2	140

(a) No oxygen.

Figure 4.30 Comparison of corrosion rates (in mm/yr) in oxygen free(hydrogen saturated) and oxygen saturated solutions [95].

Further the corrosion potential of SG tubing E_{Corr} is influenced by the concentration of oxidizing and reducing species in the water . The investigations shows that oxidizing conditions are a prerequisite of pitting for all SG tubing alloys [24]. Newman et al., showed that thiosulfate, thiocyanate, tetrathionate, and sulphide ions are all highly aggressive SCC agents for sensitized steels at room temperature. In particular, aerated sodium thiosulfate solutions as dilute as $6x10^{-7}$ molar caused SCC in constant extension rate (CER) tests.

It was proposed that maximum SCC susceptibility was associated with elemental sulphur formation in aerated thiosulfate solutions[28].Therefore maintaining an aerated condition of the test solution will be the future work to study the in-situ stress corrosion crack growth rate of Alloy 800 at room temperature in AECL recommended test environment.

4.3.1 Calibration of potential drop system

The record of potential vs. time is converted into crack length vs. time by using standards and equations that suits specimen geometry or practical calibration method can be used to do this conversion.

ASTM E-647 is available to convert the potential vs. time curve into crack length vs. time curve for a CT specimen. There are no established standards and equations for doing this conversion for C-ring specimen. ASTM E-647 standard recommends using an experimental calibration procedure for complex geometry. Therefore an experimental calibration method should be used to convert the potential vs. time curve obtained in this work into crack length vs. time curve. Further the calibration should be done over a wider range of crack lengths than will be measured in the actual test.The experimental calibration method refers to electrical analogue method. The electrical analogue method is a 2D method. The procedure to obtain calibration curve for the case of CT specimen can be found in ASTM E-647. But this method cannot be applied for the geometry of C-ring specimen. The reason is that the equi-potential lines generated on the C-ring specimen by application of constant current has 3-D properties. Further it is difficult to make a crack of known size vs. time for the geometry of C-ring specimen.

Therefore an attempt was made to obtain a calibration curve, by using a C-ring specimen made of alloy 800 according to NACE standard TM0177-2005 with a notch of depth 0.15mm, which was prepared as explained in the Section 3.3. A deflection of 0.474 mm was applied. The experiment was conducted in air and the change in potential vs. time was recorded.

Figure 4.31 shows the changes in potential measured with time at deflection value of 0.474 mm. There is no significant average increase in the potential drop signal. This shows that there is no significant change in air gap at the notch and which in turn means that the material did not fail mechanically. Even though the applied deflection is of higher value the material did not fail which is due to the highly ductile nature of Alloy 800.

Therefore alternate calibration methods should be used to obtain calibration curves. For example, a nano-precision cutting tool may be used to increase the notch depth at known values and the change in potential drop can be recorded to obtain a calibration curve. Additionally, finite element analysis may be used to obtain the calibration curve for this type of specimen geometry.

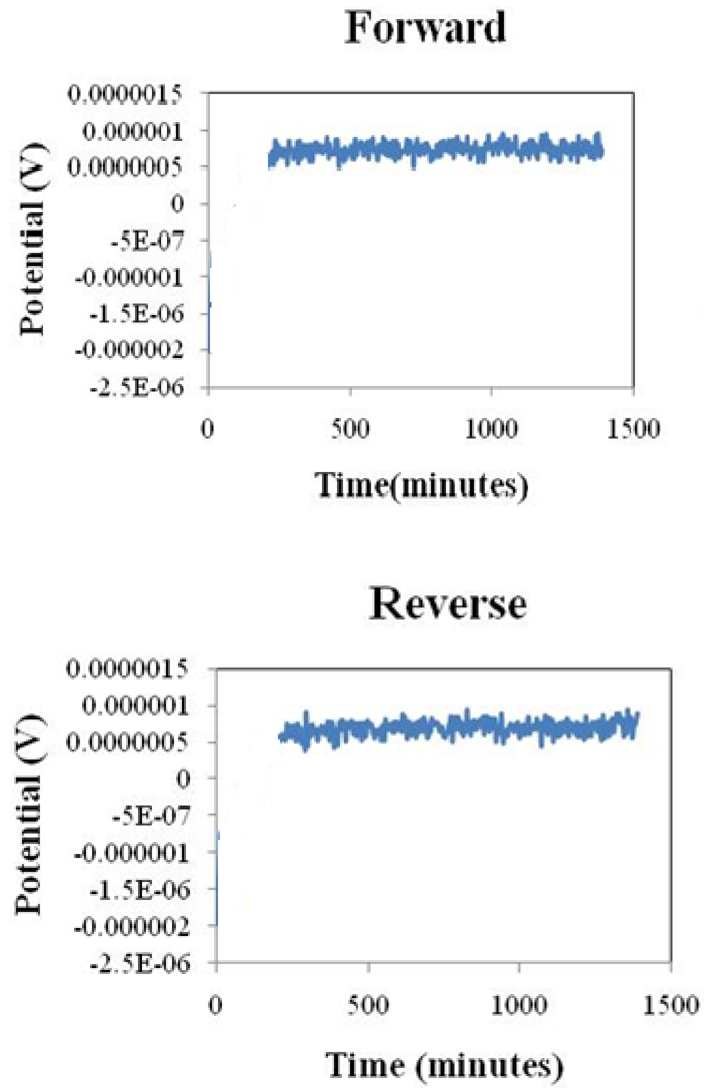

Figure 4.31 Change of measured potential as a function of test time for C-ring specimen with notch for calibration in air at applied deflection of 0.474 mm.

4.3.2 Long time immersion test

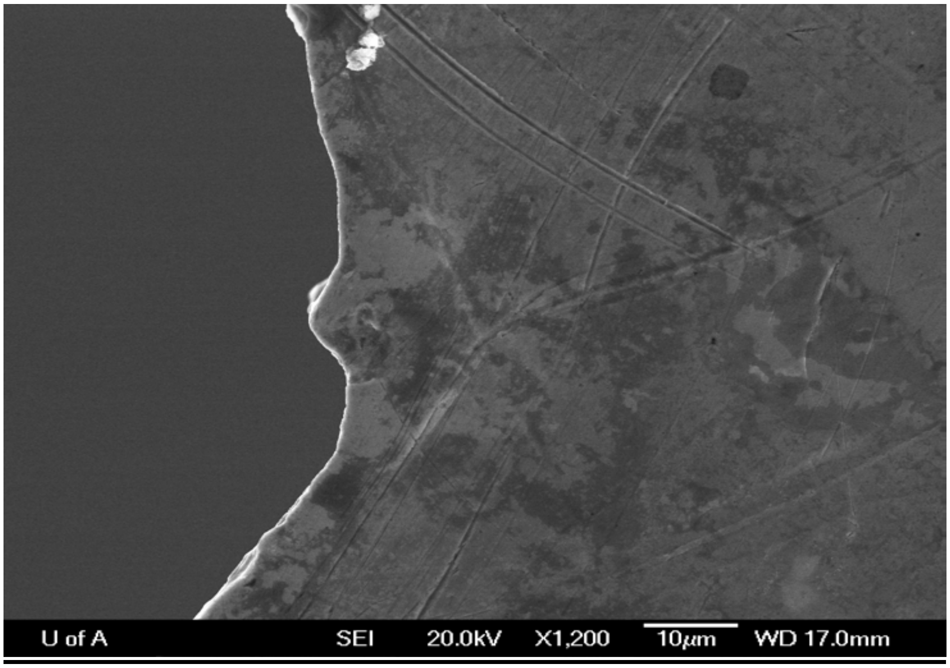

Figure 4.32 SEM morphology of C-ring specimen with notch under applied deflection(0.356 mm), immersed in NC-2-1 solution for 90 days (approximate).

The potential drop test results already concluded that there was no SCC in the NC-2-1 test environment at room temperature, open circuit conditions as explained above.

The objective of the immersion test is to find out if the increase in time of exposure of C-ring samples under deflection to the aggressive test solution NC-2-1 leads to SCC. Figure 4.32 shows the SEM morphology of Alloy 800 sample immersed in the NC-2-1 environment under applied deflection of 0.356 mm in open circuit condition. This picture showed that Alloy 800 was not susceptible to SCC in the test condition used.

Chapter 5 Conclusions & Future Work

5.1 Conclusions

1) At room temperature, with increase in the concentration of thiosulfate in the simulated SG crevice solution, pitting potential decreased and the passive range of Alloy 800 got reduced. The presence of deflection concentration shifted the OCP cathodically, increased the passive current density and decreased the pitting potential in the test solution containing higher concentration of thiosulfate. SEM morphology pictures showed that the density of pitting is high at higher concentration of thiosulfate in the test solution.
2) At room temperature, with increase in the concentration of sulphide in the test solution in simulated SG crevice solution, the OCP shifted cathodically, the material showed active dissolution behavior over a large potential range. SEM and EDX mapping showed that there are weak points on the oxide film, where sulphide could cause active dissolution. Further the comparison of maps of Fe, Cr and Ni showed that Fe is more susceptible to active dissolution by sulphide
3) Alloy 800 is not susceptible to SCC, when polarized at the fixed active-passive potential region (-350 mV) at room temperature in simulated SG crevice solution containing thiosulfate. Localized dissolution was detected, when Alloy 800 was polarized at the fixed potential in the passive region (-250 mV). Alloy 800 is susceptible to SCC at the transpassive potential region(-110 mV). SEM morphology pictures indicated the susceptibility of Alloy 800 to SCC at -110mV. Localized attacks were detected in SEM morphology pictures, when Alloy 800 sample without notch was polarized at transpassive potential. It showed that the localized attack of the oxide film as the probable reason for susceptibility of Alloy 800 to S^y-SCC.
4) EDX analysis of the corrosion product inside the pits indicated that thiosulfate promoted anodic dissolution, which in turn implied that the reduction reaction reaction of thiosulfate played a dominant role to cause metal dissolution than the repassivation reaction to form oxide film at -110 mV. XPS analysis showed evidence for the probable reduction reaction of thiosulfate to form sulphur on the surface during the

passivation of Alloy 800 which caused passivity degradation and increased the concentration of hydroxides in the passive film. This further explained the competition between the reduction reaction of thiosulfate and the dehydration of hydroxides to form oxide film on the Alloy 800 surface. SIMS analysis showed the supporting evidence for passivity degradation due to the presence of M-OH bonds at -110 mV.

5) Mott-Schottky test results in SG crevice solution containing thiosulfate show the n-type behaviour and the defects in the passive film i,e donor density increased with increase in the concentration of thiosulfate in the test solution. Mott-Schottky test results in SG crevice solution containing sulphide showed the n-type behaviour and the donor density of the passive film increased with increase in the concentration of sulphide in the test solution.
6) Potential drop test indicated that Alloy 800 was not susceptible to SCC at the rest potential in the SG crevice solution containing thiosulfate and sulphide at the room temperature.

5.2 Future work

1) To study in-situ crack growth rate using potential drop method and C-ring specimen, a more aggressive condition where Alloy 800 is susceptible to SCC should be used. In Section 4.2.1, it was concluded that Alloy 800 was susceptible to SCC at the transpassive potential region. Therefore the in-situ crack growth rate can be studied under applied potential condition in the transpassive region. Additionally maintaining an aerated condition of the test solution will be the second method to study the in-situ SCC growth rate of Alloy 800 at room temperature in AECL recommended test environment.
2) Further the effect of applied potential on the crack propagation rate of Alloy 800 due to S^y-SCC at high temperature can also be studied.
3) The S^y-SCC of Alloy 800 under different applied potentials can be investigated at high temperature.
4) The effect of applied potentials on the SCC of Alloy 800 can be studied in simulated SG crevice solution without thiosulfate and sulphide.
5) Mott-schottky tests can be conducted to study the semiconductive behavior of Alloy 800 in test solutions containing thiosulfate and sulphide at high temperature.

References:

1. (2011) Canadian Electricity Association.
2. (2010) Independent Electricity System Operator(IESO),.
3. Dutta R, Dey G, Lobo A, Purandare R, Kulkarni S. (2002) Corrosion behavior of austenitic alloy 690 under anodic and cathodic potentials. Metallurgical and Materials Transactions A, 33, 1437-1447.
4. Dutta RS, Purandare R, Lobo A, Kulkarni SK, Dey GK. (2004) Microstructural aspects of the corrosion of Alloy 800. Corrosion Science, 46, 2937-2953.
5. Dutta RS, Jagannath, Dey GK, De PK. (2006) Characterization of microstructure and corrosion properties of cold worked Alloy 800. Corrosion Science, 48, 2711-2726.
6. De PK, Ghosal SK. (1981) A Comparative Study of Stress Corrosion Cracking of Steam Generator Tube Materials in Water at 315 C. NACE.
7. Totsuka N, Lunarska E, Cragnolino G, Szklarska-Smialowska Z. (1987) Effect of Hydrogen on the Intergranular Stress Corrosion Cracking of Alloy 600 in High Temperature Aqueous Environments. NACE.
8. Totsuka N, Szklarska-Smialowska Z. (1987) Effect of Electrode Potential on the Hydrogen-Induced IGSCC of Alloy 600 in an Aqueous Solution at 350 C. NACE.
9. Shen Y, Shewmon PG. (1991) IGSCC Crack Growth of Alloy 600 and X-750 in Steam. NACE.
10. Bandy R, Rooyen DV. (1984) Stress Corrosion Cracking of Inconel Alloy 600 in High Temperature Water An Update. NACE.
11. Economy G, Jacko RJ, Pement FW. (1987) IGSCC Behavior of Alloy 600 Steam Generator Tubing in Water or Steam Tests Above 360 C. NACE.
12. De PK, Bose A. (1993) Electrochemical Corrosion Behavior of Alloy 400: Intergranular Corrosion in Acidic Na2SO4 Solutions. Corrosion, 49, 135.
13. Gadiyar HS. (1992) Workshop on Failure Analysis, Corrosion Evaluation and Metallography (FACORMET-92) Metallurgy Division, BARC. 10.
14. H.S.Gadiyar. (1995) Symposium on Current Trends in Water Chemistry of Nuclear and Thermal Power Plants and Other Related Units(CURTWAC-95), BARC. 9.
15. Moorthy PN, Mathur PK. Workshop on Failure Analysis,Corrosion Evaluation and Metallography (FACORMET-92), 1992, Metallurgy Division, BARC. 37.
16. Dutta RS, Tewari R, De PK. (2007) Effects of heat-treatment on the extent of chromium depletion and caustic corrosion resistance of Alloy 690. Corrosion Science, 49, 303-318.
17. A.J. Smith, R.P. Stratton. (1991) Proceedings of the 5th International Symposium on Environmental Degradation of Materials in Nuclear Power Systems-Water Reactors, Monterey, California, American Nuclear Society, Inc., La Grange Park, Illinois.
18. McIntyre NS, Davidson RD, Walzak TL, Brennenstuhl AM, Gonzalez F, Corazza S. (1995) The corrosion of steam generator surfaces under typical secondary coolant conditions: Effects of pH excursions on the alloy surface composition. Corrosion Science, 37, 1059-1083.
19. Tapping R. (2006) Steam Generator Aging In CANDUS: 30 Years Of Operation and R&D. 5th CNS International Steam Generator Conference
20. L.Chi, G.Goszczynski, Y.C.Lu. (2009) Test Plan for Investigating the Low Temperature Degradation of Steam Generator Tubing Materials in the Environments Containing Intermediate Oxidation State of Sulphur. AECL Report.

21. D. Durance, K. Sedman, J. Roberts, Gorman J. (2009) FFS Issues for Steam Generator Tube (Top of Tubesheet) Intergranular Attack/Stress Corrosion Cracking. Proceedings of the 17th International Conference on Nuclear Engineering (ICONE 17-75599), Brussels, Belgium, July 12-16, 2009.
22. U.E. Gustafsson, Shoemaker CE. Proceedings: Workshop on the Role of Sulphur Species on the Secondary-Side Degradation of Alloy 600 and Related Alloys.
23. Laycock NJ. (1999) Effects of Temperature and Thiosulfate on Chloride Pitting of Austenitic Stainless Steels. CORROSION, 55, 590-595.
24. Kilian R, Wieling N, Stieding L. (1991) Corrosion resistance of SG tubing material Incoloy 800 mod. and Inconel 690 TT. Materials and Corrosion, 42, 490-496.
25. R. Kilian RZ, R. Arenz, J. Beck, T. Schönherr and M. Widera. (2007) Operating Experience with Alloy 800 SG Tubing in Europe. Presentation at the 13th International Conference on Environmental Degradation of Materials in Nuclear Power Systems-Water Reactors,, Wistler, BC, Canada (2007).
26. Y.C.Lu, G.Goszczynski, S.Ramamurthy. (2009) Degradation of Alloy 800 Under Steam Generator Secondary Side Crevice Conditions. Proceedings of the 17th International Conference on Nuclear Engineering
27. Yang IJ. (1993) Localized Corrosion of Alloy 600 in Thiosulfate Solution at 25[degree]C. CORROSION, 49, 576-584.
28. Newman R, Sieradzki K, Isaacs H. (1982) Stress-corrosion cracking of sensitized type 304 stainless steel in thiosulfate solutions. Metallurgical and Materials Transactions A, 13, 2015-2026.
29. Zhang W, Newman RC. (2009) Localized corrosion of steam generator alloys at low temperature in mixed solutions of sulfate and thiosulfate. In: 14th International Conference on Environmental Degradation of Materials in Nuclear Power Systems Water Reactors 2009. Vol. 1, pp 1-8.
30. Ho JT, Yu GP. (1992) Pitting Corrosion of Inconel 600 in Chloride and Thiosulfate Anion Solutions at Low Temperature. CORROSION, 48, 147-158.
31. Haruna T, Toyota R, Shibata T. The effect of potential on initiation and propagation of stress corrosion cracks for type 304l stainless steel in a chloride solution containing thiosulfate. Corrosion Science, 39, 1873-1882.
32. Ashour EA, El Meguid, Abd EA, Ateya BG. (1997) Effects of Thiosulfate on Susceptibility of Type 316 Stainless Steel to Stress Corrosion Cracking in 3.5% Aqueous Sodium Chloride. CORROSION, 53, 612-616.
33. Gonzalez-Rodriguez JG, Salinas-Bravo VM, Martinez-Villafane A. (1999) Low-Temperature Stress Corrosion Cracking of Alloy 601 in Thiosulfate and Chloride Solutions. CORROSION, 55, 38-44.
34. Roychowdhury S, Ghosal S, De P. (2004) Role of environmental variables on the stress corrosion cracking of sensitized AISI type 304 stainless steel (SS304) in thiosulfate solutions. Journal of Materials Engineering and Performance, 13, 575-582.
35. Tsai WT, Chang CS, Lee JT. (1994) Effects of Shot Peening on Corrosion and Stress Corrosion Cracking Behaviors of Sensitized Alloy 600 in Thiosulfate Solution. CORROSION, 50, 98-105.
36. Tsai WT, Sheu MJ, Lee JT. (1996) The stress corrosion crack growth rate in sensitized alloy 600 in thiosulfate solution. Corrosion Science, 38, 33-45.
37. Laitinen TMJ. (1999) Comparison of Stainless Steels in Simulated Paper Machine Environments. CORROSION, 55, 858-869.

38. Singh PM, Perdomo JJ, Oteng JE, Mahmood J. (2004) Stress Corrosion Cracking and Corrosion Fatigue Cracking of a Duplex Stainless Steel in White Water Environments. CORROSION, 60, 852-861.
39. Chen YY, Shih HC, Liou YM, Wang LH, Oung JC. (2006) Stress Corrosion Cracking of Type 321 Stainless Steels under Simulated Petrochemical Conditions Containing Thiosulfate and Chloride. CORROSION, 62, 781-794.
40. Isaacs HS, Vyas B, Kendig MW. (1981) *Stress-corrosion cracking of sensitized stainless steel by sulfur-containing compounds*.
41. Park JO, Verhoff M, Alkire R. (1997) Microscopic behavior of single corrosion pits: the effect of thiosulfate on corrosion of stainless steel in NaCl. Electrochimica Acta, 42, 3281-3291.
42. Fang Z, Staehle RW. (1999) Effects of the Valence of Sulfur on Passivation of Alloys 600, 690, and 800 at 25[degree]C and 95[degree]C. CORROSION, 55, 355-379.
43. Ge H-H, Zhou G-D, Wu W-Q. (2003) Passivation model of 316 stainless steel in simulated cooling water and the effect of sulfide on the passive film. Applied Surface Science, 211, 321-334.
44. Staehle RW, Gorman JA. (2004) Quantitative Assessment of Submodes of Stress Corrosion Cracking on the Secondary Side of Steam Generator Tubing in Pressurized Water Reactors: Part 3. CORROSION, 60, 115-180.
45. R.H.Jones. Mechanism of Stress Corrosion Cracking.
46. M.Huang. (2009) Degradation of SG Tubing Materials in Reduced Sulphur environment. AECL Report.
47. Haruna T, Shibata T. (1994) Initiation and Growth of Stress Corrosion Cracks in Type 316L Stainless Steel during Slow Strain Rate Testing. CORROSION, 50, 785-791.
48. Duret-Thual C, Costa D, Yang WP, Marcus P. (1997) The role of thiosulfates in the pitting corrosion of Fe-17Cr alloys in neutral chloride solution: Electrochemical and XPS study. Corrosion Science, 39, 913-933.
49. Tsai WT, Kuoh CC. (1999) Corrosion Fatigue Crack Growth Rate in Sensitized Alloy 600 in Thiosulfate Solution at Room Temperature. CORROSION, 55, 554-560.
50. Staehle RW, Gorman JA. (2004) Quantitative Assessment of Submodes of Stress Corrosion Cracking on the Secondary Side of Steam Generator Tubing in Pressurized Water Reactors: Part 2. CORROSION, 60, 5-63.
51. Kelly R.G., Sculy J.R., Shoesmith D.W., Bucheit R.G. Electrochemical techniques in corrosion science and engineering Marcel Dekkar.
52. Macdonald D.D. (1992) The point defect model for the passive state Journal of Electrochemical Society, 139 3434-3449.
53. P. C. McKeighan, C. P. Tabrett, D. J. Smith. (1995) The influence of Crack Deflection on Bifurcation on DC Potential Drop Calibration. Special Applications and Advanced Techniques for Crack Size Determination, ASTM STP 1251, Amercian Society for Testing and Materials, Philadelphia.
54. W. J. Barnett aART. (1957) Crack propagation in the Hydrogen Induced Brittle Fracture of Steel Transactions, American Institute of Mining, Metallurgical, and Electronic Engineers, 20.
55. Merah N. (2000) DC Potential Drop Calibration in Creep-Fatigue Loading Conditions. Journal of Testing and Evaluation, JTEVA, 28, 301-306.
56. W. R. Catlin, D. C. Lord, T. A. Prater, Coffin LF. (1985) The Reversing DC Elctrical Potential Method. Automated Test Methods for Fracture and Fatigue Crack Growth, ASTM STP 877, W. H. Cullen, R. W. Landgraf, L. R. Daisand, and J. H. Underwood, Eds.Philadelphia,American Society for Testing and Materials Pennsylvania,.

57. Wei RP, Bazill RL. (1981) An Assessment of AC and DC potential Systems for Monitoring Fatigue Crack Growth. Fatigue Crack Growth Measuremnet and Data Analysis, ASTM STP 738, S. J. Hudak Jr., and R. J. Bucci, eds., American Society for Testing and Materials, Philadelphia, Pennsylvania.
58. Y.C. Lu, M. Huang, D. Burns, Dupuis M. (2008) Electrochemical Studies on the Interactive Effect between Calcium, Copper, Aluminum, Magnesium and Lead on SG Tube Corrosion, CANDU Owner's Group, TN-08-4067, 2008 May.
59. (2005) Laboratory Testing of Metals for Resistance to Sulfide Stress Cracking and Stress Corrosion Cracking in H2S Environments - Item No:21212 NACE INTERNATIONAL, NACE TM0177.
60. Alice DINU MA, Maria RADULESCU, Lucian VELCIU. (2006) Electrochemical studies on Stress corrosion cracking of INCOLOY-800 in caustic solution. Part II: Precracking samples. Nuclear technology and radiation protection-1/2006.
61. (Reapproved 2007) Standard Practice for Making and Using C-Ring Stress-Corrosion Test Specimens. ASTM INTERNATIONAL, G 38 – 01
62. Kuo H-S, Chang H, Tsai W-T. (1999) The corrosion behavior of AISI 310 stainless steel in thiosulfate ion containing saturated ammonium chloride solution. Corrosion Science, 41, 669-684.
63. Pickering HW, Frankenthal RP. (1972) On the Mechanism of Localized Corrosion of Iron and Stainless Steel. Journal of The Electrochemical Society, 119, 1297-1304.
64. Szklarska-Smialowska Z. (1986) Pitting corrosion of metals. National Association of Corrosion Engineers.
65. Brown BF, Fujii CT, Dahlberg EP. (1969) Methods for Studying the Solution Chemistry Within Stress Corrosion Cracks. Journal of The Electrochemical Society, 116, 218-219.
66. Ashour EA, El Meguid EAA, Ateya BG. (1997) Effects of Thiosulfate on Susceptibility of Type 316 Stainless Steel to Stress Corrosion Cracking in 3.5% Aqueous Sodium Chloride. CORROSION, 53, 612-616.
67. (2006) HSC Chemistry 5.11. Outokumpu Research, Pori, Finland.
68. (2011) http://bilbo.chm.uri.edu/CHM112/tables/KspTable.htm.
69. Macdonald DD, Syrett BC, Wing SS. (1979) CORROSION OF Cu-Ni ALLOYS 706 AND 715 IN FLOWING SEA WATER - 2. EFFECT OF DISSOLVED SULFIDE. Corrosion, 35, 367-378.
70. Shoesmith DW, Taylor P, Bailey MG, Ikeda B. (1978) Electrochemical behaviour of iron in alkaline sulphide solutions. Electrochimica Acta, 23, 903-916.
71. Shoesmith DW, Bailey MG, Ikeda B. (1978) Electrochemical formation of mackinawite in alkaline sulphide solutions. Electrochimica Acta, 23, 1329-1339.
72. Hansson EB, Odziemkowski MS, Gillham RW. (2006) Formation of poorly crystalline iron monosulfides: Surface redox reactions on high purity iron, spectroelectrochemical studies. Corrosion Science, 48, 3767-3783.
73. Betova I, Bojinov M, Hyökyvirta O, Saario T. Effect of sulphide on the corrosion behaviour of AISI 316L stainless steel and its constituent elements in simulated Kraft digester conditions. Corrosion Science, 52, 1499-1507.
74. Ma H, Cheng X, Chen S, Wang C, Zhang J, Yang H. (1998) An ac impedance study of the anodic dissolution of iron in sulfuric acid solutions containing hydrogen sulfide. Journal of Electroanalytical Chemistry, 451, 11-17.
75. Cheng X, Ma H, Chen S, Niu L, Lei S, Yu R, Yao Z. (1999) Electrochemical behaviour of chromium in acid solutions with H2S. Corrosion Science, 41, 773-788.

76. Cheng X, Ma H, Chen S, Chen X, Yao Z. (2000) Corrosion of nickel in acid solutions with hydrogen sulphide. Corrosion Science, 42, 299-311.
77. Ma H, Cheng X, Li G, Chen S, Quan Z, Zhao S, Niu L. (2000) The influence of hydrogen sulfide on corrosion of iron under different conditions. Corrosion Science, 42, 1669-1683.
78. Galtayries A, Cousi C, Zanna S, Marcus P. (2004) SO2 adsorption at room temperature on Ni(111) surface studied by XPS. Surface and Interface Analysis, 36, 997-1000.
79. Grosvenor AP, Biesinger MC, Smart RSC, McIntyre NS. (2006) New interpretations of XPS spectra of nickel metal and oxides. Surface Science, 600, 1771-1779.
80. McIntyre NS, Zetaruk DG. (1977) X-ray photoelectron spectroscopic studies of iron oxides. Analytical Chemistry, 49, 1521-1529.
81. Lu BT, Luo JL, Lu YC. (2007) A Mechanistic Study on Lead-Induced Passivity-Degradation of Nickel-Based Alloy. Journal of The Electrochemical Society, 154, C379-C389.
82. Laajalehto K, Kartio I, Nowak P. (1994) XPS study of clean metal sulfide surfaces. Applied Surface Science, 81, 11-15.
83. (2011) http://xpsfitting.blogspot.com/search/label.
84. Marcus P, Grimal JM. (1990) The antagonistic roles of chromium and sulphur in the passivation of Ni---Cr---Fe alloys studied by XPS and radiochemical techniques. Corrosion Science, 31, 377-382.
85. D.Briggs MPS. (1994) Particle surface analysis. John wiley & sons, 2nd edn.
86. Lu BT, Luo JL, Lu YC. (2008) Correlation between film rupture ductility and PbSCC of Alloy 800. Electrochimica Acta, 53, 4122-4136.
87. Biernat RJ, Robins RG. (1969) High temperature potential/ph diagrams for the sulphur-water system. Electrochimica Acta, 14, 809-820.
88. Dhawale SW. (1993) Thiosulfate: An Interesting Sulfur Oxoanion that is Useful in Both Medicine and Industry-But is Implicated in Corrosion. Journal of Chemical Education, 70, 12-null.
89. Lu BT, Tian LP, Zhu RK, Luo JL, Lu YC. Effects of dissolved calcium and magnesium ions on lead-induced stress corrosion cracking susceptibility of nuclear steam generator tubing alloy in high temperature crevice solutions. Electrochimica Acta, 56, 1848-1855.
90. Rangel CM, Silva TM, Belo MdC. (2005) Semiconductor electrochemistry approach to passivity and stress corrosion cracking susceptibility of stainless steels. Electrochimica Acta, 50, 5076-5082.
91. Vignal V, Valot C, Oltra R, Verneau M, Coudreuse L. (2002) Analogy between the effects of a mechanical and chemical perturbation on the conductivity of passive films. Corrosion Science, 44, 1477-1496.
92. S.R.Morrison. (Newyork, 1980) Electrochemistry at Semiconductor and Oxidized Metal Electrodes. Plenum press.
93. A.Palani. (University of Alberta(2008)) Effects of Magnesium on PbSCC of UNS N00800 Alloy, Master Thesis.
94. Marvasti M. Crack growth behavior of pipeline steels in near neutral pH soil environment, pp 136. University of Alberta (Canada), Canada.
95. ASM Metals Handbook- corrosion. 13.